NASA Contractor Report 3760

NASA-CR-3760 19840010194

FOR REFERENCE

NOT TO BE TAKEN FROM THIS ROOM

Control of Large Flexible Spacecraft by the Independent Modal-Space Control Method

Leonard Meirovitch and Joram Shenhar

GRANT NAG1-225
JANUARY 1984

NASA

NASA Contractor Report 3760

Control of Large Flexible Spacecraft by the Independent Modal-Space Control Method

Leonard Meirovitch and Joram Shenhar
Virginia Polytechnic Institute and State University
Blacksburg, Virginia

Prepared for
Langley Research Center
under Grant NAG1-225

National Aeronautics
and Space Administration

Scientific and Technical
Information Branch

1984

TABLE OF CONTENTS

LIST OF TABLES v

LIST OF FIGURES vii

LIST OF SYMBOLS ix

Chapter

page

I. INTRODUCTION 1

II. PROBLEM FORMULATION 13

System Discretization via Finite Element Method 13
Potential Energy 16
Kinetic Energy 23
Nonconservative Generalized Force 24
Finite Element Model 25
The Eigenvalue Problem and Modal Space Decomposition 45
Control of the Dominant Modes 48

III. LINEAR OPTIMAL CONTROL WITH QUADRATIC PERFORMANCE INDEX 52

IV. THE EFFECT OF ACTUATORS PLACEMENT ON THE MODE PARTICIPATION MATRIX 60

V. MINIMUM FUEL IN HIGH ORDER SYSTEMS 80

Problem Formulation 83
Fuel-Optimal Control for a Rigid Body Mode . . . 99
Fuel Consumed - RBM 117
Fuel-Optimal Control for an Elastic Mode . . . 118
Fuel Consumed and Final Time Selection - EM 128

VI. NUMERICAL EXAMPLES 136

Linear Optimal Control with Quadratic Performance Index 144
Minimum-Fuel Problem 151

VII. CONCLUSIONS AND RECOMMENDATIONS 159

REFERENCES 164

Appendix

page

A. LAPLACE EXPANSION FOR DETERMINANTS 167

B. MINIMUM FUEL CONTROL WITH UNSPECIFIED FINAL TIME: RIGID BODY MODE 173

Region R1 174
Region R2 177

C. MINIMUM-FUEL CONTROL WITH BOUNDED FINAL TIME: RIGID BODY MODE 180

Minimum-Time Solution 180
Switching Times tz, tw 182
First Switch Times Loci 185
Boundaries for the Reachable States 185
Plot of the Modal State Plane 186

D. MINIMUM-FUEL CONTROL: ELASTIC MODE 190

Time Scaling of the State Plane Trajectories . 190
Determination of the Costate Constants for Initial Condition Point Outside the Control Sector 192
Determination of the Costate Constants for Initial Condition Point Inside the Control Sector 195

LIST OF TABLES

Table

page

4.1. Summary of Cases from Fig. 4.2 72

6.1. System Parameters in the Linear Optimal Control Framework 145

6.2. System Parameters in the Minimum-Fuel Control Framework 152

LIST OF FIGURES

Figure

page

1.1. Beam Lattice 10

2.1. Beam Lattice Model 15

2.2. A Typical Element in Gravitation Field 21

2.3. Finite Element Models 26

3.1. Modal Damping Ratio ζ vs p 59

4.1. Triple Index Notation (i,j,k) 63

4.2. Various Actuators Configurations 68

5.1. N-Dependent Part of Modal Hamiltonian Function . . . 95

5.2. Modal Fuel-Optimal Control Function 97

5.3. Candidates for Modal Fuel-Optimal Control for RBM 104

5.4. State Plane Trajectories for RBM 106

5.5. Four Regions of Control in the State Plane for RBM 108

5.6. Modal State Plane Trajectories for RBM with Fixed Final Time 112

5.7. Modal State Trajectories Families for EM 124

5.8. Modal State Trajectory vs Modal Costate Function for EM 125

5.9. Realization of Minimum-Fuel Solution (case 1) . . 131

5.10. Realization of Minimum-Fuel Solution (case 2) . . 135

6.1. The Twelve Lowest Modes of Vibration 139

6.2. System Initial Conditions 141

6.3. Mode Participation Factors 142

6.4. Actuators Placement Configuration 143

6. 5. Actual Response at Nodes 1,3,8 and 14 146

6. 6. Modal Control Forces vs Time 148

6. 7. Actuators Forces vs Time 149

6. 8. Total Consumed Fuel 150

6. 9. Modal State-Plane Trajectories (Cases 1,2,3) . . . 153

6. 10. Modal Control Forces vs Time (Case 1) 156

6. 11. Actuators Forces vs Time (Case 1) 157

6. 12. Total Consumed Fuel (Case 1) 158

A. 1. Beam Lattice with Symmetric Actuators Configuration 170

B. 1. Control Dependence on Initial Condition Point for RBM 175

C. 1. State Plane Minimum-Time Trajectory for RBM . . . 181

C. 2. Optimal Control Regions and Switching Curves . . . 187

D. 1. Time Recovery from State Plane Description 191

D. 2. Initial Condition Point Outside the Control Sector for EM 193

D. 3. Initial Condition Point Inside the Control Sector for EM 196

LIST OF SYMBOLS

A	Cross-sectional area (II.1)[1]
	Modal plant matrix (III)
a	Weighting coefficients (V.1)
	Beam width (II.1)
B	Actuators placement transformation matrix (II.3)
	State control matrix (III)
b	Beam thickness (II.1)
C	Constraints matrix (II.1)
	Notation for the number of controlled modes (II.3)
	Mode participation matrix (V.2)
C_R	Rigid constraints matrix (II.1)
c	Subscript for cable notation (II.1)
	Number of controlled modes (IV)
d	Notation for disjoint system (II.1)
E	Modulus of elasticity (II.1)
F	Function symbol (II.1)
	Generalized force vector (II.1)
	Actuators force vector (II.3)
	Fuel consumption (V.3)

[1] The number in parenthesis denotes the chapter and section number of first occurence

f	Distributed force (II.1)
G	Shear modulus (II.1)
	Gravitation force (II.1)
g	Gravitational acceleration constant (II.1)
H	Hamiltonian function (V.1)
h	Length of finite element (II.1)
	Number of horizontal actuators on the line of symmetry (IV)
I	Area moment of inertia in bending (II.1)
I_{xG}	Mass moment of inertia of rigid end-block (II.1)
I_{yG}	Mass moment of inertia of rigid end-block (II.1)
	Identity matrix (II.2)
i,j,k	Triple index notation for actuator placement (IV)
J	Mass moment of inertia of a unit length element about the bending axis (II.1)
	Performance index (cost) (III)
J_0	Mass polar moment of inertia (II.1)
J^*	Area polar moment of inertia (II.1)
j	Notation for a typical finite element (II.1)
K	Stiffness matrix (II.1)
	Riccati matrix (coefficient) (III)
k	Shear distribution compensation factor (II.1)
L	Interpolation functions vector (II.1)
L^*	Modified interpolation functions vector (II.1)
M	Mass matrix (II.1)

	Mass of rigid end-block (II.1)
	Total order of disjoint system (II.1)
	Control bound (V.1)
M_2	Total number of second-order members (II.1)
M_4	Total number of fourth-order members (II.1)
m	Mass per unit length (II.1)
	Distributed moment (II.1)
m_2	Number of second-order members (II.1)
m_4	Number of fourth-order members(II.1)
N	System order (II.1)
	Modal force (II.2)
$\hat{N}$	Modal control bound (V.1)
n_c	Number of full non-zero control strokes (V.3)
n_e	Number of elastic modes (V.3)
n_r	Number of rigid body modes (III)
P	Axial force (II.1)
	EM costate amplitude constant (V.3)
p	Dummy variable (III)
	Number of pairs of actuators in Ξ (IV)
	Costate variable (V.1)
Q	Configuration space force (II.1)
	Modal space weighting matrix (factor) (III)
q	Generalized coordinate (II.1)
R	Notation for the number of residual modes (II.3)
	Modal control effort weighting factor (III)

	Region in modal state plane (V.2)
r	Index for modal coordinate (II.2)
r_0	Modul of initial condition position vector (V.3)
s	Notation for a typical member (II.1)
	Number of symmetric modes (IV)
T	Cable tension (II.1)
	Kinetic energy (II.1)
T_f	Final time upper bound (V.2)
t_f	Final time (V.1)
U	Modal matrix (II.2)
u	Component of displacement (II.1)
	Eigenvector (IV)
V	Potential energy (II.1)
v	Number of vertical actuators on the line of symmetry (IV)
W	Work (II.1)
w	Lateral displacement (II.1)
x	State variable (III)
x,y,z	Global coordinate set (II.1)
Z	Trajectory variable in the state plane (V.2)
α	Weighting factors (V.1)
	Control sector angle (V.3)
β	Control arc (V.3)

γ	Switch curve (V.2)
Δ	$\pm\hat{N}$ - modal control bound (V.2)
δ	Kronecker delta (II.2)
	Phase constant correction factor (V.3)
ε	Small variation (B.1)
ζ	Damping ratio factor (III)
η	RBM constate initial conditions (V.2)
	Angle in a triangle (D.3)
θ	Rotational displacement in torsion (II.1)
	EM costate phase constant (V.3)
Λ	Diagonal matrix of eigenvalues (II.2)
λ	Eigenvalue (V.1)
ν	Poisson ratio (II.1)
Ξ	Symmetric set of actuators configuration (IV)
	Modal initial condition point (V.2)
ξ	Local coordinate (II.1)
	Modal space coordinate (II.2)
ρ	Sign function (IV)
σ	Sign parameter (IV)
τ	Normalized time (V.3)
ϕ	Phase angle related to x_2 axis (V.3)
ψ	Rotation of a line element due to bending (II.1)
	Phase angle (III)
	State plane initial condition position angle (V.3)
ω	Natural frequency (II.2)

Special symbols

$(*)'=d(*)/dx$	Spatial derivative (rotation)
$(*)=d(*)/dt$	Time derivative
$(*)_2$	Notation for a second-order member
$(*)_4$	Notation for a fourth-order member
$(*)$	Vector notation
$A(*)$	Minor of the matrix A (IV)
[*]	Notation for reference

Abbreviations

bdiag	block diagonal (II.1)
dez	dead-zone function (V.1)
EM	Elastic Mode (V.3)
IMSC	Independent Modal Space Control (I)
RBM	Rigid Body Mode (V.2)

Chapter I

INTRODUCTION

The control of distributed-parameter systems represents a real challenge to the system designer, both from a theoretical and practical point of view. Distributed-parameter systems arise in various areas. In recent years, due to the interest in larger and more flexible structures, the analysis and design of such systems have steadily increased in importance [1-12]. Examples of flexible stuctures are high buildings, long bridges, large ships and submersible vessels, aircraft, rockets, missiles, satellites with flexible appendages, astronomical telescopes with large antenas, to mention just a few. As a rough approximation, these distributed-parameter systems, or at least their most essential parts, can be considered as vibrating strings, beams, membranes, plates, shells, and various combinations of these components. Such large flexible systems of this nature are usually described by a hybrid set consisting of ordinary and partial differential equations with two or more independent variables [7,9]. The determination of natural frequencies and dynamic response of engineering structures, requires normally a significant simplification of the actual geometry and an approximate method of analysis.

Classical structural dynamics problems require the derivation of the differential equations of motion of typical structural members and the determination of the solutio ns, where the latter are subject to given boundary conditions. Such closed-form solutions are limited to relatively simple geometries. However, these solutions are of great value as they provide an understanding of the dynamical behavior of typical components, such as beams and plates. For more complex structures, closed-form solutions are not possible and one must consider approximate solutions. Approximate methods can provide solutions for a wider range of problems and are capable of yielding results of acceptable accuracy with reasonable economy of computation.

The most indicated approximate methods in structural dynamics are the classical Rayleigh-Ritz and its finite element version. Substructure synthesis can also be regarded as a Rayleigh-Ritz method [13]. The classical Rayleigh-Ritz method is less versatile than the finite element method, as the latter can be used for more complex structural problems [13]. Complex structures generally represent assemblages of distributed parameter components such as plates, beams, columns, etc. Whereas many of these compo-

nents may have uniformly distributed properties and by themselves may admit closed-form eigensolutions, when they are bounded together in a single structure, the component eigensolution does not have much significance. The eigensolution of interest now is that of the complete structure and this eigensolution cannot be obtained in closed form. Therefore, spatial discretization is unavoidable.

In contrast to the classical Rayleigh-Ritz method, where the expressions for displacements are applicable to the complete domain, finite element expressions are defined only over a part of the domain, namely an element. It is typical of the finite element method, that the resulting discrete models possess a large number of degrees of freedom. Moreover, as with any approximate method, the associated algebraic eigenvalue problem is not an accurate representation of the actual system eigenvalue problem, as only the lower modes can be computed with satisfactory accuracy and the higher modes can be grossly in error.

In general, the fundamental problem of active control of flexible systems is to control a large-dimensional system with a much smaller-order controller. Quite often a large number of elastic modes may be needed to model the behavior

of a large flexible spacecraft. However, active control of all these modes is not likely to be feasible due to computation limitation and errors that arise in modeling the higher modes by the discretization process. Clearly, the controls must be restricted only to the most significant modes [4]. Furthermore, the bandwidths of actuators and sensors prevent response to the higher-frequency modes, and these higher modes cannot respond to the actual controls. The real justification for controlling only the lower modes lies in the fact that the higher frequency modes in an actual system are harder to excite. A conclusion can be drawn at this stage that a control system must be designed so as to control the modes of most significance, namely the lower modes. To guarantee that the controlled modes are sufficiently accurate, it is often necessary to consider a relatively large-order discrete system model.

The increased order of models representing modern structures and the associated control problems, have provided the motivation for developing methods permitting analysis of such systems, and providing solutions to the control problems with little computational effort. Such a method is the 'Independent Modal-Space Control' (IMSC) method [6-12]. This method is capable of carrying out the control task ef-

ficiently. Briefly, this method is based on a transformation of the system equations of motion to modal space, yielding internally independent modal equations of motion. Then, the control laws are designed in the modal space, so as to permit independent control of each individual mode, thus providing complete decoupling of the equations of motion. This approach allows complete flexibility as to which modes to control. The corresponding forces are not actual forces but more abstract modal control forces. For control implementation, the actual control forces are synthesized from the modal forces by a linear transformation. This method is easy to implement, especially for high-order systems, such as those arising from modeling complex distributed-parameter systems.

Most actuators placement concepts discussed so far in conjunction with the IMSC method [14,15], are supposed to minimize the part of energy that goes into the uncontrolled modes. Indeed, it is shown in Ref. 14 that the work done to control the controlled modes does not depend on the actuator locations. Of course, this statement holds true if the mode participation matrix is <u>nonsingular</u>. This is guaranteed to be the case for one-dimensional domains if IMSC is used, but cannot be taken for granted in the case of two-dimensional

domains, so that care must be exercised in choosing the location of the actuators.

Another argument can be found in Ref. 15, where a discussion on actuators placement is presented. It is remarked that actuator locations can be chosen based upon <u>any</u> desired criterion which makes the actuators placement as an independent design step. It is also remarked in this reference that improper choice of actuator locations can be disastrous since the actuator force, or torque, can grow without bounds as the actuator locations approch a position for which the system becomes uncontrollable. Then, the reference suggests a method for optimizing the actuator locations in order to minimize the actual control effort, ignoring the problem of controllability. In view of this, it is clear that, before discussing any minimization aspects, one must place the actuators so that the mode participation matrix is nonsingular. It should be pointed out that this problem tends to disappear as the number of actuators increases.

The minimum-fuel problem is a very important one in the design of space vehicles and various space structures, especially for those with lengthy missions. The amount of fuel or energy alloted for control is limited to such a degree

that it becomes necessary to treat fuel economy as one of the predominant factors. In such cases, it is natural to design the control system so that it consumes a minimum amount of fuel [16-23].

The total fuel consumed during control is measured by the time integral of the absolute value of the control variable. Due to some technical restrictions on the actuators, there exist limits on the magnitude of the control forces. As an example, the thrust produced by a gas jet actuator is limited in magnitude by the saturation of the power elements. Controls subject to constraints and minimizing a particular functional, such as the consumed fuel, the required energy, etc., are optimal. A control system minimizing the amount of consumed fuel, is referred to as a "minimum-fuel system".

About two decades have passed since the mathematical theory of control has been based on powerful variational techniques, such as the minimum principle of Pontryagin. This method can be used to determine necessary and sufficient conditions for the control to be optimal [16,17]. The necessary condition for optimal control usually specifies the nature of the control and the general structure of the control system.

The derivation of the optimal feedback control law, i.e., the explicit dependence of the control on the state variables, is a very complex task and in most practical cases it remains an unsolved problem [18,19]. In these cases, a trial and error process is unavoidable for the state determination. One may consider such a process as reasonable for a low-order system (fourth-order at most), but certainly not for a high-order system, where the computational difficulty is insurmountable. Unfotunately, an accurate model of a flexible structure requires a large number of degrees of freedom.

Formulation of the control law in terms of the costate variables can be accomplished regardless of the system order, but determination of the initial conditions of the costate variables for a high-order system is difficult if not impossible. The control task is made considerably simpler by using the IMSC method where the complexity inherent in a high-order system is eliminated. Using this method, the initial costate variables must be determined for a set of independent second-order ordinary differential equations, so that treatment of coupled high-order systems is avoided.

It is the goal of this study to apply control theory to a large flexible structure using the 'Independent Modal-Space Control' (IMSC) method, particularly for minimum-fuel control. For the purpose of demonstration, the analysis will be focused on a large-order flexible system in the form of a plate-like framework. The structure is a beam lattice assemblage, as can be seen in Fig. 1.1a. In addition, to permit simulation of a gravity-free environment in laboratory, a beam lattice supported by cables, as shown in Fig. 1.1b, is analyzed.

Chapter II contains the problem formulation. In the first section, the distributed-parameter system is discretized via the finite element method for both cases shown in Fig. 1.1. Then, in the second section, the eigenvalue problem is formulated and modal space decomposition is applied to the coupled equations of motion in order to transform the coupled set into a decoupled set of differential equations. The third section discusses the advantage of using a reduced-order controller, emphasizing the disadvantages in the control of the higher modes. In this section, the fundamental principles of the IMSC method are introduced, and the idea of complete decoupling of the equations of motion is established.

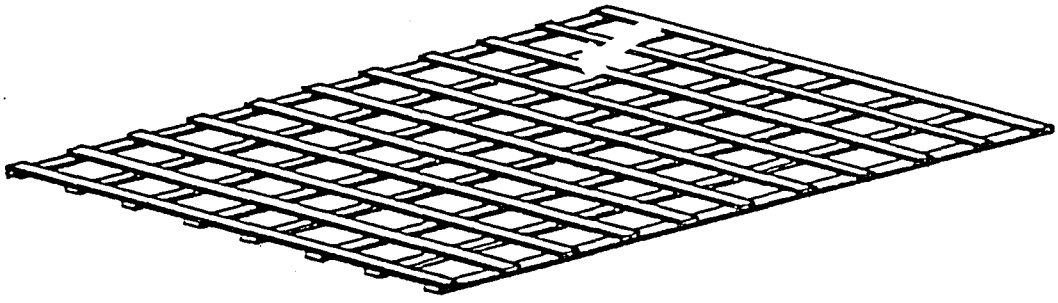

(a)

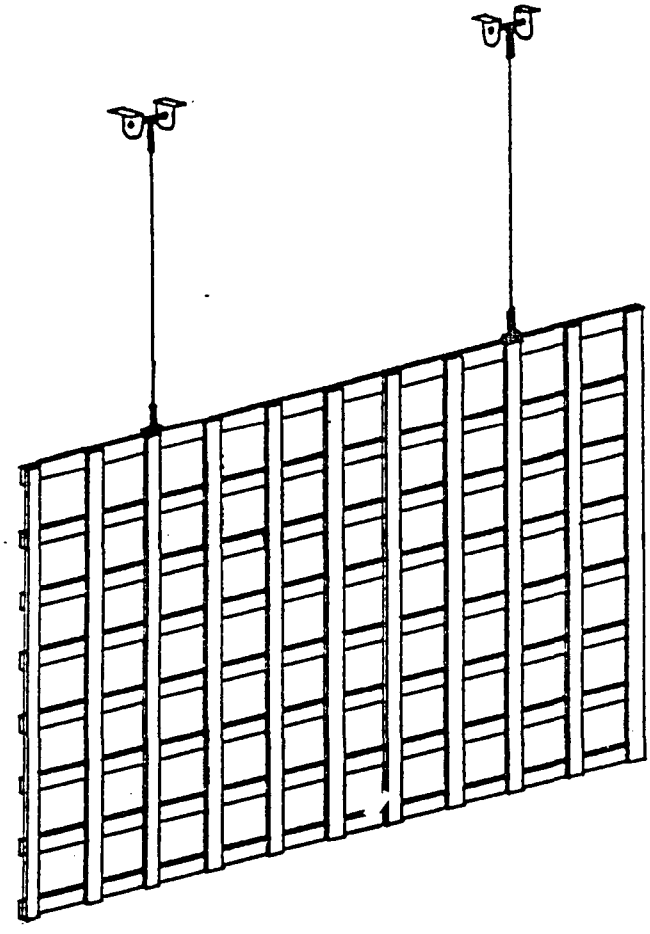

(b)

Figure 1.1: Beam Lattice
(a) Free in Space
(b) Cable Supported

Chapter III provides a discussion of linear optimal control in conjunction with quadratic performance index. The object is to suppress rigid body modes and the dominant elastic modes, thus providing attitude and shape control of a structure in a single control level policy. For control implementation, force and torque actuators, such as thrusters and momentum wheels, are used.

Chapter IV analyzes aspects of actuators placement and their effect on the condition of the mode participation matrix. The system in this discussion possesses symetric mass and stiffness properties in addition to symmetric boundary conditions. A proposition stating a sufficient condition, related to the singularity of the mode participation matrix, is introduced. A detailed proof of the proposition via Laplace expansion for determinants, concludes this chapter.

Chapter V analyses the problem of minimum-fuel in high-order system. A problem of insurmountable computational difficulty is made considerably simpler by using the IMSC method, where the complexity inherent in a high-order system is eliminated.

Chapter VI displays numerical examples based on the analysis of the beam lattice structure presented in Fig. 1.1.

Chapter VII summarizes the conclusions and provides recommendations for future research.

Chapter II

PROBLEM FORMULATION

2.1 SYSTEM DISCRETIZATION VIA FINITE ELEMENT METHOD

The equations of motion for a flexible structure can be derived by means of Hamilton's principle [24]. This derivation will lead in general, to a set of hybrid (partial and ordinary) differential equations that are difficult to handle mathematically even for simple structures and it is customary to resort to an approximate solution.

The finite element method is an approximate method of analysis which can be used to solve complex structural problems. The method consists in taking the displacement measures at discrete points in the domain as the unknowns, and defining the displacement field in terms of these discrete variables. Once the discrete displacements are known, the system motion can be described at any given point in the domain by interpolation. In order to achieve system discretization, the stiffness and mass matrices as well as the generalized force vector for the entire structure, must be obtained. In the finite element method we consider the structure to be divided into volume elements having finite

dimensions and we select certain points in the interior and boundary surfaces. The volume elements are referred as "finite" elements, since their dimensions are finite, and the boundary points are called nodal points or nodes. The various steps in a solution to any problem are:

1. Discretization of the body by selection of elements interconnected at certain nodal points.
2. Evaluation of the element stiffness, mass and force matrices.
3. Assemblage of the stiffness mass and force matrices for the system of elements-nodes and introduction of displacement boundary conditions.
4. Solution of the resulting system equations for the response, due to a given set of initial conditions, under a certain design of control law.

The system shown in Fig. 1.1 will be modeled as a reduced dimension model, assembled of flexible beams connected to each other by means of rigid blocks, as shown in Fig. 2.1. Deriving the potential and kinetic enery expressions as well as the non-conservative generalized force, are the first steps in achieving system discretization.

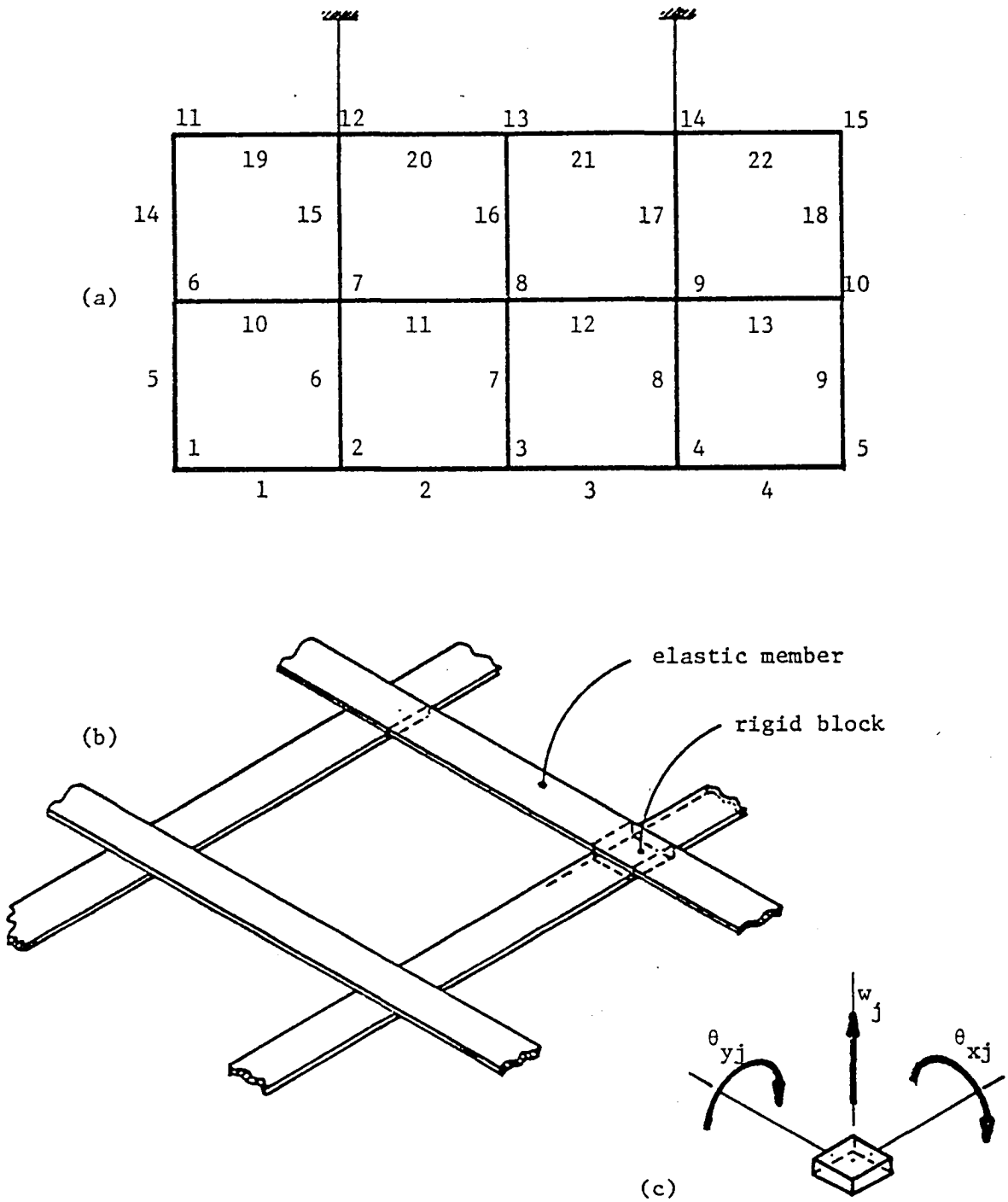

Figure 2.1: Beam Lattice Model
(a) Members and Nodes Numbering
(b) Model Members
(c) Rigid Block

2.1.1 Potential Energy

We denote a typical element by j and consider first the potential energy expression for the beam member elements. From the theory of beams, it is well known that the ratio of shear strain energy to bending strain enery is proportional to $(b/L)^2$, where b is the cross sectional height and L is the beam length. Thus, for long thin beams, the shear strain energy is very small compared to the bending strain energy. For short stubby beams, similar to those given in the beam lattice structure, the contribution of those shear effects, clearly cannot be neglected and for this reason, Timoshenko theory of beams will be considered as a mean of accounting for the effects of shear in a simple manner [25]. The total slope $\partial w/\partial x$ of the centerline that results from shear deformation and bending deformation, can be given as the sum of two parts in the following way

$$\frac{\partial w_j(x,t)}{\partial x} = \psi_j(x,t) + \beta_j(x,t) \tag{2.1}$$

where $\psi_j(x,t)$ is the rotation of line elements along the centerline due to bending only, while $\beta_j(x,t)$ accordingly, gives the shear angle at points along the centerline. As

far as shear strain is concerned, it is assumed that the shear strain is the same at all points over a given cross section of the beam. That is, the angle $\beta_j(x,t)$, used heretofore for rotation of elements along the centerline, is considered to measure the shear angle at all points in the cross section of the beam at position x. Such an assumption will greatly facilitate computation. In order to retain simplicity and still have the actual shear distribution effects, a compensation factor k is introduced and the total potential energy for the deformation field of the Timoshenko-Beam can be written as

$$V_j = \int_{x_{j-1}}^{x_j} \left[\frac{EI_j}{2} \left(\frac{\partial \psi_j}{\partial x} \right)^2 + \frac{kGA_j}{2} \left(\frac{\partial w_j}{\partial x} - \psi_j \right)^2 + \frac{GJ_j^*}{2} \left(\frac{\partial \theta_j}{\partial x} \right)^2 \right] dx \qquad (2.2)$$

where EI_j, kGA_j and GJ_j^* are the bending stiffness, the shear stiffness and tortional stiffness, respectively. k is the shear distribution compensation factor depending on the cross sectional shape and Poisson ratio ν, and is given for a rectangular cross section as

$$k = \frac{10(1+\nu)}{12 + 11\nu} \qquad (2.3)$$

To eliminate ψ_j from the total potential energy, we first derive the Euler-Lagrange equations and then substitute for ψ_j in terms of w_j. Utilizing the principle of minimum total potential energy, we can derive the equilibrium equations associated with the bending and torsion of the beam. Hence, let us insert the functional

$$F(x,w,w',\psi,\psi',\theta,\theta') = \frac{EI_j}{2}\left(\frac{d\psi_j}{dx}\right)^2 + \frac{kGA_j}{2}\left(\frac{dw_j}{dx} - \psi_j\right)^2 + \frac{GJ_j^*}{2}\left(\frac{d\theta_j}{dx}\right)^2 \quad (2.4)$$

with the three functions w_j, ψ_j, θ_j into the Euler-Lagrange equation

$$\frac{d}{dx}\left(\frac{\partial F}{\partial q_i'}\right) - \frac{\partial F}{\partial q_i} = 0 \qquad q_i = w_j,\psi_j,\theta_j \quad (2.5)$$

Then, evaluation of Eq.(2.5) for the three functions, results in the following equations

$$w: \quad \frac{d}{dx}\left[kGA_j\ (w_j' - \psi_j)\right] = 0 \quad (2.6a)$$

$$\psi: \quad \frac{d}{dx}\left[EI_j\psi_j' + kGA_j\ (w_j' - \psi_j)\right] = 0 \quad (2.6b)$$

$$\theta: \quad \frac{d}{dx}\left[GJ_j^*\theta_j\right] = 0 \quad (2.6c)$$

Considering elements with constant stiffnesses EI_j, GA_j, and GJ_j^*, Eqs.(2.6) yield

$$\frac{d\psi_j}{dx} = \frac{d^2w_j}{dx^2} \tag{2.7}$$

$$\frac{dw_j}{dx} - \psi_j = -\frac{EI_j}{kGA_j}\frac{d^3w_j}{dx^3} \tag{2.8}$$

Substituting Eqs.(2.7) and (2.8) into Eq.(2.2) and using the relation $G=E/2(1+\nu)$, the total elastic potential energy for the element can be written as

$$V_j = \int_{x_{j-1}}^{x_j} \left[\frac{EI_j}{2}\left(\frac{d^2w_j}{dx}\right)^2 + \frac{12+11\nu}{10}\frac{EI_j^2}{A_j}\left(\frac{d^3w_j}{dx^3}\right)^2 + \frac{EJ_j^*}{4(1+\nu)}\left(\frac{d\theta_j}{dx}\right)^2\right]dx \tag{2.9a}$$

where the first, second and third terms of the integrand represent the contribution of bending, shear and torsion to the total potential energy. The potential energy for a cable member element can be written as

$$V_j = \int_{x_{j-1}}^{x_j} \frac{T_c}{2}(w')^2\,dx \tag{2.9b}$$

where T_C is the cable tension [13].

In the cable supported beam lattice structure, gravity field effect plays an integral role in the expression for the total potential energy, and should be added to Eqs.(2.9). For this task we will select a typical element in gravitation field as can be seen in Fig. 2.2.
The potential energy can be regarded as resulting from the axial force acting through the shortening of the element projection on the vertical axis. Denoting a length increment along the displaced axis by ds and the projection by dy, the potential energy can be written in the form

$$V_j = \int_0^L P(y,t)(ds - dy) \tag{2.10}$$

where P(y,t) denotes the axial force due to gravity. Assuming that the shortening of the projection ds-dy is a small quantity of second order in magnitude, and retaining only quadratic terms, using the binomial expansion, the shortening of the projection can be shown to be

$$ds - dy \approx \frac{1}{2} [w'(y,t)]^2 \, dy \tag{2.11}$$

where the assumption of small motion was made. Introducing Eq.(2.11) into Eq.(2.10) and substituting P(y,t) by the actual force acting on the element

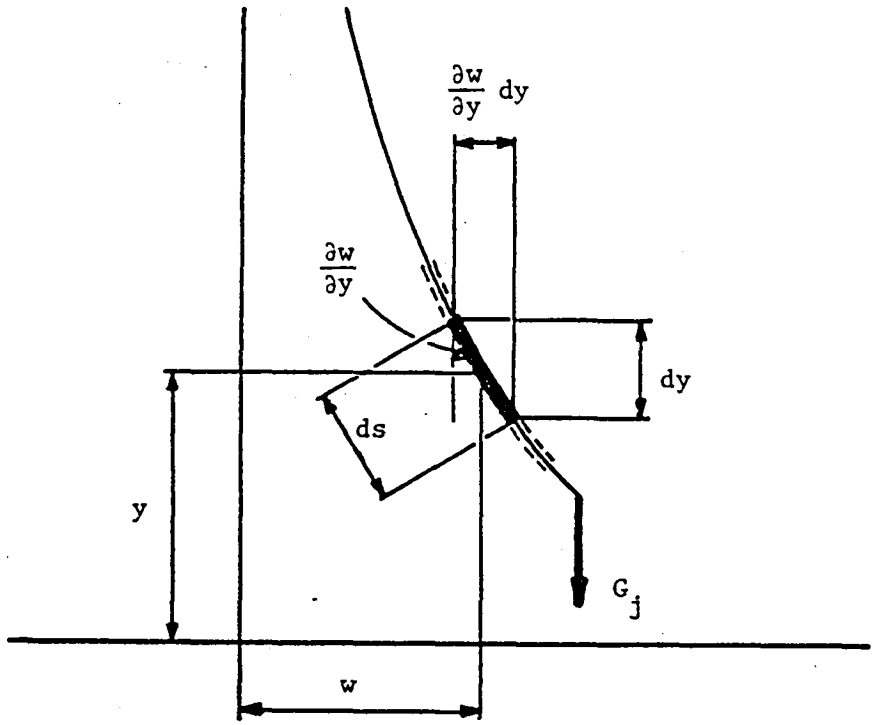

Figure 2.2: A Typical Element in Gravitation Field

$$V_j = \frac{1}{2}\int_{y_{j-1}}^{y_j} (m_j g y_j + G_j)(w_j')^2 dy \tag{2.12a}$$

where m_j is the mass per unit length and G_j is an appropiate force at the bottom end of a typical element due to the weight below. It is clear from the discussion that this type of potential energy applies only to the vertical members of the structure, while horizontal members serve as load contributors only. For this reason we wish to retain both Eqs.(2.9a) and (2.12a) separately, while combining them will be essential only when integration takes place in vertical orientation.

For the cable elements, the potential energy can be written as

$$V_j = \frac{1}{2}\int_{y_{j-1}}^{y_j} (m_{cj} g y_j + G_j)(w_j')^2 dy \tag{2.12b}$$

where m_{cj} is the mass per unit length for the cable material, and G_j is obvious, in view of Eq.(2.12a).

2.1.2 Kinetic Energy

The kinetic energy for a typical element j in a beam member can be expressed as

$$T_j = \int_{x_{j-1}}^{x_j} \left[\frac{m_j}{2} \left(\frac{\partial w_j}{\partial t} \right)^2 + \frac{J_j}{2} \left(\frac{\partial w_j'}{\partial t} \right)^2 + \frac{J_{0j}}{2} \left(\frac{\partial \theta_j}{\partial t} \right)^2 \right] dx, \tag{2.13a}$$

where m_j represents the mass per unit length, J_j is the mass moment of inertia of an element of unit length about the bending axis and J_{0_j} is the polar mass moment of inertia of an element of unit length. Moreover $\partial w_j/\partial t$ is recognized as the translational velocity, $\partial w_j'/\partial t$ as the angular velocity of the element about the bending axis and $\partial \theta_j/\partial t$ as the angular velocity of the element about the torsion axis. Accordingly, the first term of the integrand represents the translational the second the rotational and the third the torsional kinetic energy. The kinetic energy for the rigid blocks, can be written in view of the notations of Fig. 2.1c as

$$T_j = \frac{1}{2} M\dot{w}_j^2 + \frac{1}{2} I_{xG} \dot{\theta}_{xj}^2 + \frac{1}{2} I_{yG} \dot{\theta}_{yj}^2 \tag{2.13b}$$

where M is the mass of the rigid block and I_{xG} and I_{yG} are its mass moment of inertia about its lateral axes x and y,

respectively. For the cable elements, the kinetic energy can be written as

$$T_j = \int_{y_{j-1}}^{y_j} \frac{m_{cj}}{2} (\dot{w}_j)^2 dy \tag{2.13c}$$

2.1.3 Nonconservative Generalized Force

In the derivation of the discretized system equations of motion, we are making use of the virtual work concept in order to obtain the nonconservative generalized force expression

$$\delta W_j = \int_{x_{j-1}}^{x_j} [f_{wj} \quad m_{wj}' \quad m_{\theta j}] \, \delta[w_j \quad w_j' \quad \theta_j]^T \, dx \tag{2.14}$$

where f_{wj}, m_{wj}', and $m_{\theta j}$ are the distributed force and two moment components associated with the displacements w_j, w_j', and θ_j, respectively.

2.1.4 Finite Element Model

See also Meirovich [13], chapter 9.

Referring to Fig. 2.3a we express the displacement components at any point inside the element j in the form

$$w_j(\xi,t) = \underset{\sim}{L}_w^T(\xi)\ \underset{\sim}{w}_j(t) \tag{2.15a}$$

$$\theta_j(\xi,t) = \underset{\sim}{L}_\theta^T(\xi)\ \underset{\sim}{\theta}_j(t) \tag{2.15b}$$

where

$$\underset{\sim}{L}_w(\xi) = [L_{w_1}(\xi)\quad L_{w_2}(\xi)\quad L_{w_3}(\xi)\quad L_{w_4}(\xi)]^T \tag{2.16a}$$

$$\underset{\sim}{L}_\theta(\xi) = [L_{\theta_1}(\xi)\quad L_{\theta_2}(\xi)]^T \tag{2.16b}$$

are vectors of interpolation functions and

$$\underset{\sim}{w}_j(t) = [w_{j-1}(t)\quad hw'_{j-1}(t)\quad w_j(t)\quad hw'_j(t)]^T \tag{2.17a}$$

$$\underset{\sim}{\theta}_j(t) = [\theta_{j-1}(t)\quad \theta_j(t)]^T \tag{2.17b}$$

are vectors of nodal displacements where h is the length of the element. To satisfy compatibility, it is necessary that the interpolation functions vector be continuous up to the

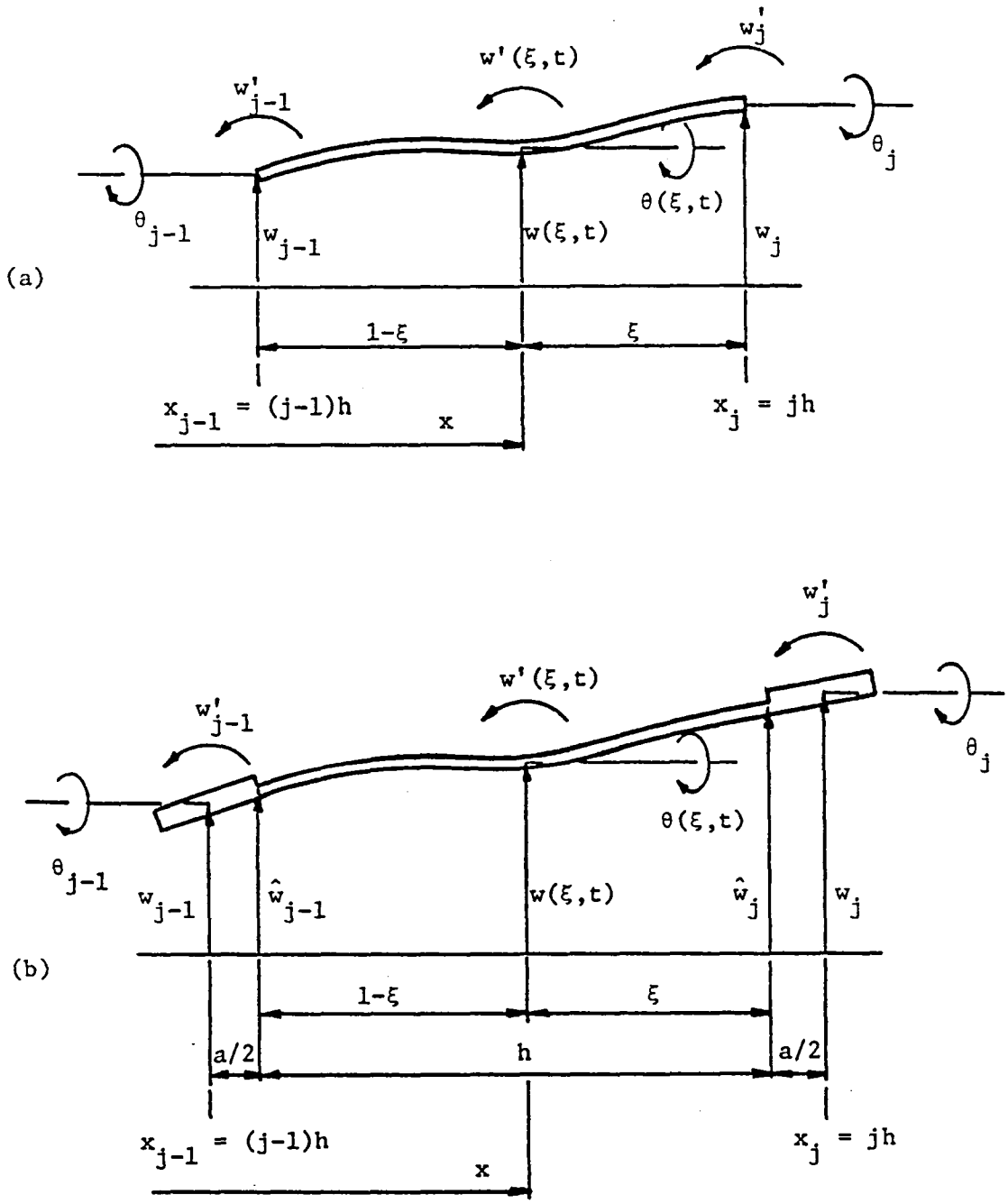

Figure 2.3: Finite Element Models
(a) A Typical Finite Element j
(b) A Typical Member with Rigid Blocks

derivative of one order lower than the highest derivative appearing in the associated differential equation. Most of the element formulations that have been developed are based on polynomial expansions. Therefore, for a beam in bending represented by a fourth order differential equation, cubic polynomials are admissible, while for the torsion part that is represented by a second order differential equation, linear polynomials are admissible. For the discretization process at hand, we select the following interpolation functions

$$L_{w_1}(\xi) = 3\xi^2 - 2\xi^3 \ , \quad L_{w_2}(\xi) = \xi^2 - \xi^3$$

$$L_{w_3}(\xi) = 1 - 3\xi^2 + 2\xi^3 \ , \quad L_{w_4}(\xi) = -\xi + 2\xi^2 - \xi^3 \tag{2.18a}$$

$$L_{\theta_1}(\xi) = \xi \ , \quad L_{\theta_2}(\xi) = 1 - \xi \tag{2.18b}$$

For a member with rigid blocks, the following relations can be derived in view of Fig. 2.3b.

$$w(\xi,t) = \underset{\sim}{L}_w^T(\xi)\ \hat{\underset{\sim}{w}}_j(t) = \underset{\sim}{L}_w^{*T}(\xi)\ \underset{\sim}{w}_j(t) \tag{2.19}$$

$$\hat{w}_{j-1} = w_{j-1} + w'_{j-1}\frac{a}{2} \ , \quad \hat{w}'_{j-1} = w'_{j-1} \tag{2.20a,b}$$

$$\hat{w}_j = w_j - \hat{w}_j\frac{a}{2} \ , \quad \hat{w}'_j = w'_j \tag{2.20c,d}$$

Referring to Eqs.(2.16a) and (2.17a) and substituting Eqs.(2.20) into (2.19), we obtain

$$\hat{\underset{\sim}{w}}_j(t) = C_R \, \underset{\sim}{w}_j(t) \tag{2.21}$$

where C_R is the rigid constraints transformation matrix

$$C_R = \begin{bmatrix} 1 & \frac{a}{2h} & 0 & 0 \\ 0 & 1 & 0 & 0 \\ 0 & 0 & 1 & -\frac{a}{2h} \\ 0 & 0 & 0 & 1 \end{bmatrix} \tag{2.22}$$

Substituting Eq.(2.21) into Eq.(2.19), the modified interpolation function vector $\underset{\sim}{L}^*_w(\xi)$ becomes

$$\underset{\sim}{L}^*_w(\xi) = C_R^T \, \underset{\sim}{L}_w(\xi) \tag{2.23}$$

We will use two reference systems, local and global. For a single element, nodal variables refer to local numbering system, but for an assembly of elements we shall refer to global system. The relation between global and local coordinates x and ξ respectively, can be concluded from Fig. 2.3

$$\xi = \frac{jh - x}{h} \quad , \qquad dx = -h \, d\xi \tag{2.24}$$

The element beam matrices can be obtained in terms of the local coordinate ξ by substituting Eq.(2.24) into (2.9a). The potential energy for a typical element j in the beam lattice has the form

$$V_j = \frac{h}{2}\int_0^1 \left\{ EI_j \frac{1}{h^4}\left[\frac{d^2 w_j(\xi,t)}{d\xi^2}\right]^2 + \frac{12+11\nu}{10}\frac{EI_j^2}{A_j}\frac{1}{h^6}\left[\frac{d^3 w_j(\xi,t)}{d\xi^3}\right]^2 + \frac{EJ_j^*}{4(1+\nu)}\left[\frac{d\theta_j(\xi,t)}{d\xi}\right]^2\right\} d\xi \tag{2.25a}$$

Inserting Eqs.(2.15) into (2.25a), one obtains

$$V_j = \frac{1}{2}\underset{\sim}{w}_j^T(t)\, K_{wj}\, \underset{\sim}{w}_j(t) + \frac{1}{2}\underset{\sim}{\theta}_j^T(t)\, K_{\theta j}\, \underset{\sim}{\theta}_j^T(t) \tag{2.25b}$$

where

$$K_{wj} = \frac{1}{h^3}\int_0^1 EI_j \frac{d^2\underset{\sim}{L}_w(\xi)}{d^2\xi}\cdot\frac{d^2\underset{\sim}{L}_w^T(\xi)}{d\xi^2}\, d\xi + \frac{1}{h^5}\int_0^1 \frac{12+10\nu}{10}\frac{EI_j^2}{A_j}\frac{d^3\underset{\sim}{L}_w(\xi)}{d\xi^3}\frac{d^3\underset{\sim}{L}_w^T(\xi)}{d\xi^3}\, d\xi \tag{2.26a}$$

$$K_{\theta j} = \frac{1}{h}\int_0^1 \frac{EJ_j^*}{4(1+\nu)}\frac{d\underset{\sim}{L}_\theta(\xi)}{d\xi}\frac{d\underset{\sim}{L}_\theta^T(\xi)}{d\xi}\, d\xi \tag{2.26b}$$

are element stiffness matrices associated with the transverse and torsional motions, respectively. Using Eqs.(2.16) and (2.18), the element stiffness matrices become

$$K_{wj} = \frac{EI}{h^3}\begin{bmatrix} 12 & 6 & -12 & 6 \\ & 4 & -6 & 2 \\ & & 12 & -6 \\ \text{symm.} & & & 4 \end{bmatrix} + \frac{12+11\nu}{10}\frac{EI^2}{Ah^5}\begin{bmatrix} 144 & 72 & -144 & 72 \\ & 36 & -72 & 36 \\ & & 144 & -72 \\ \text{symm.} & & & 36 \end{bmatrix} \tag{2.27a}$$

$$K_{\theta j} = \frac{EJ^*}{4(1+\nu)h}\begin{bmatrix} 1 & -1 \\ -1 & 1 \end{bmatrix} \tag{2.27b}$$

where all parameters are assumed to be constant throughout the element. The potential energy for an element j in a cable suspension is obtained by substituting Eq.(2.24) into (2.9b). The result is

$$V_j = \frac{h_c}{2}\int_0^1 T_c \frac{1}{h_c^2}\left[\frac{dw_j(\xi,t)}{d\xi}\right]^2 d\xi \tag{2.28a}$$

Using Eq.(2.15)

$$V_j = \frac{1}{2}\, \underset{\sim}{w}_j^T(t)\, K_{cj}\, \underset{\sim}{w}_j(t) \tag{2.28b}$$

where

$$K_{cj} = \frac{1}{h_c}\int_0^1 T_c \frac{d\underset{\sim}{L}_\theta(\xi)}{d\xi}\frac{d\underset{\sim}{L}_\theta^T(\xi)}{d\xi}\, d\xi \tag{2.29}$$

using the linear interpolation functions Eqs.(2.16b) and (2.18b), the cable element stiffness matrix becomes

$$K_{cj} = \frac{T_c}{h} \begin{bmatrix} 1 & -1 \\ -1 & 1 \end{bmatrix} \tag{2.30}$$

Following this pattern, the additional stiffness matrix due to gravity contribution can be obtained from Eq.(2.12a)

$$V_j = \frac{h}{2} \int_0^1 [m_j g(1-\xi)h + G_j] \left[\frac{dw_j(\xi,t)}{d\xi}\right]^2 d\xi = \frac{1}{2} \underset{\sim}{w}_j^T(t)\ K_{Gj}\ \underset{\sim}{w}_j(t) \tag{2.31}$$

where

$$K_{Gj} = \int_0^1 \left(m_j g + \frac{G_j}{h}\right) \frac{d\underset{\sim}{L}_w(\xi)}{d\xi} \frac{d\underset{\sim}{L}_w^T(\xi)}{d\xi}\, d\xi - \int_0^1 m_j g\xi \frac{d\underset{\sim}{L}_w(\xi)}{d\xi} \frac{d\underset{\sim}{L}_w^T(\xi)}{d\xi}\, d\xi \tag{2.32}$$

Using Eqs.(2.16) and (2.18)

$$K_{Gj} = \frac{1}{30}\left(mg + \frac{G}{h}\right)\begin{bmatrix} 36 & 3 & -36 & 3 \\ & 4 & -3 & -1 \\ & & 36 & -3 \\ \text{symm.} & & & 4 \end{bmatrix} - \frac{mg}{60}\begin{bmatrix} 36 & 0 & -36 & 6 \\ & 6 & 0 & -1 \\ & & 36 & -6 \\ \text{symm.} & & & 2 \end{bmatrix} \tag{2.33}$$

The potential energy due to gravity contribution for element j in the cable suspension, is similar to Eq.(2.28), or

$$V_j = \frac{1}{2}\, \underset{\sim}{w}_j^T(t)\, K_{CGj}\, \underset{\sim}{w}_j(t) \tag{2.34}$$

Since cables in transverse vibration and beam in torsional vibration represent entirely analogous dynamical systems from a mathematical point of view, the same interpolation functions can be used for both cases. Therefore, K_{cGj} in Eq.(2.34) has the form

$$K_{CGj} = \int_0^1 \left(m_{cj}g + \frac{G_j}{h_c}\right) \frac{d\underset{\sim}{L}_\theta(\xi)}{d\xi}\, \frac{d\underset{\sim}{L}_\theta^T(\xi)}{d\xi} - \int_0^1 m_{cj}g\xi\, \frac{d\underset{\sim}{L}_\theta(\xi)}{d\xi}\, \frac{d\underset{\sim}{L}_\theta^T(\xi)}{d\xi}\, d\xi \tag{2.35}$$

Using Eqs.(2.16b) and (2.18b)

$$K_{CGj} = \left(\frac{3}{2}\, m_c g + \frac{G}{h_c}\right)\begin{bmatrix} 1 & -1 \\ -1 & 1 \end{bmatrix} \tag{2.36}$$

A similar pattern is adopted to obtain the element mass matrix, where the assumption of a member consisting of one element is made. Substituting Eq.(2.24) into (2.13a)

$$T_j = \frac{h}{2} \int_0^1 \left\{ m_j [\dot{w}_j(\xi,t)]^2 + J_j \frac{1}{h^2} \left[\frac{d\dot{w}(\xi,t)}{d\xi} \right]^2 + J_{0j} [\dot{\theta}_j(\xi,t)]^2 \right\} d\xi \tag{2.37a}$$

inserting Eqs.(2.19) and (2.23) into Eq.(2.37a), one obtains

$$T_j = \frac{1}{2} \dot{\underset{\sim}{w}}_j^T(t) \; C_R^T \, M_{wj} \; C_R \; \dot{\underset{\sim}{w}}_j(t) + \frac{1}{2} \dot{\theta}_j^T(t) \; M_{\theta j} \; \dot{\theta}_j(t) \tag{2.37b}$$

where

$$M_{wj} = h \int_0^1 m_j \; \underset{\sim}{L}_w(\xi) \; \underset{\sim}{L}_w^T(\xi) \; d\xi + \frac{1}{h} \int_0^1 J_j \; \frac{d\underset{\sim}{L}_w(\xi)}{d\xi} \cdot \frac{d\underset{\sim}{L}_w^T(\xi)}{d\xi} \; d\xi \tag{2.38a}$$

$$M_{\theta j} = h \int_0^1 J_{0j} \; \underset{\sim}{L}_\theta(\xi) \; \underset{\sim}{L}^T(\xi) \; d\xi \tag{2.38b}$$

$C_R^T M_{wj} C_R$ and $M_{\theta j}$ are element mass matrices associated with the transverse and torsional motion. Using Eqs.(2.16) and (2.18), the element mass matrices become

$$C_R^T M_{wj} C_R = C_R^T \left\{ \frac{mh}{420} \begin{bmatrix} 156 & 22 & 54 & -13 \\ & 4 & 13 & -3 \\ & & 156 & -22 \\ \text{symm.} & & & 4 \end{bmatrix} + \frac{J}{30h} \begin{bmatrix} 36 & 3 & -36 & 3 \\ & 4 & -3 & -1 \\ & & 36 & -3 \\ \text{symm.} & & & 4 \end{bmatrix} \right\} C_R \tag{2.39a}$$

$$M_{\theta j} = \frac{J_0 h}{6} \begin{bmatrix} 2 & 1 \\ 1 & 2 \end{bmatrix} \tag{2.39b}$$

where all the parameters were assumed to be constant throughout the element. The kinetic energy for element j in the cable suspension is obtained by substituting Eq.(2.24) into (2.13b), so that

$$T_j = \frac{h_c}{2} \int_0^1 m_{cj} [\dot{w}_j(\xi,t)]^2 \, d\xi \tag{2.40a}$$

Using again the linear interpolation functions Eqs.(2.16b) and (2.18b), we obtain the cable element mass metrix

$$T_j = \frac{1}{2} \dot{\underset{\sim}{w}}_j^T(t) \, M_{cj} \, \dot{\underset{\sim}{w}}_j^T(t) \tag{2.40b}$$

where

$$M_{cj} = \frac{m_c\ h_c}{6} \begin{bmatrix} 2 & 1 \\ 1 & 2 \end{bmatrix} \tag{2.41}$$

The discrete element force vector can be obtained from Eq.(2.14). Using local coordinate ξ

$$\delta W_j = h \int_0^1 \left\{ f_{wj}\ \delta w_j(\xi,t) - m'_{wj}\ \frac{1}{h}\ \delta \left[\frac{dw_j(\xi,t)}{d\xi} \right] + m_{\theta j}\ \delta\theta_j(\xi,t) \right\} \delta\xi \tag{2.42a}$$

Substituting Eqs.(2.15) into (2.42a)

$$\begin{aligned} \delta W_j &= h \int_0^1 f_{wj}\ \underset{\sim}{L}_w^T(\xi)\ C_R\ \delta \underset{\sim}{w}_j(t)\ d\xi - \int_0^1 m'_{wj}\ \frac{d\underset{\sim}{L}_w^T(\xi)}{d\xi}\ C_R\ \delta \underset{\sim}{w}_j(t) d\xi \\ &\quad + h \int_0^1 m_{\theta j}\ \underset{\sim}{L}_\theta^T(\xi)\ C_R\ \delta\theta_j(t)\ d\xi \\ &= \underset{\sim}{F}_{wj}^T\ \delta \underset{\sim}{w}_j(t) + \underset{\sim}{F}_{\theta j}^T\ \delta \underset{\sim}{\theta}_j(t) \end{aligned} \tag{2.42b}$$

where

$$\underset{\sim}{F}_{wj} = h \int_0^1 f_{wj}\ C_R^T\ \underset{\sim}{L}_w(\xi) d\xi - \int_0^1 m'_{wj}\ C_R^T\ \frac{d\underset{\sim}{L}_w(\xi)}{d\xi}\ d\xi \tag{2.43a}$$

$$\underset{\sim}{F}_{\theta j} = h \int_0^1 m_{\theta j}\ \underset{\sim}{L}_\theta(\xi)\ d\xi \tag{2.43b}$$

are the element generalized force vectors.

We will regard the forcing functions as concentrated forces and moments acting at the element nodes. These forces and torques can be represented as distributed forces and torques by writing them in the form $F_i \delta(\xi-\xi_i)$ and $M_j \delta(\xi-\xi_j)$ where $\delta(\xi-\xi_i)$ and $\delta(\xi-\xi_j)$ are spatial delta functions. Substituting these expressions into Eqs.(2.43), we can write

$$\underset{\sim}{F}_{wj} = [h\ F_{j-1} \quad M_{wj-1} \quad h\ F_j \quad M_{wj}]^T \tag{2.44a}$$

$$\underset{\sim}{F}_{\theta j} = [h\ M_{\theta j-1} \quad h\ M_{\theta j}]^T \tag{2.44b}$$

where F_{j-1}, $M_{wj=1}$, $M_{\theta j-1}$ and F_j, M_{wj}, $M_{\theta j}$ are concentrated forces, bending moments and torques at the j-1 and j nodes respectively.

The potential energy, kinetic energy and virtual work for member s are obtained by summing up the contributions of the individual elements, in a process known as "assembling". Two types of members participate in the assembly, beams and cable supports which are regarded as 4th and 2nd order members respectively, according to the degree of their differential equations of motion. With this notation it will prove convenient to introduce a $3(m_4+1)$ and a (m_2+1) dimensional displacement vectors for a 4th and a 2nd order mem-

ber, where m_4 and m_2 are numbers of elements in these type of members, respectively. For a beam-member

$$\underset{\sim}{u}_{s4} = [w_0 \quad hw_0' \quad w_1 \quad hw_1' \quad \ldots \quad w_{m4} \quad hw_{m4}' \quad \theta_0 \quad \theta_1 \quad \ldots \quad \theta_{m4}]^T \tag{2.45a}$$

and for a cable-member

$$\underset{\sim}{u}_{s2} = [w_0 \quad w_1 \quad \ldots \quad w_{m2}]^T \tag{2.45b}$$

The member stiffness matrix can be written in a block diagonal form as follows. Starting with a beam member, we have

$$K_{s4} = \left[\begin{array}{c|c} K_w & 0 \\ \hline 0 & K_\theta \end{array}\right]_{3(m_4+1)} \tag{2.46}$$

where each block can be schematically displayed as follows

$K_w =$ 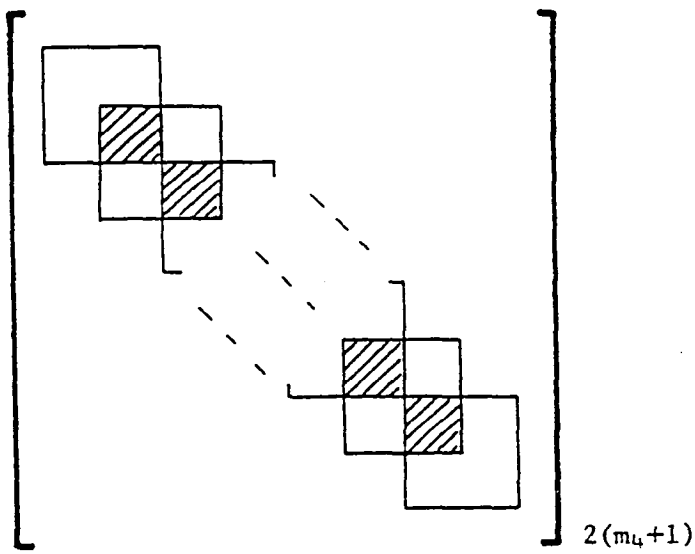 $_{2(m_4+1)}$ (2.47a)

$K_\partial =$ 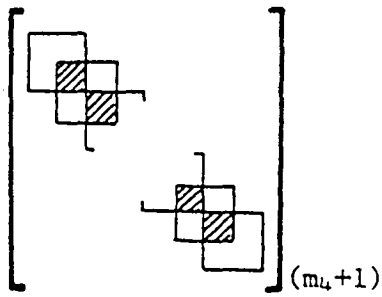 (m_4+1) (2.47b)

in which the shaded blocks indicate summation of the overlaping entries. We notice the distinction between a vertical member and a horizontal member in the beam lattice. The former is affected by gravity, while the latter serves just as a load contributor. Therefore, for a vertical beam member, using Eqs.(2.27) and (2.33), we obtain

$$K_w = \frac{EI}{h^3}\begin{bmatrix} 12 & 6 & -12 & 6 & & & & & & & \\ 6 & 4 & -6 & 2 & & & & & & & \\ -12 & -6 & 24 & 0 & -12 & 6 & & & & & \\ 6 & 2 & 0 & 8 & -6 & 2 & & & 0 & & \\ & & -12 & -6 & 24 & 0 & & & & & \\ & & 6 & 2 & 0 & 8 & & & & & \\ & & & & & & \ddots & & & & \\ & & & & & & & 24 & 0 & -12 & 6 \\ & & & 0 & & & & 0 & 8 & -6 & 2 \\ & & & & & & & -12 & -6 & 12 & -6 \\ & & & & & & & 6 & 2 & -6 & 4 \end{bmatrix} +$$

$$+\frac{12+11\nu}{10}\frac{EI^2}{Ah^5}\begin{bmatrix} 144 & 72 & -144 & 72 & & & & & & \\ 72 & 36 & -72 & 36 & & & & & & \\ -144 & -72 & 288 & 0 & -144 & 72 & & & 0 & \\ 72 & 36 & 0 & 72 & -72 & 36 & & & & \\ & & -144 & -72 & 288 & 0 & & & & \\ & & 72 & 36 & 0 & 72 & & & & \\ & & & & & & \ddots & & & \\ & & & & & & 288 & 0 & -144 & 72 \\ & & & 0 & & & 0 & 72 & -72 & 36 \\ & & & & & & -144 & -72 & 144 & -72 \\ & & & & & & 72 & 36 & -72 & 36 \end{bmatrix} +$$

$$+\frac{1}{30}\left(mg+\frac{G}{h}\right)\begin{bmatrix} 36 & 3 & -36 & 3 & & & & & & \\ 3 & 4 & -3 & -1 & & & & & & \\ -36 & -3 & 72 & 0 & -36 & 3 & & & 0 & \\ 3 & -1 & 0 & 8 & -3 & -1 & & & & \\ & & -36 & -3 & 72 & 0 & & & & \\ & & 3 & -1 & 0 & 8 & & & & \\ & & & & & & \ddots & & & \\ & & & & & & 72 & 0 & -36 & 3 \\ & & & 0 & & & 0 & 8 & -3 & -1 \\ & & & & & & -36 & -3 & 36 & -3 \\ & & & & & & 3 & -1 & -3 & 4 \end{bmatrix} +$$

$$
-\frac{mg}{60}\begin{bmatrix}
36 & 0 & -36 & 6 & & & & & & & \\
0 & 6 & 0 & -1 & & & & & & & \\
-36 & 0 & 72 & -6 & -36 & 6 & & & & & \\
6 & -1 & -6 & 8 & 0 & -1 & & & 0 & & \\
 & & -36 & 0 & 72 & -6 & & & & & \\
 & & 6 & -1 & -6 & 8 & & & & & \\
 & & & & & & \ddots & & & & \\
 & & & & & & & 72 & -6 & -36 & 6 \\
 & & & 0 & & & & -6 & 8 & 0 & -1 \\
 & & & & & & & -36 & 0 & 36 & -6 \\
 & & & & & & & 6 & -1 & -6 & 2
\end{bmatrix} \tag{2.48a}
$$

$$
K_\theta = \frac{EJ^*}{4(1+\nu)h}\begin{bmatrix}
1 & -1 & & & & \\
-1 & 2 & -1 & & 0 & \\
 & -1 & 2 & & & \\
 & & & \ddots & & \\
 & & & & 2 & -1 \\
 & 0 & & & -1 & 1
\end{bmatrix} \tag{2.48b}
$$

Here, we should note that for a horizontal beam-member, only the first two matrices in Eq.(2.48a) are to be included. Finally, for a cable-member, the stiffness matrix can be obtained using Eqs.(2.30) and (2.36), with the result

$$K_{s_2} = \left(\frac{3}{2} m_c g + \frac{T_c + G}{h}\right) \begin{bmatrix} 1 & -1 & & & & \\ -1 & 2 & -1 & & 0 & \\ & -1 & 2 & & & \\ & & & \ddots & & \\ & & & & 2 & -1 \\ & 0 & & & -1 & 1 \end{bmatrix} \tag{2.49}$$

A similar pattern can be hold to obtain the mass matrices for a beam-member as well as for a cable-member.

For the member force vector, we can write

$$\underset{\sim}{F}_{s_4} = [\underset{\sim}{F}_w^T \quad \underset{\sim}{F}_\theta^T]^T_{3(m_4+1)} \tag{2.50}$$

where $\underset{\sim}{F}_w$ and $\underset{\sim}{F}_\theta$ are $2(m_4+1)$ and (m_4+1) vectors respectively, obtained from Eqs.(2.44) in a manner similar to the member stiffness and mass matrices.

Making use of the above matrices and vectors, the members equations of motion can be written in the matrix form

$$M_{s_4} \ddot{\underset{\sim}{u}}_{s_4} + K_{s_4} \underset{\sim}{u}_{s_4} = \underset{\sim}{F}_{s_4} \qquad s_4 = 1,2,\ldots,M_4 \tag{2.51a}$$

$$M_{s_2} \ddot{\underset{\sim}{u}}_{s_2} + K_{s_2} \underset{\sim}{u}_{s_2} = \underset{\sim}{0} \qquad s_2 = 1,2,\ldots,M_2 \tag{2.51b}$$

for a 4th and 2nd order members respectively. M_4 and M_2 represent the number of 4th and 2nd order members in the structure. It will prove convenient to consider the total dimension of the beam lattice according to the number of beam members along each side. Let n_a and n_b represent these numbers along the lattice sides a and b respectively, and n_c, the number of cable members in each cable branch,

$$M_4 = n_a(n_b+1) + n_b(n_a+1) \tag{2.52a}$$

$$M_2 = 2n_c \tag{2.52b}$$

Equations (2.51) represent a set of $M=M_4+M_2$ disjoint equations for the independent members in the entire structure. For the assemblage of discrete members, the boundary displacements must match. The displacements at the nodes shared by several members must be the same for every such member and corresponding forces should be statically equivalent to the applied forces. Note that displacements include rotations and forces include torques. At this point let us introduce the $N_d=3M_4(m_4+1)+M_2(m_2+1)$ dimensional disjoint displacement and force vectors

$$\underset{\sim}{u}_d = [\underset{\sim}{u}_{41}^T \quad \underset{\sim}{u}_{42}^T \quad \cdots \quad \underset{\sim}{u}_{4M_4}^T \quad \underset{\sim}{u}_{21}^T \quad \underset{\sim}{u}_{22}^T \quad \cdots \quad \underset{\sim}{u}^T{}_{2M_2}]^T \tag{2.53a}$$

$$\underset{\sim}{F}_d = [\underset{\sim}{F}_{41}^T \quad \underset{\sim}{F}_{42}^T \quad \cdots \quad \underset{\sim}{F}_{4M_4}^T \quad \underset{\sim}{0}_{21}^T \quad \underset{\sim}{0}_{22}^T \quad \cdots \quad \underset{\sim}{0}_{2M_2}^T]^T \tag{2.53b}$$

as well as the disjoint mass and stiffness matrices

$$M_d = \left[\begin{array}{c|c} b \text{ diag } M_{s_4} & 0 \\ \hline 0 & b \text{ diag } M_{s_2} \end{array}\right] , \quad K_d = \left[\begin{array}{c|c} b \text{ diag } K_{s_4} & 0 \\ \hline 0 & b \text{ diag } K_{s_2} \end{array}\right]$$

$$s_4 = 1,2,\ldots,M_4 \qquad\qquad s_2 = 1,2,\ldots,M_2 \qquad (2.54a,b)$$

With these expressions, the equations of motion for the disjoint structure, have the reduced matrix form

$$M_d \ddot{\underset{\sim}{u}}_d + K_d \underset{\sim}{u}_d = \underset{\sim}{F}_d \qquad (2.55)$$

It is clear that the disjoint vector $\underset{\sim}{u}_d$ contains local coordinates some of which are redundant for the description of the assembled structure. It will prove convenient to introduce a new displacement vector $\underset{\sim}{q}$ representing the nodal displacements of the complete structure in terms of components along the global system coordinates. The total number of nodes in the entire structure can be determined in terms of n_a, n_b, n_c, and m_4, m_2, M_4, M_2

$$N_4 = (n_a+1)(n_b+1) + M_4(m_4-1) \quad , \quad N_2 = 2n_c - 2 + M_2(m_2-1) \qquad (2.56a,b)$$

In view of this number, the order of the independent global coordinates vector $\underset{\sim}{q}$ is

$$N_q = 3[(n_a+1)(n_b+1) + M_4(m_4-1) + [2n_c - 2 - M_2(m_2-1)] \qquad (2.57)$$

The relation between the vectors $\underset{\sim}{u}_d$ and $\underset{\sim}{q}$ can be written in a matrix form as

$$\underset{\sim}{u}_d(t) = C\ \underset{\sim}{q}(t) \tag{2.58}$$

C is a $N_d x N_q$ rectangular matrix reflecting the constraints expressions, relating the disjoint structure in the local coordinate set to the assembled continuous structure in the global coordinate set. Introducing Eq.(2.58) into Eq.(2.55) and premultiplying by C^T, the structure equations of motion will take the matrix form

$$M\ddot{\underset{\sim}{q}}(t) + K\ \underset{\sim}{q}(t) = \underset{\sim}{Q}(t) \tag{2.59}$$

where

$$M = C^T M_d C \quad , \quad K = C^T K_d C \quad , \quad \underset{\sim}{Q} = C^T \underset{\sim}{F}_d \tag{2.60a,b,c}$$

and

$$\underset{\sim}{q} = [w_1\ \theta_{x_1}\ \theta_{y_1}\ w_2\ \theta_{x_2}\ \theta_{y_2}\ \cdots\ w_{N_4}\ \theta_{xN_4}\ \theta_{yN_4}\ w_{N_4+1}\ w_{N_4+2}\ \cdots\ w_{N_4+N_2}]^T \tag{2.61}$$

$\underset{\sim}{q}$ is the nodal displacement vector and $\underset{\sim}{Q}$ represents the vector of nodal control forces. The elements in the nodal displacement vector, w_i, θ_{xi}, θ_{yi} are the nodal global coordinates, i.e., lateral displacement and two rotations respectively, in the ith node. To add the rigid blocks con-

tribution to the kinetic energy, we can associate the velocity components of Eq.(2.13b) $\dot{w}_j$, $\dot{\theta}_{xj}$, $\dot{\theta}_{yj}$, with the appropriate nodal velocities $\dot{q}_i$, $\dot{q}_{i+1}$, $\dot{q}_{i+2}$, respectively, and simply add the mass and two moments of inertia of these blocks to the related entries in the main diagonal of the system mass matrix.

2.2 THE EIGENVALUE PROBLEM AND MODAL SPACE DECOMPOSITION

The object is to reduce the transverse motion of the structure to zero. This can be done most effectively by active control techniques. Customarily, controls are designed by working with the state equations of motion. In the state-space framework, methods have been developed for state and output feedback problems which have been proved to be computationally attractive. It turns out that for a discretized structure, as described by Eq.(2.59), a configuration space approach is simpler and more useful.

To achieve the control task, the IMSC method is employed. As a first step, it is necessary to solve the eigenvalue problem associated with Eq.(2.59), where the latter can be written as

$$\omega_r^2 \, M \, \underset{\sim}{q}_r = K \, \underset{\sim}{q}_r \qquad r = 1,2,\ldots,Nq \qquad (2.62)$$

M and K are real symmetric and positive definite matrices, so that all the eigenvalues ω_r^2 are real and positive, where the ω_r's represent the natural frequencies of the system and $\underset{\sim}{q}_r$ are the associated orthogonal set of eigenvectors. The eigenvectors can be normalized by setting

$$\underset{\sim}{q}_r^T M \underset{\sim}{q}_r = \delta_{rs} \quad , \quad \underset{\sim}{q}_r^T K \underset{\sim}{q}_r = \omega_r^2 \delta_{rs} \qquad r,s = 1,2,\ldots,Nq \quad (2.63a,b)$$

where δ_{rs} is the Kronecker delta. Arranging the eigenvectors in a $N_q x N_q$ modal matrix

$$U = [\underset{\sim}{q}_1 \quad \underset{\sim}{q}_2 \quad \cdots \quad \underset{\sim}{q}_{Nq}] \qquad (2.64)$$

Eqs.(2.63) can be rewritten in the compact matrix form

$$U^T M U = I \quad , \quad U^T K U = \Lambda \qquad (2.65)$$

where I is the identity matrix of order N_q and Λ is the diagonal matrix of eigenvalues.

Using the expansion theorem [24], the response of the system at any time can be expressed as a linear combination of the eigenvectors. Defining $\underset{\sim}{\xi}(t)$ as a N_q dimensional modal space vector, we introduce the linear transformation

$$\underset{\sim}{q}(t) = U\underset{\sim}{\xi}(t) \qquad (2.66)$$

Substituting Eq.(2.66) into Eq.(2.59), premultiplying by U^T and using Eq.(2.65), we obtain the modal equation

$$\ddot{\underset{\sim}{\xi}}(t) + \Lambda\, \underset{\sim}{\xi}(t) = \underset{\sim}{N}(t) \tag{2.67}$$

where

$$\underset{\sim}{N}(t) = U^T \underset{\sim}{Q}(t) \tag{2.68}$$

is the N_q - vector of generalized control forces associated with the modal vector $\underset{\sim}{\xi}(t)$. Eq.(2.67) represents a set of N_q modal equations

$$\ddot{\xi}_r(t) + \omega_r^2\, \xi_r(t) = N_r(t) \qquad r = 1,2,\ldots,Nq \tag{2.69}$$

Although Eqs.(2.69) appear as a decoupled set, modal coordinate recoupling occurs in general through the control forces, as can be recognized from Eq.(2.68). To achieve a complete decoupled form, each modal control force N_r must depend on the rth mode only, which is the essence of the IMSC method.

2.3 CONTROL OF THE DOMINANT MODES

The fundamental problem of active control of a flexible system, is to control a large-dimensional system with a much smaller-order controller. Although a large number of elastic modes may be needed to model the behavior of a large flexible structure, active control of all of these modes is out of question due to computation limitations and errors in the higher modes because of the discretization process. Clearly, the controls must be restricted to the most significant modes, which are the lower modes.

The justification for controlling lower modes only lies in the fact that higher frequency modes are very difficult to excite. Furthermore, the bandwidths of actuators and sensors cannnot respond to the higher frequency modes. Hence, although Eqs.(2.69) permit independent control of all the discretized system modes, we will concentrate in controlling only a number of dominant modes. This number can be determined by examining the modes participation in the response. To accomplish this, the eigensolution will be rearranged according to the increasing order of the eigenvalues and only the first c of Eqs.(2.69) will be retained for the control task.

Perhaps this is the point to emphasize the unique advantage of the Independent Modal Space Control method. After the system equations have been transformed to the modal space, the control laws will be designed in the modal space, permitting independent control of each individual mode. This approach allows a complete flexibility as to which mode to control. For control implementation, the actual control forces are synthesized from the modal control forces by a linear transformation, as we shall see latter in this section. It appears that this approach is simpler to implement, especially for high-order system such as those arising from modeling complex distributed-parameter systems. Let us assume that only a subset of the modeled modes will be controlled and use the subscripts C and R to denote the controlled and residual (uncontrolled) modes, respectively. Then, introducing the partitioned forms

$$\underset{\sim}{\xi}(t) = \left\{ \begin{array}{c} \underset{\sim}{\xi}_c \\ \hline \underset{\sim}{\xi}_R \end{array} \right\} , \quad \Lambda = \left[\begin{array}{c|c} \Lambda_c & 0 \\ \hline 0 & \Lambda_R \end{array} \right] , \quad \underset{\sim}{N} = \left\{ \begin{array}{c} \underset{\sim}{N}_c \\ \hline \underset{\sim}{N}_R \end{array} \right\} , \quad U = [U_c \mid U_R] \tag{2.70a,b,c,d}$$

Equation (2.67) can be separated into the two equations

$$\ddot{\underset{\sim}{\xi}}_c + \Lambda_c \underset{\sim}{\xi}_c = \underset{\sim}{N}_c \tag{2.71a}$$

$$\ddot{\underset{\sim}{\xi}}_R + \Lambda_R \underset{\sim}{\xi}_R = \underset{\sim}{N}_R \tag{2.71b}$$

where

$$\underset{\sim}{N}_c = U_c^T \underset{\sim}{Q} \quad , \quad \underset{\sim}{N}_R = U_R^T \underset{\sim}{Q} \tag{2.72a,b}$$

are the partitioned parts of the control vector.
Substitution of Eq.(2.70a) into Eq.(2.66), yields the configuration space displacement vector

$$\underset{\sim}{q}(t) = U_c \underset{\sim}{\xi}_c(t) + U_R \underset{\sim}{\xi}_R(t) \tag{2.73}$$

Assuming that the contribution of the uncontrolled modal vector $\underset{\sim}{\xi}_R(t)$ to the actual response is negligible, we can truncate Eq.(2.73) by ignoring $U_R \underset{\sim}{\xi}_R(t)$.

For control implementation, thruster and torquer actuators will be placed at some nodes, the number of which equals to the number of controlled modes. The control forces are first designed as generalized forces in the modal space, and then synthesized to form the actual actuator forces.
The discrete forcing vector $\underset{\sim}{Q}(t)$ in Eq.(2.59) will be generated by using c discrete actuators

$$\underset{\sim}{Q}(t) = B \underset{\sim}{F}(t) \tag{2.74}$$

where $\underset{\sim}{F}(t)$ is a c-dimensional vector of thrusters and torquers, while B is a full rank $N_q$xc modal participation ma-

trix. Substituting Eq.(2.74) into Eq.(2.72a), the expression for the actual actuators forces is

$$\underset{\sim}{F}(t) = (U_c^T B)^{-1} \underset{\sim}{N}_c(t) \tag{2.75}$$

where the actuators are placed so that $(U_C^T B)$ is a nonsingular matrix.

Substituting Eqs.(2.74) and (2.75) into Eq.(2.72b), the residual modal force vector is obtained as

$$\underset{\sim}{N}_R(t) = U_R^T B(U_c^T B)^{-1} \underset{\sim}{N}_c(t) \tag{2.76}$$

We can summarize now the modal equations of the controlled and uncontrolled modes as follows:

$$\ddot{\underset{\sim}{\xi}}_c(t) + \Lambda_c \underset{\sim}{\xi}_c(t) = \underset{\sim}{N}_c(t) \tag{2.77a}$$

$$\ddot{\underset{\sim}{\xi}}_R(t) + \Lambda_R \underset{\sim}{\xi}_R(t) = U_R^T B(U_c^T B)^{-1} \underset{\sim}{N}_c(t) \tag{2.77b}$$

Equations (2.77) illustrate clearly that the c entries of the modal vector $\underset{\sim}{\xi}_c(t)$ can be controlled independently, while the R entries of the residual part of the modal vector $\underset{\sim}{\xi}_R(t)$ are excited by the spillover of the control forces into the uncontrolled modes.

Chapter III

LINEAR OPTIMAL CONTROL WITH QUADRATIC PERFORMANCE INDEX

An optimal control system is defined as one in which a certain performance index is minimized. Selecting the proper performance index for a complex control system is in general a difficult task. As stated in the previous chapter, independent control of the modes is achieved if the control force associated with each modal coordinate, depends only on this coordinate. This guarantees complete decoupling of the modes. In view of this approach, we can determine a performance criterion for each mode independently. Because every modal coordinate is controlled independently of any other modal coordinate, the overall system cost will then be the sum of all modal costs

$$J_c = \sum_{r=1}^{c} J_r \tag{3.1}$$

Evidently J_c is a minimum if every J_r in the summation is a minimum, because minimization of each term can be carried out independently. At this point we abandon the configuration space expression from chapter II and replace the second-order modal equations Eqs.(2.71a) by first-order modal state equations.

Let us consider the modal state variables

$$x_{1r}(t) = \xi_r(t) \quad , \quad x_{2r}(t) = \dot{\xi}_r(t) \qquad r = 1,2,\ldots,c \tag{3.2a,b}$$

In view of this state definition the modal Eq.(2.71a) can be written as pairs of first-order differential equations

$$\dot{\underset{\sim}{x}}_r(t) = A_r \, \underset{\sim}{x}_r(t) + \underset{\sim}{B}_r \, N_{cr}(t) \qquad r = 1,2,\ldots,c \tag{3.3}$$

where

$$\underset{\sim}{x}_r(t) = [x_{1r}(t) \quad x_{2r}(t)]^T \quad , \quad A_r = \begin{bmatrix} 0 & 1 \\ -\omega_r^2 & 0 \end{bmatrix} \quad , \quad \underset{\sim}{B}_r = [0 \quad 1]^T \tag{3.4a,b,c}$$

This type of state definition is different from the one used in the IMSC method [26]. In Ref. 26, the modal velocity is eigenvalue-dependent such that the modal matrix A_r is skew symmetric in ω_r and vanishes from the modal equations for possible rigid body modes. To handle the entire system in presence of rigid body modes, dual-level control scheme was introduced, in which the first level is a proportional control providing control to the rigid body modes. This control provides "artificial" stiffness rendering the stiffness matrix positive definite. Second level controls are then designed to provide final control to the complete system. The state defined by Eqs.(3.2) permits one control policy for the entire system, including control of the rigid-body modes.

In view of the state Eqs.(3.3), we consider the following performance indices

$$J_r = \int_0^{t_f} (\underset{\sim}{x}_r^T Q_r \underset{\sim}{x}_r + R_r N_r^2) \, dt \qquad r = 1,2,\ldots,c \tag{3.5}$$

where t_f is the final time, Q_r are 2x2 weighting matrices and R_r are weighting factors. For the rigid body modes, Q_r are chosen independently of the eigenvalues, or

$$Q_r = \begin{bmatrix} Q_{11r} & 0 \\ 0 & Q_{22r} \end{bmatrix} \qquad r = 1,2,\ldots,n_r \tag{3.6}$$

For the elastic modes, Q_r are chosen as

$$Q_r = \begin{bmatrix} \omega_r^2 & 0 \\ 0 & 1 \end{bmatrix} \qquad r = n_r+1,n_r+2,\ldots,c \tag{3.7}$$

In view of Eq.(3.7) the first term of the integrand in Eq.(3.5) represents the total energy associates with the controlled elastic modes. R_r is the modal control effort expenditure during the interval $(0,t_f)$. Increasing R_r, places a havier penalty on the control effort.

The minimization of the modal cost J_r leads to the optimal controls [16,17]

$$N_r(t) = - R_r^{-1} B_r^T K_r \underset{\sim}{x}_r(t) \qquad r = 1,2,\ldots,c \tag{3.8}$$

where $K_r(t)$ is the 2x2 symmetric matrix satisfying the modal differential matrix Riccati equation

$$\dot{K}_r = - Q_r + K_r B_r R_r^{-1} B_r^T K_r - K_r A_r - A_r^T K_r \qquad (3.9)$$

$$r = 1,2,\ldots,c$$

The steady-state solution is of great interest and will be obtained by setting $\dot{K}_r=0$ in Eqs.(3.9). This yields the algebraic matrix Riccati equation. With the notation

$$K_r = \begin{bmatrix} K_{11r} & K_{12r} \\ K_{21r} & K_{22r} \end{bmatrix} \qquad r = 1,2,\ldots,c \qquad (3.10)$$

the solution to the gain coefficients K_{11r}, K_{12r}, K_{22r} can be shown to be

$$K_{11r} = \left[(Q_{22r} - 2R_r\,\omega_r^2)(Q_{11r} + R_r\,\omega_r^4) + 2R_r^{-1}\,(R_r\omega_r^4+R_rQ_{11r})^{\frac{3}{2}}\right]^{\frac{1}{2}} \qquad (3.11a)$$

$$K_{22r} = \left[R_r\,Q_{22r} - 2R_r^2\,\omega_r^2 + 2R_r(R_r^2\,\omega_r^4 + R_r\,Q_{11r})^{\frac{1}{2}}\right]^{\frac{1}{2}} \qquad (3.11b)$$

$$K_{12r} = - R_r\,\omega_r^2 + (R_r^2\,\omega_r^4 + R_r\,Q_{11r})^{\frac{1}{2}} \qquad (3.11c)$$

$$r = 1,2,\ldots,c$$

where Q_{11r}, Q_{22r} are general coefficients of the diagonal weighting matrix Q_r. Substituting Eqs.(3.11) into Eqs.(3.8) and using Eqs.(3.2), the optimal modal controls are obtained in the form

$$N_r(t) = -\frac{K_{12r}}{R_r}\,\xi_r(t) - \frac{K_{22r}}{R_r}\,\dot{\xi}_r(t) \qquad r = 1,2,\ldots,c \tag{3.12}$$

Insertion of Eqs.(3.12) into Eqs.(2.71a) results in the second-order differential equations

$$\ddot{\xi}_r(t) + \frac{K_{22r}}{R_r}\,\dot{\xi}_r(t) + \left(\omega_r^2 + \frac{K_{12r}}{R_r}\right)\xi_r(t) = 0 \qquad r = 1,2,\ldots,c \tag{3.13}$$

The general solution to Eqs.(3.13) is known to be

$$\xi_r(t) = \frac{\xi_r(0)}{(1-\zeta_r^2)^{\frac{1}{2}}}\,e^{-\zeta_r\,\omega_{nr}t}\cos(\omega_{dr}\,t - \psi_r) + \frac{\dot{\xi}_r(0)}{\omega_{dr}}\,e^{-\zeta_r\,\omega_{nr}t}\sin(\omega_{dr}t)$$

$$r = 1,2,\ldots,c \tag{3.14}$$

where

$$\omega_{nr}^2 = \omega_r^2 + \frac{K_{12r}}{R_r} \tag{3.15a}$$

$$\zeta_r = \frac{K_{22r}}{2(R_r^2\,\omega_r^2 + R_r\,K_{12r})^{\frac{1}{2}}} \tag{3.15b}$$

$$\omega_{dr} = \omega_{nr}\,(1-\zeta_r^2)^{\frac{1}{2}} \tag{3.15c}$$

$$\psi_r = \arctan \frac{\zeta_r}{(1 - \zeta_r^2)^{\frac{1}{2}}} \qquad r = 1,2,\ldots,c \quad (3.15d)$$

Eqs.(3.14) imply that $1-\zeta_r^2>0$, which places a lower bound on the control factors R_r. Using Eqs.(3.11b,c) and (3.15b), we obtain

$$R_r > \frac{Q_{22r}^2}{4(Q_{11r} + Q_{22r}\,\omega_r^2)} \qquad r = 1,2,\ldots,c \qquad (3.16)$$

From Eq.(3.16), in view of Eq.(3.6) and (3.7)

$$R_r > \frac{Q_{22r}^2}{4Q_{11r}} \qquad r = 1,2,\ldots,n_r \qquad (3.17a)$$

for a rigid body mode and

$$R_r > \frac{1}{8\omega_r^2} \qquad r = n_r+1,n_r+2,\ldots,c \quad (3.17b)$$

for an elastic mode.

Substituting Eqs.(3.11b,c) into Eq.(3.15b), and setting $Q_{11r}=\omega_r^2$ and $Q_{22r}=1$, we obtain

$$\zeta_r = \frac{1}{2}\left[\frac{1 - 2p + 2p^{\frac{1}{2}}\,(1 + p)^{\frac{1}{2}}}{p^{\frac{1}{2}}\,(1 + p)^{\frac{1}{2}}}\right]^{\frac{1}{2}} \qquad r = 1,2,\ldots,c \qquad (3.18)$$

where p is a dummy variable

$$p = R_r \, \omega_r^2 \qquad r = 1,2,\ldots,c \qquad (3.19)$$

Figure 3.1 provides a plot of the modal damping factor ζ_r vs p. Using this plot and in conjunction with Eq.(3.19), one can select the desired control weighting factors R_r (r=1,2,...,c) to meet certain modal response performance criteria, such as settling time, etc. A numerical example for linear optimal control of the beam lattice is presented in Ch. VI.

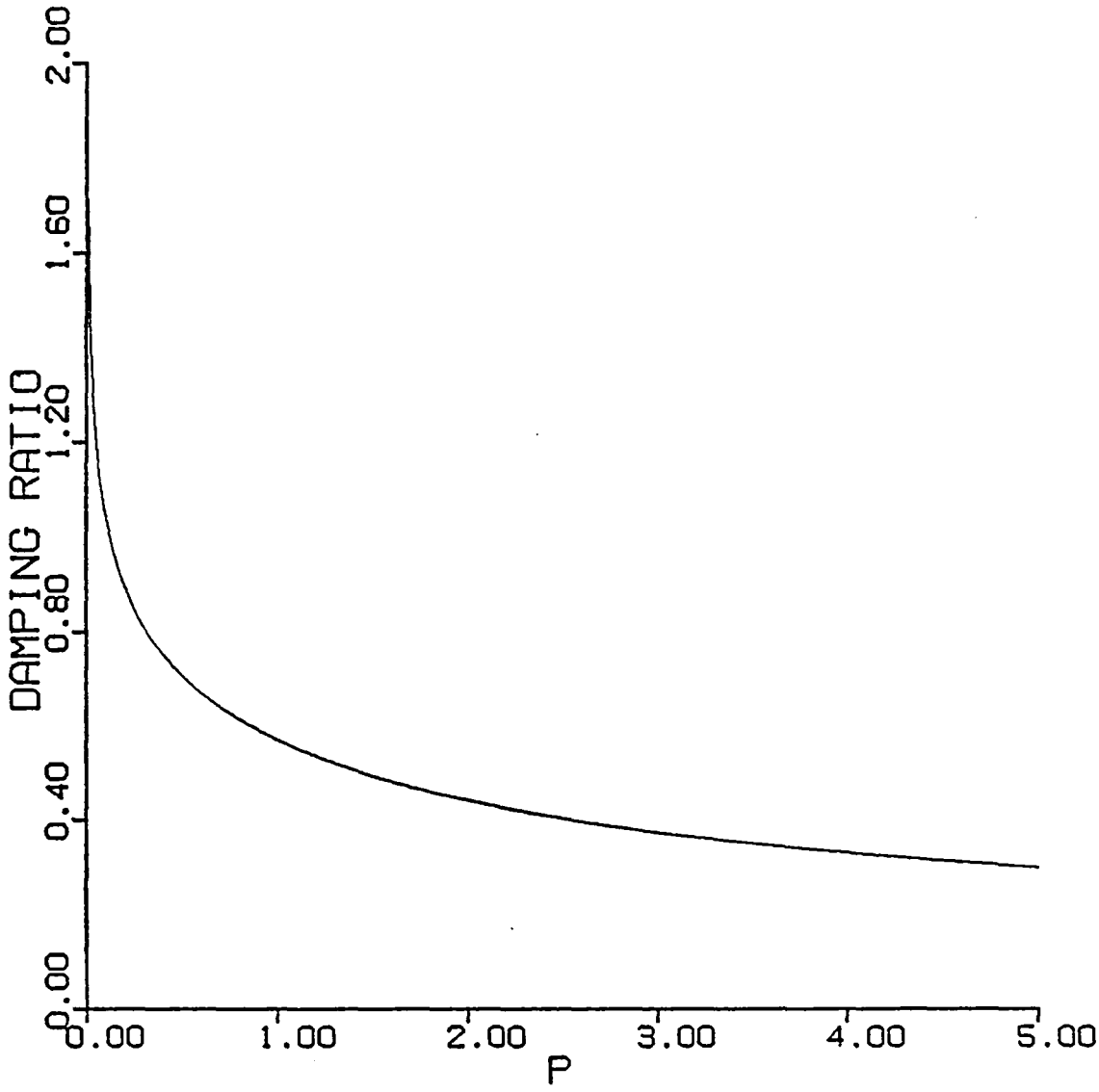

Figure 3.1: Modal Damping Ratio ζ vs p

Chapter IV

THE EFFECT OF ACTUATORS PLACEMENT ON THE MODE PARTICIPATION MATRIX

Most actuators placement concepts discussed so far in conjunction with the IMSC method [14,15] are directed toward minimizing the energy that goes into the uncontrolled modes. These concepts provide guidelines for achieving this goal. However, there are some other constraints that must be satisfied in conjunction with the minimal solution.

It has been shown that the work done to control the controlled modes does not depend on the actuator locations. Of course, this statement holds true if the mode participation matrix is <u>nonsingular</u>. This is the case for a one-dimensional domain if IMSC is used. This cannot be taken for granted in the case of two-dimensional domains, so that care must be exercised in choosing the location of the actuators. In view of this, it is clear that, before discussing minimization aspects, one must place the actuators so that the mode participation matrix is nonsingular.

In this chapter we establish a sufficient condition for the mode participation matrix $U_C^T B$ that asserts its singular-

ity, where U_C^T is the cxn upper part of the modal matrix and B is a full rank nxc actuators placement matrix, in which n is the order of the system and c is the number of controlled modes. The analysis provides a method of recognizing undesirable actuators placement configurations.

We start by examining the structure of the modal matrix U. The nxn modal matrix has the modal vectors as its columns. Furthermore, the modes are arranged in increasing order of magnitude of the associated eigenvalues. We confine our discussion to a structure of the type shown in Fig. 4.1. Because the system possesses symmetric mass and stiffness properties, in addition to symmetrical boundary conditions, the solution of the eigenvalue problem consists of eigenvectors of two types, namely, symmetric and antisymmetric with respect to the center lines of the system. These center lines are chosen to coincide with the reference axes x and y, as shown in Fig. 4.1. It will prove convenient to work with a triple index notation (i,j,k) where the first two indices i and j represent nodal coordinates, as shown in Fig. 4.1 and the third index k represents the actuator type applied at the particular node. Moreover, k=1 represents a force vector or translation in the z direction, perpendicular to the lattice plane, k=2 and k=3 represent

torque vectors or rotations in the x and y directions respectively.

We recall that n_a and n_b represent the numbers of beam members along the sides of the lattice and that n_c is the number of cable members in each cable branch. With no loss of generality, we consider one element per member so that the order of the system in Eq.(2.57) is $n=3(n_a+1)(n_b+1)$.

The modal matrix can be written as

$$U=(\underset{\sim}{u}_1 \ \underset{\sim}{u}_2 \ \ldots \underset{\sim}{u}_c \ \ldots \underset{\sim}{u}_n) \tag{4.1}$$

where

$$\underset{\sim}{u}_\ell = \begin{Bmatrix} u_\ell\left(-\frac{n_a}{2}, -\frac{n_b}{2}, 1\right) \\ u_\ell\left(-\frac{n_a}{2}, -\frac{n_b}{2}, 2\right) \\ u_\ell\left(-\frac{n_a}{2}, -\frac{n_b}{2}, 3\right) \\ u_\ell\left(-\frac{n_a}{2}+1, -\frac{n_b}{2}, 1\right) \\ \vdots \\ u_\ell\,(i,j,k) \\ \vdots \\ u_\ell\left(\frac{n_a}{2}, \frac{n_b}{2}, 3\right) \end{Bmatrix} \quad \begin{array}{l} \ell \in \{1,2,\ldots,n\} \\ i \in \left\{-\frac{n_a}{2}, -\frac{n_a}{2}+1, \ldots, \frac{n_a}{2}-1, \frac{n_a}{2}\right\} \\ j \in \left\{-\frac{n_b}{2}, -\frac{n_b}{2}+1, \ldots, \frac{n_b}{2}-1, \frac{n_b}{2}\right\} \\ k \in \{1,2,3\} \end{array} \tag{4.2}$$

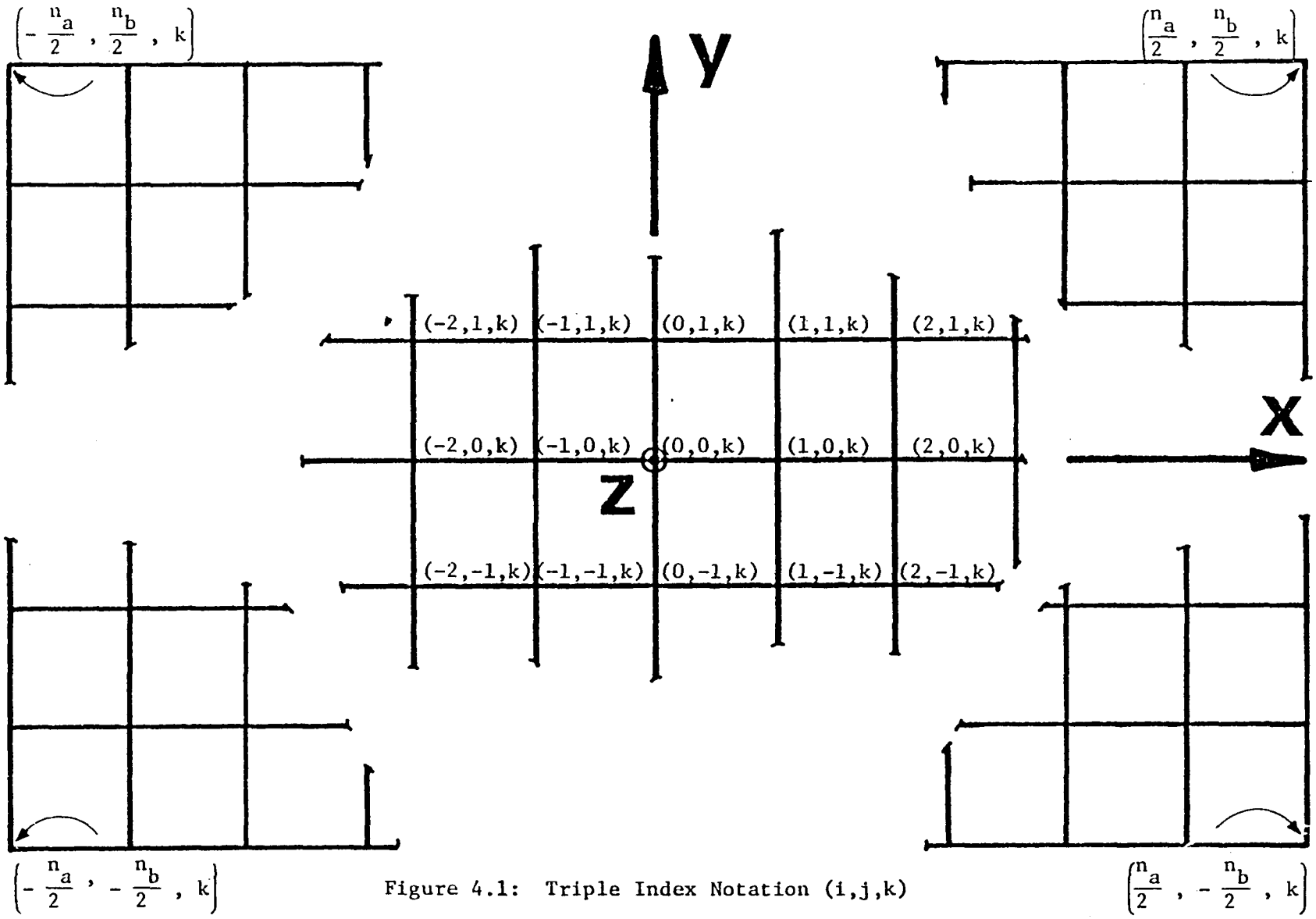

Figure 4.1: Triple Index Notation (i,j,k)

in which the arguments of the entries in $\underset{\sim}{u}_\ell$ are ordered triples of rationals (i,j,k), ordered in increasing lexicographical order of the ordered triples (j,i,k).

<u>Note</u>: (i_1,j_1,k_1) preceedes (i_2,j_2,k_2) in lexicographical increasing order if and only if

$i_1<i_2$

or, $i_1=i_2$ and $j_1<j_2$

or, $i_1=i_2$ and $j_1=j_2$ and $k_1<k_2$

By virtue of the symmetry and antisymmetry of the modes, we introduce the following relations:

<u>Definition</u>

A mode is said to be symmetric if

$$\begin{aligned} u(i,j,1)&= u(-i,j,1) \\ u(i,j,2)&= u(-i,j,2) \\ u(i,j,3)&=-u(-i,j,3) \end{aligned} \tag{4.3a,b,c}$$

implying

$$u(0,j,3)=0 \tag{4.3d}$$

A mode is said to be antisymmetric if

$$\begin{aligned} u(i,j,1)&=-u(-i,j,1) \\ u(i,j,2)&=-u(-i,j,2) \\ u(i,j,3)&= u(-i,j,3) \end{aligned} \tag{4.4a,b,c}$$

implying

$$u(0,j,1)= u(0,j,2)=0 \tag{4.4d}$$

The matrix

$$U_C^T=[\underset{\sim}{u}_1 \ \underset{\sim}{u}_2 \ \ldots \underset{\sim}{u}_c]^T \tag{4.5}$$

contains the first c rows of the transposed modal matrix U. As far as the actuator placement matrix B is concerned, we let

$$\Xi=\{(i_1,j_1,k_1),(i_2,j_2,j_2),\ldots,(i_c,j_c,k_c)\} \tag{4.6}$$

be a subset of the set of all arguments of the entries of any column in the modal matrix U.

We recall the definition of the standard unit vector

$$\underset{\sim}{e}_i^n=[0,\ldots,0,1,0,\ldots 0]^T \tag{4.7}$$

which is a vector of n coordinates with a unit in its ith entry and zeros elsewhere, $i\in\{1,\ldots,n\}$. Using Eqs.(4.6) and (4.7), the actuators matrix can be written as

$$B = [\underset{\sim}{e}^n(i_1,j_1,k_1) \ , \ \ldots \ , \ \underset{\sim}{e}^n(i_c,j_c,k_c)] \tag{4.8}$$

B has full rank if no two ordered triples of Ξ in Eq.(4.6) are identical. Multiplication of the matrices in Eqs.(4.6) and (4.8), results in the product

$$U_C^T B = \begin{bmatrix} u_1(i_1,j_1,k_1) & \dots & u_1(i_c,j_c,k_c) \\ u_2(i_1,j_1,k_1) & \dots & u_2(i_c,j_c,k_c) \\ \vdots & & \\ u_c(i_1,j_1,k_1) & \dots & u_c(i_c,j_c,k_c) \end{bmatrix} \tag{4.9}$$

We recognize that $U_C^T B$ is a minor of the transposed modal matrix U. We propose to use the shorthand notation

$$U_C^T B = U^T \begin{pmatrix} 1 & 2 & \dots & c \\ (i_1,j_1,k_1) & (i_2,j_2,k_2) & \dots & (i_c,j_c,k_c) \end{pmatrix} \tag{4.10}$$

Here, the first row indicates the selected rows of U^T and the second row indicates the selected columns of U^T in producing the minor $U_C^T B$.

The actuators placement over the domain can have either symmetric or asymmetric configuration.

<u>Definition</u>

We state that a set Ξ of actuators exhibits a symmetric configuration if

$$(i,j,k) \in \Xi \text{ implies } (-i,j,k) \in \Xi \tag{4.11}$$

<u>Remark</u>

Without constraints, any ordered triples of Ξ of the form (0,j,k) do not affect the symmetry of the configuration of actuators.

As illustrations, we selected six cases displayed in Fig. 4.2. The control scheme provides control of the first six modes by means of six thrust and torque actuators. Three cases represent asymmetric and three symmetric actuators configurations. Cases a, b, and c present a variety of asymmetric actuators placement configurations. It is not a difficult task to show by examining the determinant of the matrix, that all the three cases yield regular matrices $U_C^T B$. On the other hand, the last three cases d, e, and f present a variety of symmetric actuators placement configurations. Although cases d, e, and f are of the same kind, namely, symmetric, the nature of the resulting matrices $U_C^T B$ is not of the same kind. Cases d and e yield zero determinant of the matrix $U_C^T B$, proving $U_C^T B$ singular in both, while case f yields a non-zero determinant, proving $U_C^T B$ for this case regular. Cases e and f seem to be similar, although the first resulted in a singular matrix, while the second in a regular one. The question arises now as to how to distinguish beetween such two cases and how to avoid singularity.

Notation

Let Ξ be a symmetric configuration of actuators

Case	Actuators Configuration	Nature of $U_C^T B$
a	asymmetric 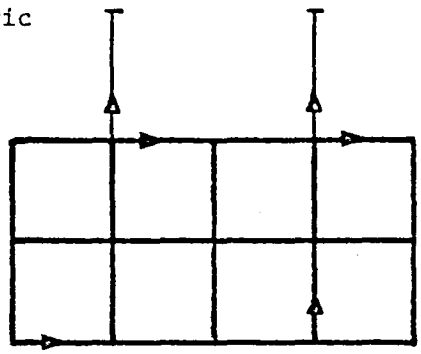	regular
b	asymmetric 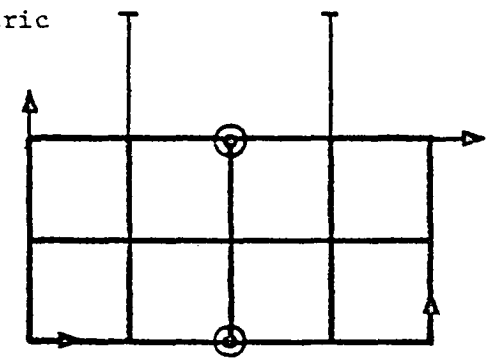	regular
c	asymmetric 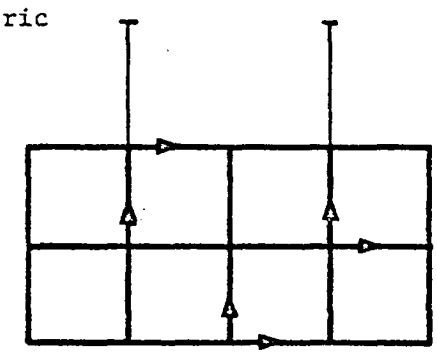	regular

Notation: ○ force vector in the z direction (k=1)
→ torque vector in the x direction (k=2)
↑ torque vector in the y direction (k=3)

Figure 4.2: Various Actuators Configurations

Case	Actuators Configuration	Nature of $U_C^T B$
d	symmetric 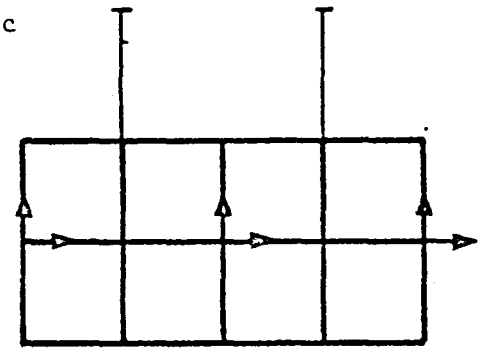	singular
e	symmetric 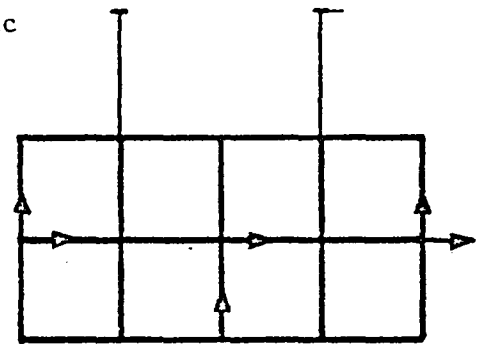	singular
f	symmetric 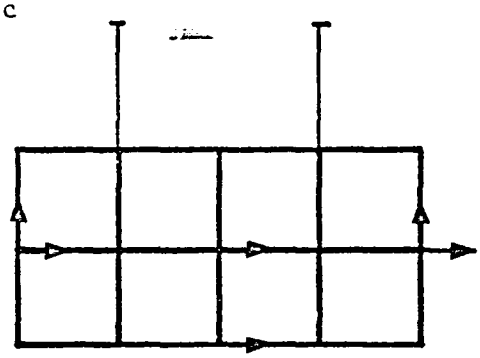	regular

Figure 4.2: (cont.)

- We denote by 2p the number of actuators in Ξ of the form (i,j,k) such that $i \neq 0$.

<u>Remark</u>: There are exactly p actuators in Ξ having $i>0$

<u>Remark</u>: There are exactly c-2p actuators on the axis of symmetry i.e., the y axis. Note that c is the total number of actuators which is also the number of controlled modes. From this follows that there are in Ξ exactly c-2p actuators (i,j,k) having i=0.

- We denote by h the number of actuators in Ξ of the forms (0,j,1) and (0,j,2), for some j.
- We denote by v the number of actuators in Ξ of the form (0,j,3), for some j. Clearly, c=2p+h+v
- We denote by s the number of symmetric modes in the modal matrix U among the selected first c controlled modes.

<u>Proposition</u>

Let Ξ be a symmetric configuration of actuators with disposition 2p, h, and v. A sufficient condition for the mode participation matrix $U_C^T B$ to be singular is

$$p+h<s \tag{4.12}$$

<u>Explanation</u>

The proposition states that for the matrix $U_C^T B$ to be singular, the number of actuator pairs p, in addition to the number of actuators h with force or torque vectors, not paral-

lel to the axis of symmetry, must be less than the number s of symmetric modes controlled.

Next, let us examine the cases of Fig. 4.2. The order of the system in Fig. 4.2 is n=45. The solution to the eigenvalue problem can show that among the first six eigenvectors, four have symmetric and two have antisymmetric modes shapes, so that s=4. A summary of the cases in Fig. 4.2, is given in Tab. 4.1. It is clear from the table that there is no conflict between the results obtained using the theorem and those obtained by inspecting directly the determinant of the matrix $U_C^T B$.

Conjecture

If Ξ is not a symmetric configuration or if Ξ is a symmetric configuration with $p+h \geq s$, then $U_C^T B$ is regular. If this conjecture is true, then the condition in the theorem is necessary and sufficient for $U_C^T B$ to be singular provided that Ξ has a symmetric configuration. Otherwise, if Ξ is not a symmetric configuration set, the conjecture asserts that $U_C^T B$ is regular. Before proceeding with the proof of the theorem, we will mention the following important lemma

Laplace Expansion of a Determinant

The classical Laplace expansion for determinants has the form

TABLE 4.1

Summary of Cases from Fig. 4.2

Case	p	h	v	p+h	s	Result	$U_C^T B$
a					4	Ξ is not a symmetric configuration, therefore p, h, and v are undefined	
b					4		
c					4		
d	2	1	1	3	4	p+h < s	singular
e	2	1	1	3	4	p+h < s	singular
f	2	2	0	4	4	p+h = s	regular

$$\det A = \sum_{\substack{\text{all } j_1,j_2,\ldots,j_p \\ \text{such that} \\ 1\leq j_1<j_2<\ldots<j_p\leq n}} (-1)^{\sum_{k=1}^{p}(i_k+j_k)} \det A \begin{pmatrix} i_1 & i_2 & \ldots & i_p \\ j_1 & j_2 & \ldots & j \end{pmatrix} \cdot \det A \begin{pmatrix} i'_1 & i'_2 & \ldots & i'_{n-p} \\ j'_1 & j'_2 & \ldots & j'_{n-p} \end{pmatrix} \tag{4.13}$$

where

$$A \begin{pmatrix} i_1 & i_2 & \ldots i_p \\ & & \\ j_1 & j_2 & \ldots j_p \end{pmatrix}$$

denotes the minor of the matrix A obtained by the selected rows $i_1, i_2, \ldots, i_p$ and selected columns $j_1, j_2, \ldots, j_p$.
In the sum, there are $\binom{n}{p}$ terms as the number of selection of ordered p indices. The sum is extended over all p-tuples $1\leq j_1<j_2<\ldots<j_p\leq n$, where $j'_1, j'_2, \ldots j'_{n-p}$ denote the complementary set of indices to $j_1, j_2, \ldots, j_p$ in $1,2,\ldots,n$ arranged in natural order, and similarly $i'_1, i'_2, \ldots, i'_{n-p}$ denote the complementary set of indices to $i_1, i_2, \ldots, i_p$ in $1,2,\ldots,n$ (see examples in Appendix A.)

<u>Proof of Proposition</u>

Consider a set Ξ with a symmetric configuration of actuators, with disposition 2p, h, and v. This represents a set Ξ of the form

$$\Xi = \{(i_1,j_1,k_1),\ \ldots,\ (i_p,j_p,k_p),\ (-i_1,j_1,k_1),\ \ldots\ (-i_p,j_p,k_p),$$
$$(0,j_{p+1},k_{p+1}),\ \ldots,\ (0,j_{p+h},k_{p+h}),$$
$$(0,j_{p+h+1},3),\ \ldots,\ (0,j_c,3)\} \tag{4.14}$$

where $i_1,\ldots,i_p$ are not zero, and $k_{p+1},\ldots k_{p+h} \in \{1,2\}$.

Let $p+h<s$ hold true. We have now to show that $U_C^T B$ is singular, i.e., that $\det(U_B^T B)=0$. By virtue of the fact that a change of rows (columns) in a determinant only affects the sign of the determinant, the vanishing of $\det(U_C^T B)$ is invariant under such changes. Let us perform changes of rows in $U_C^T B$, such that the first s rows will represent the s symmetric modes and the rest c-s rows will represent the antisymmetric modes, renumbering the rows accordingly.

Let us now perform changes of columns in $U_C^T B$ such that the new order of the columns will be

$(i_1,j_1,k_1),(-i_1,j_1,k_1),\ldots,(i_p,j_p,k_p),(-i_p,j_p,k_p)$	2p triples
$(0,j_{p+1},k_{p+1}),\ldots,(0,j_{p+h},k_{p+h})$	h triples
$(0,j_{p+h+1},3),\ldots,(0,j_c,3)$	v triples

Explicitly,

$$\det\,(U_C^T\,B) =$$

$$= \sigma\cdot\det\left|\begin{array}{cccc|cc}
\multicolumn{4}{c|}{\overbrace{\hphantom{u_1(i_1,j_1,k_1)\quad u_1(-i_1,j_1,k_1)\quad \ldots\quad u_1(i_p,j_p,k_p)\quad u_1(-i_p,j_p,k_p)}}^{\text{block P}}} & & \\
u_1(i_1,j_1,k_1) & u_1(-i_1,j_1,k_1) & \ldots & u_1(i_p,j_p,k_p) & u_1(-i_p,j_p,k_p) & \\
u_2(i_1,j_1,k_1) & u_2(-i_1,j_1,k_1) & \ldots & u_2(i_p,j_p,k_p) & u_2(-i_p,j_p,k_p) & \\
\vdots & & & & & \\
u_s(i_1,j_1,k_1) & u_s(-i_1,j_1,k_1) & \ldots & u_s(i_p,j_p,k_p) & u_s(-i_p,j_p,k_p) & \\
u_{s+1}(i_1,j_1,k_1) & u_{s+1}(-i_1,j_1,k_1) & \ldots & u_{s+1}(i_p,j_p,k_p) & u_{s+1}(-i_p,j_p,k_p) & \\
\vdots & & & & & \\
u_c(i_1,j_1,k_1) & u_c(-i_1,j_1,k_1) & \ldots & u_c(i_p,j_p,k_p) & u_c(-i_p,j_p,k_p) &
\end{array}\right|$$

$$\left|\begin{array}{cc|cc}
\multicolumn{2}{c|}{\overbrace{\hphantom{u_1(0,j_{p+1},k_{p+1})\quad \ldots u_1(0,j_{p+h},k_{p+h})}}^{\text{block H}}} & \multicolumn{2}{c}{\overbrace{\hphantom{u_1(0,j_{p+h+1},3)\quad \ldots u_1(0,j_c,3)}}^{\text{block V}}} \\
u_1(0,j_{p+1},k_{p+1}) & \ldots u_1(0,j_{p+h},k_{p+h}) & u_1(0,j_{p+h+1},3) & \ldots u_1(0,j_c,3) \\
u_2(0,j_{p+1},k_{p+1}) & \ldots u_2(0,j_{p+h},k_{p+h}) & u_2(0,j_{p+h+1},3) & \ldots u_2(0,j_c,3) \\
\vdots & & & \\
u_s(0,j_{p+1},k_{p+1}) & \ldots u_s(0,j_{p+h},k_{p+h}) & u_s(0,j_{p+h+1},3) & \ldots u_s(0,j_c,3) \\
u_{s+1}(0,j_{p+1},k_{p+1}) & \ldots u_{s+1}(0,j_{p+h},k_{p+h}) & u_{s+1}(0,j_{p+h+1},3) & \ldots u_{s+1}(0,j_c,3) \\
\vdots & & & \\
u_c(0,j_{p+1},k_{p+1}) & \ldots u_c(0,j_{p+h},k_{p+h}) & u_c(0,j_{p+h+1},3) & \ldots u_c(0,j_c,3)
\end{array}\right|$$

where $\sigma \in \{+1, -1\}$ (4.15)

Note the blocks division P, H, and V in Eq.(4.15) where block P relates to the actuators located off the axis of symmetry, block H to the actuators type k=1 and k=2 that are on this axis and block V relates to the actuators type k=3 located along the axis of symmetry of the domain.

Noticing the fact that the vanishing of $\det(U_C^T B)$ is invariant under rows (columns) elementary transformations, we make use of the modes symmetry properties, as described by Eqs.(4.3) and (4.4) to perform such operations on the columns of the determinant in Eq.(4.15).

$$\det(U_C^T B) =$$

$$= \sigma \cdot \det \begin{vmatrix} \overbrace{\begin{matrix} u_1(i_1,j_1,k_1) & 0 & \ldots u_1(i_p,j_p,k_p) & 0 \\ u_2(i_1,j_1,k_1) & 0 & \ldots u_2(i_p,j_p,k_p) & 0 \\ \vdots & & & \\ u_s(i_1,j_1,k_1) & 0 & \ldots u_s(i_p,j_p,k_p) & 0 \end{matrix}}^{\text{block P}} \\ \begin{matrix} u_{s+1}(i_1,j_1,k_1) & \rho_1 2u_{s+1}(i_1,j_1,k_1) & \ldots u_{s+1}(i_p,j_p,j_p) & \rho_p 2u_{s+1}(i_p,j_p,k_p) \\ \vdots & & & \\ u_c(i_1,j_1,k_1) & \rho_1 2u_c(i_1,j_1,k_1) & \ldots u_c(i_p,j_p,k_p) & \rho_p 2u_c(i_p,j_p,k_p) \end{matrix} \end{vmatrix}$$

$$
\begin{array}{c}
\overbrace{\hphantom{u_1(0,j_{p+1},k_{p+1}) \;\cdots\; u_1(0,j_{p+h},k_{p+h})}}^{\text{block H}} \quad \overbrace{\hphantom{0 \;\cdots\; 0}}^{\text{block V}} \\
\left|\begin{array}{ccc|ccc}
u_1(0,j_{p+1},k_{p+1}) & \cdots & u_1(0,j_{p+h},k_{p+h}) & 0 & \cdots & 0 \\
u_2(0,j_{p+1},k_{p+1}) & \cdots & u_2(0,j_{p+h},k_{p+h}) & 0 & \cdots & 0 \\
\vdots & & & & & \\
u_s(0,j_{p+1},k_{p+1}) & \cdots & u_s(0,j_{p+h},k_{p+h}) & 0 & \cdots & 0 \\
0 & \cdots & 0 & u_{s+1}(0,j_{p+h+1},3) & \cdots & u_{s+1}(0,j_c,3) \\
\vdots & & & & & \\
0 & \cdots & 0 & u_c(0,j_{p+h+1},3) & \cdots & u_c(0,j_c,3)
\end{array}\right|
\end{array}
$$

where $\sigma \in \{+1, -1\}$ (4.16)

The final form as obtained in Eq.(4.16) is a result of the following operations:

Consider column 2ℓ and column $2\ell-1$ for any $\ell \in \{1,2,\ldots,p\}$. If k_ℓ is 1 or 2, then in order to achieve zeros in the first s rows in column 2ℓ of block P, we subtract column $2\ell-1$ from column 2ℓ. If k_ℓ is 3, then in order to achieve the same goal, we add column $2\ell-1$ to column 2 . The columns $2\ell-1$ for $\ell \in \{1,2,\ldots p\}$ remain as they are. The parameter ρ_ℓ that appears in block P, represents a sign function $\rho_\ell(k)=(-1)^{\frac{1}{2}k(3-k)}$ such that $\rho_\ell(1)=\rho_\ell(2)=-1$ and $\rho_\ell(3)=+1$. Applying Laplace expansion Eq.(4.13) to the determinant of Eq.(4.16)

$$\det(U_C^T B) = \sigma \cdot \det(\widetilde{U_C^T B}) = \sigma \Sigma (-1)^{1+2+\ldots+s+j_1+j_2+\ldots+j_s}$$

$$\cdot \det \widetilde{U_C^T B} \begin{pmatrix} 1 & 2 & \ldots & s \\ j_1 & j_2 & \cdots & j_s \end{pmatrix} \cdot \det \widetilde{U_C^T B} \begin{pmatrix} s+1 & s+2 & \ldots & c \\ j_1' & j_2' & \cdots & j_{c-s}' \end{pmatrix} \quad (4.17)$$

where the sum is as indicated in Eq.(4.13). In this expansion, $\widetilde{U_C^T B}$ denotes the rearranged matrix as in Eq.(4.16), the rows (columns) numbering is also with respect to the new arrangement, and the choice of first fixed s rows was made.

<u>Claim</u>

$$\det \widetilde{U_C^T B} \begin{pmatrix} 1 & 2 & \ldots & s \\ j_1 & j_2 & \cdots & j_s \end{pmatrix} = 0 \quad (4.18)$$

for any $j_1, j_2, \ldots, j_s$ such that $1 \le j_1 < j_2 < \ldots < j_s \le c$

<u>Proof of Claim</u>

The matrix

$$U_C^T B \begin{pmatrix} 1 & 2 & \ldots s \\ & & \\ j_1 & j_2 & \cdots j_s \end{pmatrix}$$

has at most p+h nonzero columns. By assumption, $p+h<s$. Therefore, this matrix of order s has at least $s-p-h>0$ null

columns. Because s, p, and h are integers, s-p-h is an integer also, and a positive one. Hence, at least one column of the above mentioned matrix is zero, so that the determinant of the matrix is zero. This concludes the proof of the claim.

In view of this claim, we have

$$\det(U_C^T B)=0 \tag{4.19}$$

because its expansion in Eq.(4.17) is really a sum of zeros. This proves that $U_C^T B$ is singular, which concludes the proof of proposition.

Chapter V

MINIMUM FUEL IN HIGH ORDER SYSTEMS

The minimum fuel problem became a very important one in recent space vehicles, especially in those that are launched for lengthy missions. The amount of fuel or energy alloted for the control system is limited to such a degree that it becomes necessary to treat fuel economy as the predominant factor in many systems. In such cases, it is natural to design the control so that it consumes a minimum amount of fuel.

There are many problems where the control variables F(t) are directly proportional to the rate of fuel flow, like the flow from a gas jet for attitude control or shape control of a large flexible spacecraft. Almost invariably in these problems, the total fuel available is limited. Therefore, it is desirable to accomplish each control correction with a minimum amount of fuel. The total fuel consumed during control action is measured by the time integral of the absolute value of the control variable. Due to technical restrictions on the actuators, there are limits on the magnitude of the control forces. As an example, the thrust

produced by a gas jet actuator is limited in magnitude due to the saturation of the power elements. Systems characterized by a restriction on the control and subjected to the minimization of a particular functional, such as the consumed fuel, the required energy, etc., are optimal. We refer to a control system minimizing the amount of consumed fuel, as a "minimum-fuel system".

About two decades have passed since the development of powerful variational techniques in the theory of control, such as the minimum principle of Pontryagin. This principle can be used to determine necessary and sufficient conditions for the control function to be optimal [16,17]. The necessary condition usually specifies the nature of the control and the general structure of the control system. Unfortunately, the derivation of the optimal fedback control law, i.e., the explicit dependence of the control on the instantaneous values of the state variables, is a very complex task and for most practical cases it remains an unsolved problem [18,19]. In these cases, a trial and error process is unavoidable for the state determination. One may consider such a process as reasonable for a low-order system (fourth order at most), but certainly not for a high-order system, where the computational difficulty is insurmontable.

However, it is unexpected that a reasonably accurate model of a flexible structure can be represented by a low-order system.

Formulation of the control law in terms of the costate variables can be accomplished regardless of the system order. Yet, determination of the initial conditions of the costate variables for a high-order system is difficult, if not impossible. The control task is made considerably simpler by using the IMSC method, where the complexity inherent in a high-order system is reduced. Using this method, the initial constate variables must be determined for a set of independent second-order ordinary differential equations, so that treatment of the coupled high-order system is avoided. According to this approach, to each of the decoupled modes, independent control policy can be specified so as to permit independent control of each individual mode. With this method, the cumbersome minimum fuel problem in the high-order system is reduced to n fuel minimization problems of the decoupled set of n second-order modal space systems.

After the control design task has been carried out in the modal space, and modal control functions have been found, these generalized control forces are synthesized to obtain the actual actuators forces.

5.1 PROBLEM FORMULATION

In formulating the minimum fuel problem, we begin with the discretized time-invariant structure equations of motion of order n

$$M\,\ddot{\underset{\sim}{q}}(t) + K\,\underset{\sim}{q}(t) = \underset{\sim}{Q}(t) \tag{5.1}$$

where $\underset{\sim}{Q}(t)$ is the discrete forcing vector, generated using c actuators, or as many as the number of controlled modes,

$$\underset{\sim}{Q}(t) = B \cdot \underset{\sim}{F}(t) \tag{5.2}$$

where $\underset{\sim}{F}(t)$ is the c-dimensional vector of thrusters and tourquers and B is a full rank nxc actuators placement transformation matrix.

The problem of minimum-fuel control can be stated as follows: Assume that the control $F_i(t)$ is proportional to the rate of flow of fuel. Then the total fuel consumed J(F) during a time interval $(0, t_f)$ that is also a measure of control effort, can be expressed in terms of the time integral of the sum of the absolute control values as follows:

$$J(\underset{\sim}{F}) = \int_0^{t_f} \left(\sum_{i=1}^{c} \alpha_i |F_i(t)| \right) dt \tag{5.3}$$

where α_i are nonegative weighting factors and t_f is some unspecified final time. In most practical systems, the magnitude of each of the control functions $F_i(t)$ $(i=1,2,\ldots,c)$ is limited due to the saturation of the power elements. Therefore, it is assumed that the controls have to satisfy the constraints

$$|F_i(t)| \leqslant M_i \qquad i = 1,2,\ldots,c \qquad (5.4)$$

where M are positive constants.

It is assumed that at $t_0=0$ the system (5.1) is in the initial state $\underset{\sim}{q}(t_0)$, $\dot{\underset{\sim}{q}}(t_0)$. Then, the control task amounts to driving the system from its initial state to a final specified state $q(t_f)$, $\dot{q}(t_f)$ in finite time.

The essence of the control problem is to determine a control vector $\underset{\sim}{F}(t)$ subjected to the constraints (5.4), such that the final state is reached with a minimum amount of fuel $J(\underset{\sim}{F})$.

As stated already, the problem can be decomposed into a set of n second-order decoupled optimal control problems, which reduces the amount of complexity arising in high-order system. In the formulation, we employ theoretical results de-

veloped in Refs. 16,17 to obtain the necessary condition for the optimal minimum-fuel control.

The modal linear time-invariant plant is described by the matrix differential equation

$$\dot{\underset{\sim}{x}}_r(t) = A_r \, \underset{\sim}{x}_r(t) + \underset{\sim}{b} \, N_r(t) \qquad r = 1,2,\ldots,c \qquad (5.5)$$

where

$$\underset{\sim}{x}_r = [x_{1r} \;\; x_{2r}]^T \;, \quad A_r = \begin{bmatrix} 0 & 1 \\ -\omega_r^2 & 0 \end{bmatrix} \;, \quad \underset{\sim}{b} = [0 \;\; 1]^T \qquad (5.6a,b,c)$$

$$x_{1r}(t) = \xi_r(t) \;, \quad x_{2r} = \dot{\xi}_r(t) \qquad (5.6d)$$

$\xi_r(t)$ and $\dot{\xi}_r(t)$ are modal displacement and modal velocity respectively, $\underset{\sim}{x}_r(t)$ is a 2x1 vector, A_r is a 2x2 matrix and $N_r(t)$ is the scalar modal control function.

To apply the IMSC method, one must seek the minimization of modal cost functions rather than the minimization of the global cost given in Eq.(5.3). To derive independent modal cost functions, a decomposition of the global cost into modal costs, dependent on the associated modal control forces and modal coordinates only, is essential.

It turns out that a complete decomposition of the global cost for fuel minimization problem, as it appears in Eq.(5.3), into equivalent independent modal costs is not feasible, so that we resort to another approach.

Using Eqs.(2.72a) and (5.2), the modal control vector is obtained as

$$\underset{\sim}{N}_c(t) = C\,\underset{\sim}{F}(t) \tag{5.7}$$

where

$$C = U_c^T B \tag{5.8}$$

is the system cxc mode participation matrix. We employ norm-one measurement for the configuration space actuator force vector $\underset{\sim}{F}(t)$. By definition, norm-one is the sum of the absolute values of the vector entries which resembles exactly the global cost presented by Eq.(5.3), or

$$|\underset{\sim}{F}(t)|_1 \triangleq \sum_{i=1}^{c} |F_i(t)| \tag{5.9}$$

This norm is defined for the n dimensional Euclidean vector space R^n and has all the properties of a regular vector norm, as shown in Ref. 29.

The related matrix norm is defined as

$$\|C\|_1 \triangleq \max_j \sum_{i=1}^{c} |c_{ij}| \qquad \text{(column sum)} \tag{5.10}$$

Using these norm definitions we can write the norm-one relation, applied to the control vector transformation in Eq.(5.7), as

$$|\underset{\sim}{F}(t)| \leqslant \|C^{-1}\| \; |\underset{\sim}{N}_c(t)| \tag{5.11}$$

With no loss of generality, we assign the values $\alpha_i=1$ for all $i=1,2,\ldots,c$ as weighting factors in the cost Eq(5.3). Note that the derivation can be easily modified if those assumptions are not made. We propose to minimize the modal fuel expenditure by minimizing the norm-one of the modal control vector. This vector consists of independent control entries, so that minimization of its norm-one can be carried out by minimizing each entry independently. Integrating Eq.(5.11) on $(0,t_f)$ will result in a cost inequality that provides an upper bound to the global cost of Eq.(5.3)

$$\int_0^{t_f} |\underset{\sim}{F}(t)|\,dt \leqslant \|C^{-1}\| \int_0^{t_f} |\underset{\sim}{N}(t)|\,dt \tag{5.12}$$

where $\int_0^{t_f} |\underset{\sim}{F}(t)|_1 dt$ is the fuel cost function and $\int_0^{t_f} |\underset{\sim}{N}(t)|_1 dt$ is its modal counterpart.

It was stated earlier that the magnitude of each actuator force is bounded due to limitations on the forces char-

acteristics, as can be seen in Eq.(5.4). These bounds must be transformed to modal forces bounds before the modal minimum-fuel problem can be formulated. We use the norm of Eq.(5.7) to determine modal control bounds. Eq.(5.4) in conjunction with the norm-one definition of Eq.(5.9) provide the bound to the norm of the actuators force vector, or

$$|\underset{\sim}{F}(t)| = \sum_{i=1}^{c} |F_i(t)| \leqslant \sum_{i=1}^{c} M_i \tag{5.13}$$

Applying norm-one measurement to Eq.(5.7), we obtain

$$|\underset{\sim}{N}_c(t)| \leqslant \|C\| \; |\underset{\sim}{F}(t)| \leqslant \|C\| \sum_{i=1}^{c} M_i \tag{5.14}$$

and, because $|\underset{\sim}{N}_c(t)|_1 = \sum_{i=1}^{c} |N_i(t)|$, it turns out that

$$\sum_{i=1}^{c} |N_i(t)| \leqslant \|C\| \sum_{i=1}^{c} M_i \tag{5.15}$$

which is a total bound.

In the IMSC method, the modal controls act independently of each other, so that each control must have its own bound. To achieve this requirement, we introduce weighting coefficients a_i such that

$$|N_i| \leqslant a_i \; \|C\| \sum_{j=1}^{c} M_j \tag{5.16}$$

where

$$\sum_{i=1}^{c} a_i = 1 \quad , \quad a_i \geqslant 0 \tag{5.17}$$

One way of generating these coefficients is to select them inversely proportional in some manner to the eigenvalues. In a case where n_r rigid body modes are present, as well as $c-n_r$ elastic modes, one may choose

$$a_i = \frac{1}{c} \quad , \qquad i = 1,2,\ldots,n_r \tag{5.18}$$

for the rigid body modes, and

$$a_i = \frac{(c-n_r)}{c(c-n_r-1)} \left(1 - \frac{\lambda_i}{\sum_{j=1}^{c} \lambda_j} \right) \qquad i = n_r+1, n_r+2, \ldots, c \tag{5.19}$$

for the elastic modes.

Clearly, any other set of weighting coefficients can be used as long as Eq.(5.17) is satisfied.

The essence of the IMSC method is to design the control laws in the modal space for each of the controlled modes independently. Then, realization of the actual force vector is made by modal synthesis. It can be shown [17,18] that for modal minimum-fuel problem the controls appear as a non-linear "bang-off-bang" type, that use the maximum values of the modal control forces. This means that the norm of the modal control vector will reach its upper bound in Eq.(5.15) very often. In such case, through substitution of Eq.(5.14)

into Eq.(5.11), we see that the norm of actuators forces would exceed its bounds, or

$$|\underset{\sim}{F}(t)| \leqslant \|C^{-1}\| \; \|C\| \sum_{i=1}^{c} M_i \tag{5.20}$$

where $\|C^{-1}\|\|C\| > 1$ is the <u>condition number</u> of the mode participation matrix C, which is unacceptable. To circumvent this problem, it is necessary to modify Eq.(5.13) by dividing each control bound by the condition number of the matrix C, so that

$$|\underset{\sim}{F}(t)| \leqslant \frac{1}{\|C^{-1}\| \; \|C\|} \cdot \sum_{i=1}^{c} M_i \tag{5.21}$$

Eq.(5.21) provides the <u>effective upper bounds</u> on actuators forces, where its modal counterpart will be obtained as the modified Eq.(5.14)

$$|\underset{\sim}{N}_c(t)| \leqslant \frac{1}{\|C^{-1}\|} \sum_{i=1}^{c} M_i \tag{5.22}$$

Clearly, the condition number plays the role of a "figure of merit" in the control effectiveness.

Now, we are ready to formulate the modal minimum-fuel problem for the linear time invariant modal plant described by the modal differential equations (5.5). Because of limitations on actuators power, the norm of the modal control force vector is bounded as given in Eq.(5.22). Using the weighted decomposition scheme given by Eqs. (5.16-19), the modal forces bounds can be given for each mode as

$$|N_r(t)| \leqslant a_r \frac{1}{\|C^{-1}\|} \sum_{i=1}^{c} M_i \triangleq \hat{N}_r \qquad r = 1,2,\ldots,c \qquad (5.23)$$

The task of the modal controls is to drive the initial modal states $\underset{\sim}{x}_{0r}$ to final desired states $\underset{\sim}{x}_{fr}$ (the origin for example), by appropriate optimal control signals $N_r(t)$, minimizing the performance indices $J_r(N_r)$. In our case, the modal fuel functionals are given by

$$J_r(N_r) = \int_0^{t_f} |N_r(t)|\,dt \qquad r = 1,2,\ldots,c \qquad (5.24)$$

The minimum principle of Pontryagin [16] can be used to derive the necessary condition for the optimal modal minimum-fuel control. Using Eqs.(5.5) and (5.24), we introduce the modal Hamiltonian functional

$$H_r(\underset{\sim}{x}_r,\underset{\sim}{p}_r,N_r,t) = |N_r(t)| + \underset{\sim}{p}_r^T(t)\ (A_r\ \underset{\sim}{x}_r(t) + \underset{\sim}{b}\ N_t(t)) \qquad r = 1,2,\ldots,c \tag{5.25}$$

where $\underset{\sim}{p}_r(t)=[p_{1r}(t)\ p_{2r}(t)]^T$ is the 2x1 vector of Lagrange multipliers known as the modal costate vector.

The necessary conditions for minimization are given by

$$\dot{\underset{\sim}{x}}_r(t) = \frac{\partial H_r}{\partial \underset{\sim}{p}_r} \qquad t \in \{0,t_f\}\ ,\quad r = 1,2,\ldots,c \tag{5.26}$$

$$\dot{\underset{\sim}{p}}_r(t) = -\frac{\partial H_r}{\partial \underset{\sim}{x}_r} \qquad t \in \{0,t_f\}\ ,\quad r = 1,2,\ldots,c \tag{5.27}$$

$$0 = \frac{\partial H_r}{\partial N_r} \qquad t \in \{0,t_f\}\ ,\quad r = 1,2,\ldots,c \tag{5.28}$$

subject to the boundary conditions

$$\underset{\sim}{x}_r(0) = \underset{\sim}{x}_{0r} \tag{5.29a}$$

$$\underset{\sim}{x}_r(t_f) = \underset{\sim}{x}_{fr} \tag{5.29b}$$

$$H_r(\underset{\sim}{x}_r(t_f),\underset{\sim}{p}_r(t_f),N_r(t_f),t_f) = 0 \qquad r = 1,2,\ldots,c \tag{5.29c}$$

The object is to determine the 2c constants of integration and t_f.

Because the cost functional is not a function of $\underset{\sim}{p}_r(t)$, it follows that Eqs.(5.26) are identical to Eqs.(5.5), the modal plant equations. Eqs.(5.27) lead to the adjoint-costate system of differential equations

$$\dot{\underset{\sim}{p}}_r(t) = - A_r^T \underset{\sim}{p}_r(t) \qquad r = 1,2,\ldots,c \qquad (5.30)$$

The control $N_r(t)$ minimizing the Hamiltonian H_r absolutely is a function of $\underset{\sim}{x}_r$, $\underset{\sim}{p}_r$ and t. This functional dependence of N_r is a necessary condition on the control function $N_r(t)$, which is the one that minimizes the performance index $J_r(N_r)$. It can be stated that the optimal control $N_r(t)$ minimizing the performance index $J_r(N_r)$, Eq.(5.24), must by necessity minimize the Hamiltonian H_r, Eq.(5.25), absolutely.

The formal minimization technique, Eqs.(5.28), leads to an unrealistic result. However,

$$\min_{\substack{N_r \\ |N_r| \leqslant \hat{N}_r}} H_r(\underset{\sim}{x}_r,\underset{\sim}{p}_r,N_r,t) = \underset{\sim}{p}_r^T(t)\, A_r\, \underset{\sim}{x}_r(t) + \min_{\substack{N_r \\ N_r \leqslant \hat{N}_r}} \{|N_r(t)| + \underset{\sim}{p}_r^T(t)\, \underset{\sim}{b}\, N_r(t)\}$$

$$r = 1,2,\ldots,c \qquad (5.31)$$

does provide an absolute minimum to the Hamiltonian function.

The shaded area in Fig. 5.1 provides the value of $|N_r(t)| + \underset{\sim}{p}_r^T(t)\underset{\sim}{b}N_r(t)$ versus $\underset{\sim}{p}_r(t)\underset{\sim}{b}$ depending on the value of $N_r(t)$. From the plot, it is clear that H_r takes its smallest value at each instant t if the term $|N_r(t)| + \underset{\sim}{p}_r^T(t)\underset{\sim}{b}N_r(t)$ maintains its largest negative value at all times. This can be achieved by selecting $N_r(t)$ along the solid lines providing the lower bounds of the shaded area. Hence, we consider the switching functions

$$N_r(t) = -\hat{N}_r \operatorname{sgn}\{\underset{\sim}{p}_r^T(t) \cdot \underset{\sim}{b}\} \qquad |\underset{\sim}{p}_r^T(t)\,\underset{\sim}{b}| > 1 \tag{5.32a}$$

$$N_r(t) = 0 \qquad |\underset{\sim}{p}_r^T(t)\,\underset{\sim}{b}| < 0 \tag{5.32b}$$

$$0 < N_r(t) < \hat{N}_r \qquad \underset{\sim}{p}_r^T(t)\,\underset{\sim}{b} = -1 \tag{5.32c}$$

$$-\hat{N}_r < N_r(t) < 0 \qquad \underset{\sim}{p}_r^T(t)\,\underset{\sim}{b} = +1 \tag{5.32d}$$

$$r = 1,2,\ldots,c$$

Equations(5.32) describe the characteristics of a relay with dead zone. We can use the definition of a dead-zone function, denoted by dez(*), as given in Ref. 17, to write these equations in a compact form

$$N_r(t) = -\hat{N}_r \operatorname{dez}\{\underset{\sim}{p}_r^T(t)\,\underset{\sim}{b}\} \qquad r = 1,2,\ldots,c \tag{5.33}$$

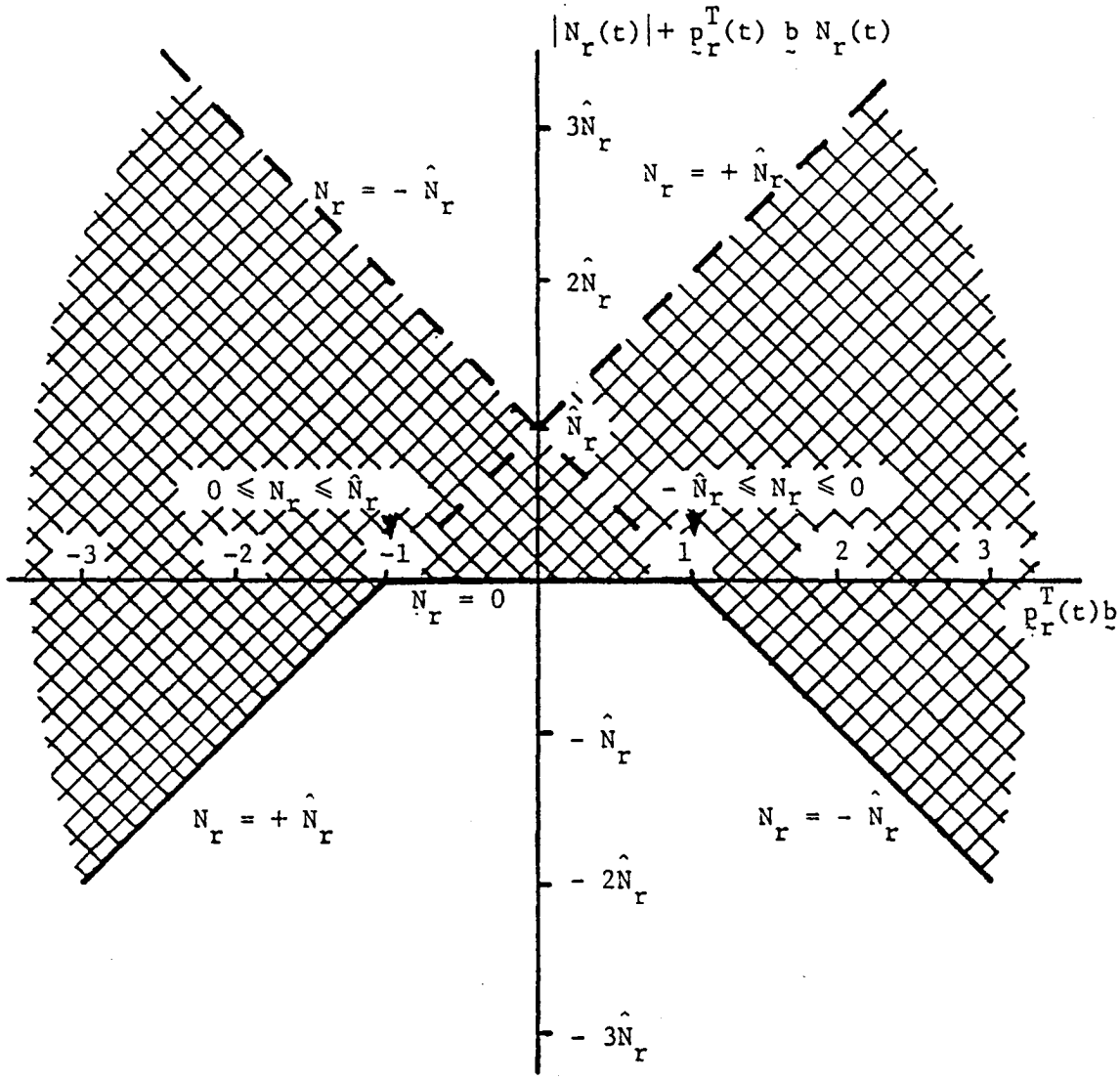

Figure 5.1: N-Dependent Part of Modal Hamiltonian Function

An illustration of Eqs.(5.33) for the rth mode fuel-optimal control is given in Fig. 5.2. Equations (5.32) provide the modal control law for the modal minimum-fuel operation, where $N_r(t)$, $(r=1,2,\ldots,c)$ are piecewise constants functions with values of $+\hat{N}_r, 0$, or $-\hat{N}_r$, as given in Eqs.(5.32a,b). If however, there are time intervals $(t_1,t_2)_r$ of finite durations, during which one or more modal necessary conditions, given by Eqs.(5.31), provide no information about the behavior of the controls $N_r(t)$, then $(t_1,t_2)_r$ are <u>singular intervals</u> and the appropriate $N_r(t)$ are singular controls in these particular modes. Such a situation occurs when $|\underset{\sim}{p}_r^T\underset{\sim}{b}|=1$. We observe that Eqs.(5.32a,b) specify the magnitude and the polarity of the fuel optimal control $N_r(t)$ in terms of $\underset{\sim}{p}_r(t)$ uniquely, provided $|\underset{\sim}{p}_r^T\underset{\sim}{b}|\neq 1$. When $|\underset{\sim}{p}_r^T\underset{\sim}{b}|=1$, as in Eqs.(5.32c,d), the fuel-optimal control polarity is specified, but not the magnitude. These considerations lead to the distinction between <u>normal</u> modal fuel-optimal problem and <u>singular</u> modal fuel-optimal problem.

We use results from Ref. 16 to show that singular intervals can exist only in the controls of rigid body modes but never in the controls of elastic modes. The condition is based upon the matrix $E_r^T A_r$ where A_r is the modal plant matrix and E_r is the 2x2 modal controllability matrix, given as

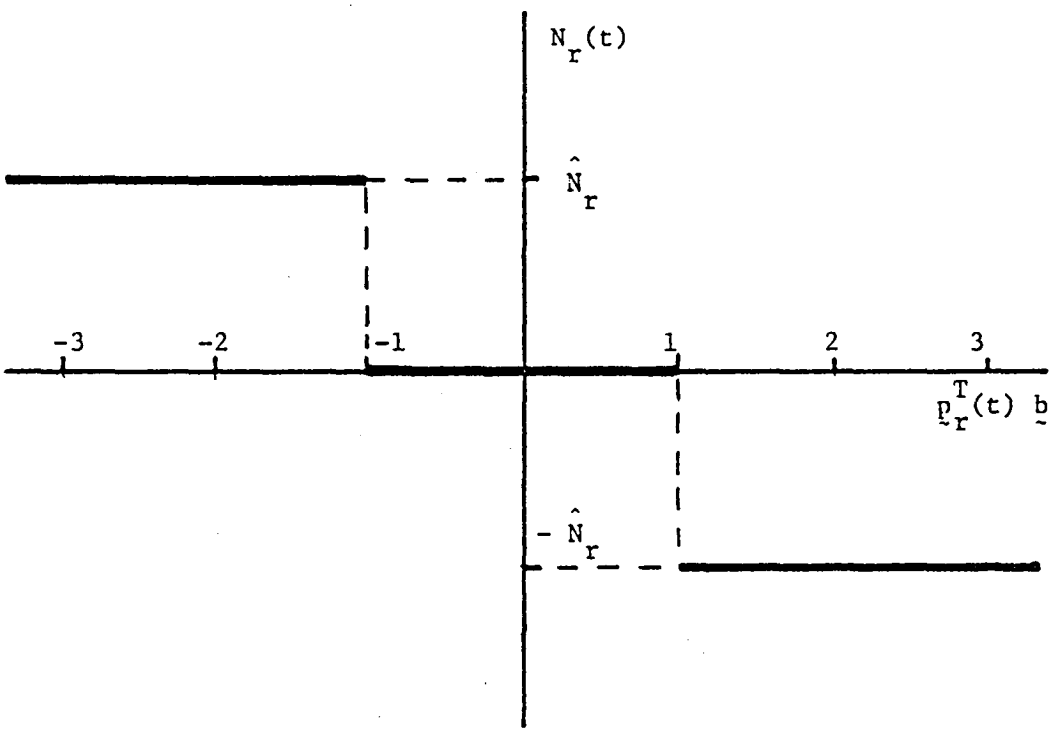

Figure 5.2: Modal Fuel-Optimal Control Function

$$E_r = [b \mid A_r\, b] \tag{5.34}$$

It is shown, that a necessary condition for a singular interval to exist requires that the matrix $[b \;\; A_r b]^T A_r^T$ be singular. This occurs when either the modal system, Eqs.(5.5) and (5.6), is not completely controllable, in which case $[b \;\; A_r b]$ is singular, or when the modal plant matrix A_r is singular. The modal controllability matrix has the non-singular form

$$E_r = \begin{bmatrix} 0 & 1 \\ 1 & 0 \end{bmatrix} \tag{5.35}$$

for both rigid or elastic modes, provided all modes are controllable. In contrast to the controllability matrix, the modal plant matrix A_r, given by Eq.(5.6b), becomes singular in the case of a rigid body mode for which $\omega_r=0$.
Hence, a necessary condition for a singular interval to exist is for the system given by Eqs.(5.5) and(5.6) not to be completely controllable, or for the plant matrix A_r to be singular.

In view of the above discussion, it is clear that each of the two mode-types, namely, rigid body modes and elastic

modes, possesses different properties. Therefore, it is appropriate to discuss the design of modal fuel-optimal control policies for these two unlike modes separately.

5.2 FUEL-OPTIMAL CONTROL FOR A RIGID BODY MODE

The control of a rigid body mode (RBM) in the modal space, resembles a single-axis attitude control of a unit-inertia space vehicle. Rigid body modes from the set of decoupled differential equations for the number of controlled modes described by Eqs.(2.77a), have the form

$$\ddot{\xi}_r(t) = N_r(t) \qquad r = 1,2,\ldots,n_r \qquad (5.36)$$

where n is the number of rigid body modes. Using the same state variable definition as in Eq.(5.6d), the modal state vector $\underset{\sim}{x}_r(t)$ satisfies the matrix differential equation

$$\begin{Bmatrix} \dot{x}_{1r}(t) \\ \dot{x}_{2r}(t) \end{Bmatrix} = \begin{bmatrix} 0 & 1 \\ 0 & 0 \end{bmatrix} \begin{Bmatrix} x_{1r}(t) \\ x_{2r}(t) \end{Bmatrix} + \begin{Bmatrix} 0 \\ 1 \end{Bmatrix} N_r(t) \qquad r = 1,2,\ldots,n_r \qquad (5.37)$$

It is desired to drive the modal plant from an arbitrary initial state given by

$$x_{1r}(0) = \xi_r(0) = \xi_{0r} \quad , \quad x_{2r}(0) = \xi_r(0) = \dot{\xi}_{0r} \quad r = 1,2,\ldots,n_r \qquad (5.38)$$

to a desired final state, say the origin, using a minimum amount of modal fuel, or

$$J_r(N_r) = \int_0^{t_f} |N_r(t)|dt \qquad r = 1,2,\ldots,n_r \quad (5.39)$$

subject to the constraints

$$|N_r(t)| \leqslant \hat{N}_r \qquad r = 1,2,\ldots,n_r \quad (5.40)$$

where $\hat{N}_r$ is the saturation value for the modal control force, as defined by Eq.(5.23), and t_f is the final time, which is free.

To this end, introduce the modal Hamiltonian

$$H_r(\underset{\sim}{x}_r,\underset{\sim}{p}_r,N_r,t) = |N_r(t)| + p_{1r}(t)\, x_{2r}(t) + p_{2r}(t)\, N_r(t) \qquad (5.41)$$
$$r = 1,2,\ldots,n_r$$

where, the costate variables p_{ir} (i=1,2) are the solutions of the adjoint system differential equations

$$\begin{Bmatrix} \dot{p}_{1r}(t) \\ \dot{p}_{2r}(t) \end{Bmatrix} = \begin{bmatrix} 0 & 0 \\ -1 & 0 \end{bmatrix} \begin{Bmatrix} p_{1r}(t) \\ p_{2r}(t) \end{Bmatrix} \qquad r = 1,2,\ldots,n_r \quad (5.42)$$

Note that even if the controls $N_r(t)$ are given as a function of time, Eqs.(5.42) will not uniquely define a vector $\underset{\sim}{p}_r(t)$,

because both the initial and terminal (final) conditions have been imposed on $\underset{\sim}{x}_r$, and no $\underset{\sim}{p}_r(0)$ boundary condition has been specified.

The minimization of the Hamiltonian H_r with respect to $N_r(t)$, leads to the control law

$$N_r(t) = -\hat{N}_r \text{ dez } \{p_{2r}(t)\} \qquad r = 1,2,\ldots,n_r \quad (5.43)$$

The optimization problem Eqs.(5.37) and (5.39) has thus been transformed into the problem of finding the solutions to the set of simultaneous Eqs.(5.37) and (5.42), with the control $N_r(t)$ given by Eqs.(5.43), with the boundary conditions

$$\underset{\sim}{x}_r(0) = \underset{\sim}{x}_{0r} \quad , \quad \underset{\sim}{x}_r(t_f) = \underset{\sim}{0} \quad (5.44)$$

specified, but with the final time t_f unspecified. The knowledge that the optimum $N_r(t)$ has the form of Eqs.(5.43) simplifies the optimization problem immeasurably. An important comment should be made at this stage: The Pontryagin theorem provides a necessary condition for the optimal control but not a sufficient one. In other words, if the theorem provides as a solution only one control function, this function is an optimum. However, more than one control function may satisfy the theorem, in which case it is necessary to search further for the optimum.

The solution to the costate equations, Eqs.(5.42) becomes

$$p_{1r}(t) = \eta_{1r} \tag{5.45a}$$

$$p_{2r}(t) = \eta_{2r} - \eta_{1r}\, t \tag{5.45b}$$

where

$$\eta_{1r} = p_{1r}(0) \quad , \quad \eta_{2r} = p_{2r}(0) \qquad r = 1,2,\ldots,n_r \tag{5.45c}$$

are unspecified constants.

Even though $p_{2r}(t)$ is not known as a function of time, the mere fact that $p_{2r}(t)$ is linear in time requires that $N_r(t)$ from Eqs.(5.43), must proceed in time as a nonrepeating sequence of values of the form $\{\pm\hat{N}\ ,0,\mp\hat{N}\ \}$ or any part of it. In view of this realization, if $\eta_{1r} \neq 0$ the only nine modal control sequences that can be candidates for the fuel-optimal control are

$$\{0\},\ \{+\hat{N}_r\},\ \{-\hat{N}_r\},\ \{+\hat{N}_r,0\},\ \{-\hat{N}_r,0\},\ \{0,+\hat{N}_r\},\ \{0,-\hat{N}_r\},$$
$$\{+\hat{N}_r,0,-\hat{N}_r\},\ \{-\hat{N}_r,0,+\hat{N}_r\} \qquad r = 1,2,\ldots,n_r \tag{5.46}$$

Figure 5.3 provides a description of these control sequences versus their costate counterparts. A control sequence like $\{-\hat{N}_r,0,+\hat{N}_r\}$ means that first $N\ (t)=-\hat{N}_r$, then $N_r(t)=0$ and finally $N_r(t)=+N_r$ are applied in this order. Therefore, in order to transfer the state to the origin from any point in the state plane, it will be necessary to use one of the con-

trol sequences given in Eqs.(5.46). Clearly, any other control sequence will violate the necessary condition for minimum-fuel control.

Solution to the state equations is obtained simply through a direct integration of Eqs.(5.37) with the initial state given by Eqs.(5.38) for the optimal control given by Eqs.(5.43). The solutions are

$$x_{1r}(t) = \xi_{0r} + \dot{\xi}_{0r}\, t \qquad r = 1,2,\ldots,n_r \quad (5.47a)$$

$$x_{2r}(t) = \dot{\xi}_{0r} \qquad r = 1,2,\ldots,n_r \quad (5.47b)$$

for $N_r(t)=0$ and

$$x_{1r}(t) = \xi_{0r} + \dot{\xi}_{0r}\, t + \frac{1}{2}\Delta_r t^2 \qquad r = 1,2,\ldots,n_r \quad (5.48a)$$

$$x_{2r}(t) = \dot{\xi}_{0r} + \Delta_r\, t \qquad r = 1,2,\ldots,n_r \quad (5.48b)$$

for $N_r(t)=\pm\hat{N}_r \stackrel{\Delta}{=} \Delta_r$.

State plane trajectories are then obtained by eliminating the time t from Eqs.(5.47) and (5.48)

$$x_{2r} = \dot{\xi}_{0r} = \text{const} \qquad r = 1,2,\ldots,n_r \quad (5.49)$$

$$x_{1r} = \xi_{0r} - \frac{1}{2\Delta_r}\dot{\xi}_{0r}^2 + \frac{1}{2\Delta_r}x_{2r}^2 \qquad r = 1,2,\ldots,n_r \quad (5.50)$$

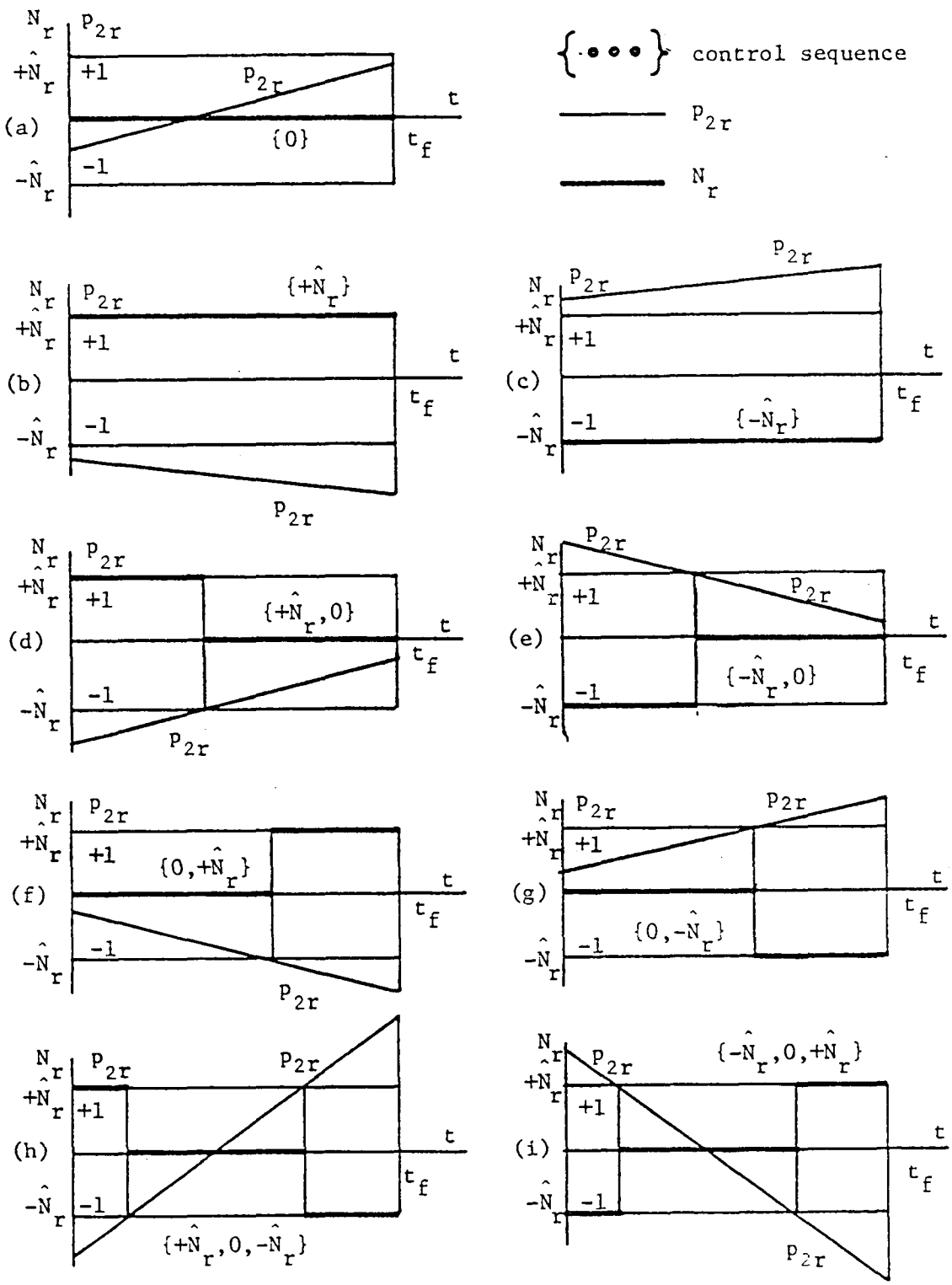

Figure 5.3: Candidates for Modal Fuel-Optimal Control for RBM

Equations (5.49) and (5.50), as well as Fig. 5.4a,b display these trajectories in the cases for which $N_r(t)=0$ and $N_r(t)=\pm\hat{N}_r$, respectively. Clearly, from Fig. 5.4, the only state that may be driven to the origin, using the control $N_r(t)=0$ is the state (0,0) itself. Moreover, for any other state, it is necessary that either $N_r(t)=+\hat{N}_r$ or $N_r(t)=-\hat{N}_r$ will be the final control portion, approaching the origin along the trajectories labeled as γ^+ and γ^- in Fig. 5.4b respectively.

From Eq.(5.50) it is clear that

$$\gamma_r^+ = \{(x_{1r},x_{2r}) : x_{1r} = \frac{1}{2\hat{N}_r} x_{2r}^2 \quad ; \quad x_{2r} \leqslant 0\} \qquad r = 1,2,\ldots,n_r \tag{5.51}$$

$$\gamma_r^- = \{(x_{1r},x_{2r}) : x_{1r} = -\frac{1}{2\hat{N}_r} x_{2r}^2 \quad ; \quad x_{2r} \geqslant 0\} \qquad r = 1,2,\ldots,n_r \tag{5.52}$$

The union of these two curves constructs the final switch curve γ_r for the modal minimum-fuel operation

$$\gamma_r = \{(x_{1r},x_{2r}) : x_{1r} = -\frac{1}{2\hat{N}_r} x_{2r}|x_{2r}|\} \qquad r = 1,2,\ldots,n_r \tag{5.53}$$

Based on these observations, clearly the fuel optimal solution depends on the modal initial state $(\xi_{0r},\dot{\xi}_{0r})$. Hence, we observe four regions in the modal state plane

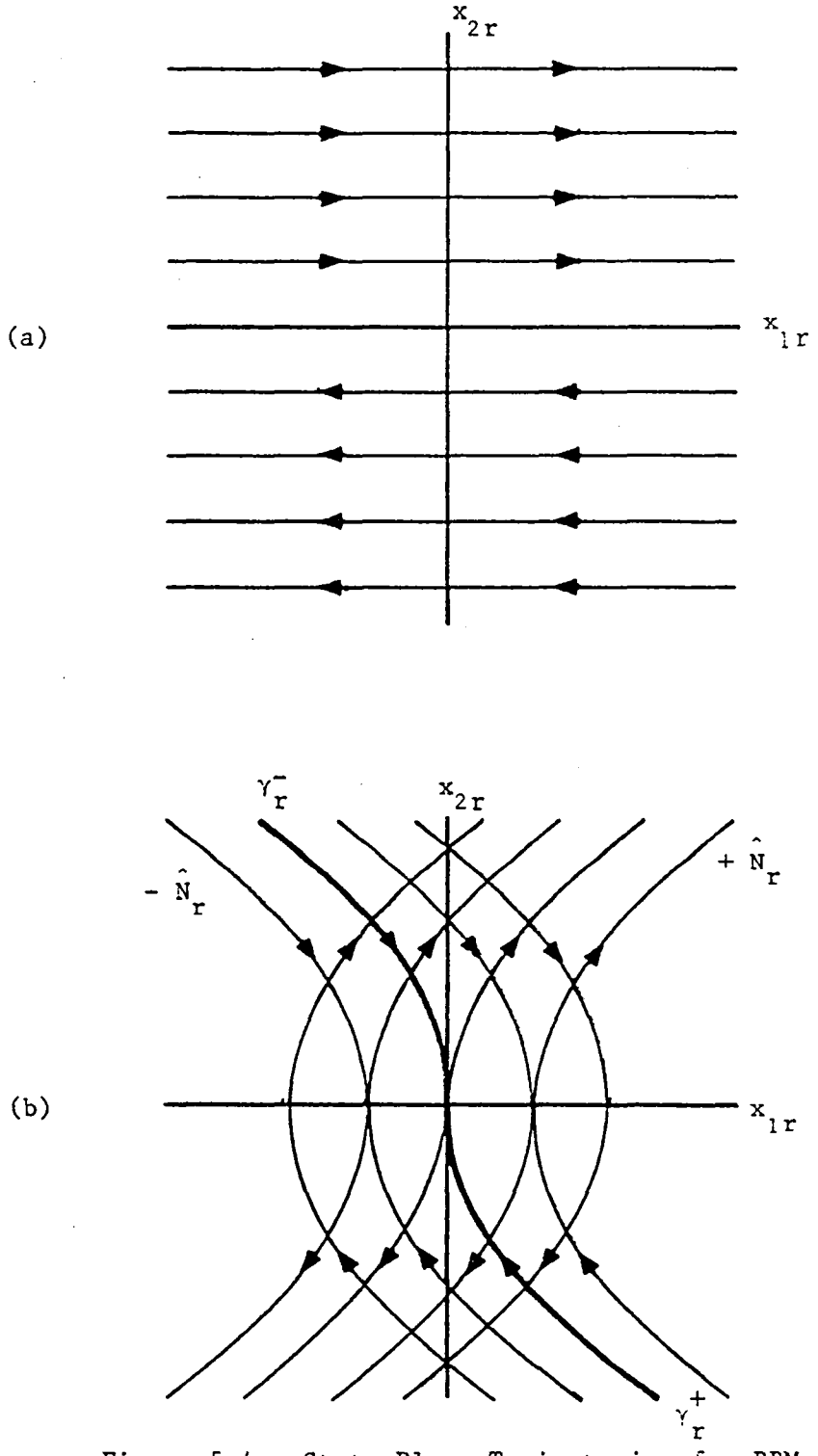

Figure 5.4: State Plane Trajectories for RBM
(a) $N_r(t) = 0$
(b) $N_r(t) = \pm \hat{N}_r$

$$R_1 = \{(x_{1r},x_{2r}) : x_{2r} \geqslant 0 \quad ; \quad x_{1r} > -\frac{1}{2\hat{N}_r} x_{2r}^2\} \tag{5.54a}$$

$$R_2 = \{(x_{1r},x_{2r}) : x_{2r} > 0 \quad ; \quad x_{1r} \leqslant -\frac{1}{2\hat{N}_r} x_{2r}^2\} \tag{5.54b}$$

$$R_3 = \{(x_{1r},x_{2r}) : x_{2r} \leqslant 0 \quad ; \quad x_{1r} < \frac{1}{2\hat{N}_r} x_{2r}^2\} \tag{5.54c}$$

$$R_4 = \{(x_{1r},x_{2r}) : x_{2r} < 0 \quad ; \quad x_{1r} \geqslant \frac{1}{2\hat{N}_r} x_{2r}^2\} \tag{5.54d}$$

These four regions are displayed in Fig. 5.5, as well as four cases of modal initial states, one in each of these regions.

It is shown in Appen. B that if $(\xi_{0r},\dot{\xi}_{0r}) \in R_1 \cup R_3$, then minimum-fuel control does not exist. If $(\xi_{0r},\dot{\xi}_{0r}) \in R_2 \cup R_4$, then the control sequence $\{0,-\hat{N}_r\}$ is a minimum-fuel control for $(\xi_{0r},\dot{\xi}_{0r}) \in R_2$, and $\{0,+\hat{N}_r\}$ is a minimum-fuel control for $(\xi_{0r},\dot{\xi}_{0r}) \in R_4$. Hence, depending on the initial state, there may or may not exist a fuel-optimal solution.

Fuel optimal systems with unspecified final time have the unfortunate property that the control resulting for the minimum expenditure of fuel, usually requires infinite final

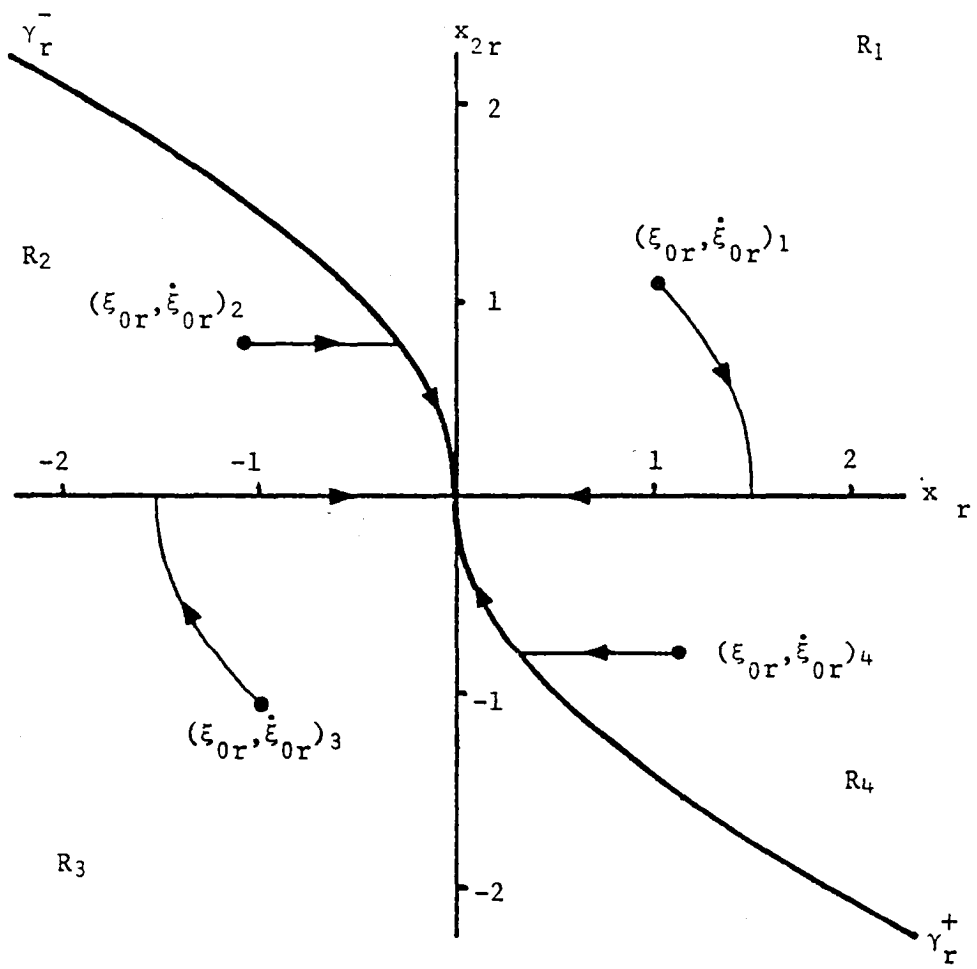

Figure 5.5: Four Regions of Control in the State Plane for RBM

time (See Appen. B). We could accept limitations of this type if the space under consideration is the configuration space, by limiting the initial state of the problem with unspecified final time just to a state subspace R_2UR_4. In general, it is very unlikely to expect the modal initial conditions obtained by the linear transformation Eq.(2.66) to have a specified distribution in the modal space and still deal with a practical problem. Solution to the minimum-fuel problem must be capable of handling any initial conditions in the modal state plane. We can clearly conclude from Eq.(B1.7) that, to assure the existence of a solution in region R_1UR_3, the response time, i.e., the final time t_f, must be either fixed a priori, or bounded from above by a fixed time T_f such that $t_f \leq T_f$. Thus we have to recognize the fact that bounding the response time will penalize fuel expenditure.

From the minimum-fuel solution, we can see that mode r arrives at the origin at a final time t_f, depending on the initial state, such that $t_{f\,min\,min} < t_{fr} < \infty$, where $t_{f\,min\,min}$ is the lower bound, i.e., the shortest time period in the minimum-time solution to reach the origin among all cont-

rolled modes, and t_f is the final time of the rth mode (See Appen. C for the minimum time solution for a second-order system). It is understood that the "modal mission" is incomplete as long as the last mode in the control scheme has not reached the specified target. Thus, the control task is to drive all the modes in the control scheme to the target (origin) in a bounded period of time. For the same reason, it is clear that no advantage is gained in driving one mode in a shorter time period then the others, consuming unecessary fuel. Therefore, we base our discussion on the premise that <u>all the modes in the control scheme are designed to arrive at the origin simultaneously</u>.

<u>Definition</u>

We shall say that T_f is a minimum upper bound for the control operation if

$$t_{f\ \mathbf{min\text{-}max}} \leqslant T_f \leqslant \infty \tag{5.55}$$

where $t_{f\ \min\ \max}$ is the largest minimum-time solution to reach the origin among all controlled modes. Certainly, T_f may be selected larger then the minimum upper bound to meet some fuel constrains.

Figure 5.6 displays a typical optimal path in the state plane for fixed final time with the control sequence

$\{-\hat{N}_r, 0, +\hat{N}_r\}$. To specify the control uniquely, two switch times t_z and t_w must be determined. This is done in Appen. C, where the switch times are obtained in the form

$$t_z = \frac{1}{2}\left\{T_f + t_0 + \frac{\dot{\xi}_{0r}}{\hat{N}_r} - \left[\left(T_f - t_0 - \frac{\dot{\xi}_{0r}}{\hat{N}_r}\right)^2 - \frac{4\xi_{0r}}{\hat{N}_r} - \frac{2\dot{\xi}_{0r}^2}{\hat{N}_r^2}\right]^{\frac{1}{2}}\right\} \tag{5.56a}$$

$$t_w = \frac{1}{2}\left\{T_f + t_0 + \frac{\dot{\xi}_{0r}}{\hat{N}_r} + \left[\left(T_f - t_0 - \frac{\dot{\xi}_0}{\hat{N}_r}\right)^2 - \frac{4\xi_{0r}}{\hat{N}_r} - \frac{2\dot{\xi}_{0r}}{\hat{N}_r^2}\right]^{\frac{1}{2}}\right\} \tag{5.56b}$$

From Eqs.(5.56) it is clear that both switch times depend on the modal initial conditions $(\xi_{0r}, \dot{\xi}_{0r})$ as well as on the specified final time T_f.

Before describing the optimal control for the minimum-fuel problem with specified final time, we recall one of the results obtained in Appen. B. It has been shown in case B.2, for the initial modal state $(\xi_{0r}, \dot{\xi}_{0r}) \epsilon R_4$, that the final time for the minimum-fuel problem, given by Eq.(B2.2), is

$$t_f = t_0 - \left(\frac{1}{2\hat{N}_r}\dot{\xi}_{0r} + \frac{\xi_{0r}}{\dot{\xi}_{0r}}\right) \tag{5.57}$$

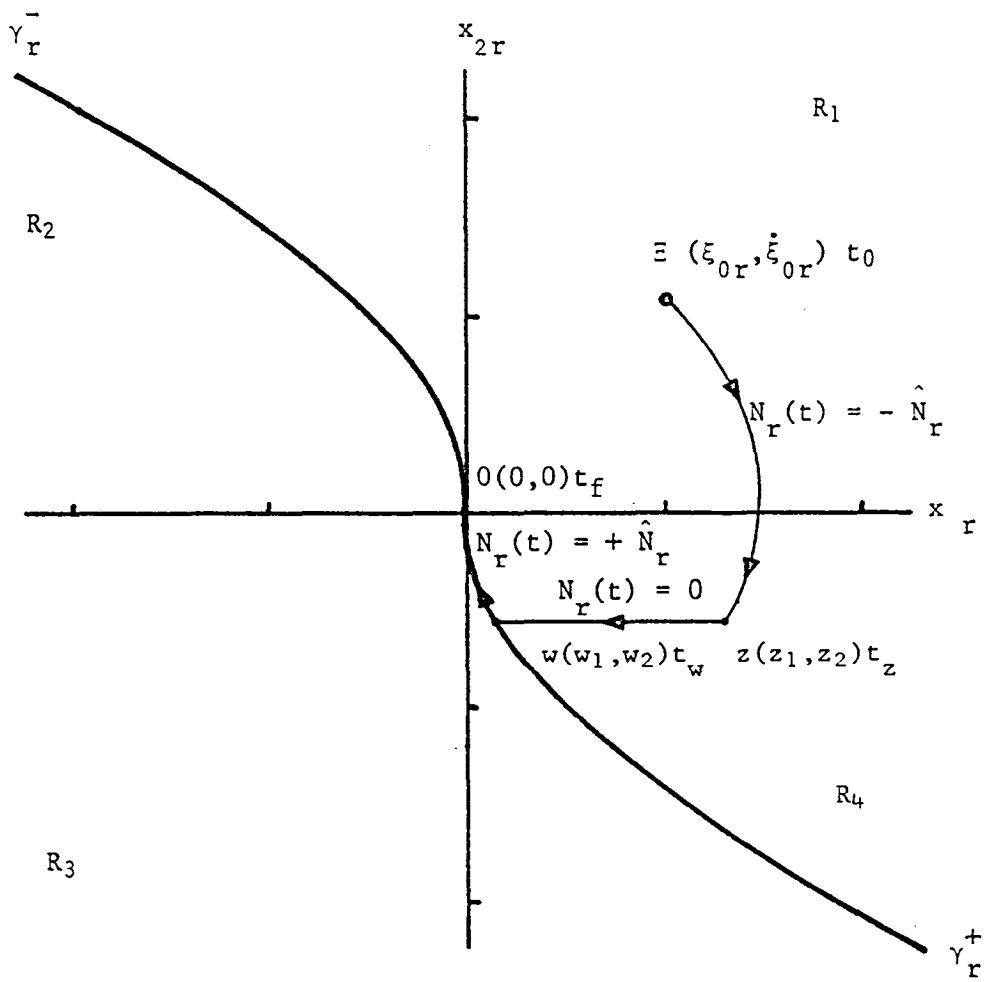

Figure 5.6: Modal State Plane Trajectories for RBM with Fixed Final Time

If the specified final time is $T_f > t_f$, where t_f is given by Eq.(5.57), clearly the state will reach the origin in less than the specified final time T_f with the minimum-fuel optimal control sequence $\{0, +N_r\}$. In this case, an exception is made by permitting the state to arrive at the origin not at the specified final time, because any adjustment to the final time will either result in the same fuel consumption or it will increase the fuel consumption, in contradiction to the basic approach for fuel minimization.

Related to the four state space regions R_1 to R_4, the minimum-fuel optimal control law has the following expressions:

$$
\left.
\begin{aligned}
&\left.\begin{aligned}
N_r(t) &= -\hat{N}_r \quad \text{for } t_0 \leqslant t < t_z \\
N_r(t) &= 0 \quad \text{for } t_z \leqslant t < t_w \\
N_r(t) &= +\hat{N}_r \quad \text{for } t_w \leqslant t \leqslant T_f
\end{aligned}\right\}
\begin{aligned}
&(\xi_{0r}, \dot{\xi}_{0r}) \in R_1 \text{ for all } T_f \\
&(\xi_{0r}, \dot{\xi}_{0r}) \in R_4 \text{ for } T_f \leqslant t_f^0
\end{aligned} \\
&\text{and we will select} \\
&\left.\begin{aligned}
N_r(t) &= 0 \quad \text{for } t_0 \leqslant t < t_1 \\
N_r(t) &= +\hat{N}_r \quad \text{for } t_1 \leqslant t < t_f^0 \\
N_r(t) &= 0 \quad \text{for } t_f^0 \leqslant t \leqslant T_f
\end{aligned}\right\}
(\xi_{0r}, \dot{\xi}_{0r}) \in R_4 \text{ for } T_f > t_f^0 \\
&\text{where} \\
&t_1 = t_0 + \frac{1}{2\hat{N}_r}\dot{\xi}_{0r} - \frac{\xi_{0r}}{\dot{\xi}_{0r}} \\
&t_f^0 = t_0 - \frac{1}{2\hat{N}_r}\dot{\xi}_{0r} - \frac{\xi_{0r}}{\dot{\xi}_{0r}} \\
&t_z = \frac{1}{2}\left\{T_f + t_0 + \frac{\dot{\xi}_{0r}}{\hat{N}_r} - \left[\left(T_f - t_0 - \frac{\dot{\xi}_{0r}}{\hat{N}_r}\right)^2 - \frac{4\xi_{0r}}{\hat{N}_r} - \frac{2\dot{\xi}_{0r}^2}{\hat{N}_r^2}\right]^{\frac{1}{2}}\right\} \\
&t_w = \frac{1}{2}\left\{T_f + t_0 + \frac{\dot{\xi}_{0r}}{\hat{N}_r} + \left[\left(T_f - t_0 - \frac{\dot{\xi}_{0r}}{\hat{N}_r}\right)^2 - \frac{4\xi_{0r}}{\hat{N}_r} - \frac{2\dot{\xi}_{0r}^2}{\hat{N}_r^2}\right]^{\frac{1}{2}}\right\}
\end{aligned}
\right\} \quad (5.58a)
$$

$$\left.\begin{array}{ll}
N_r(t) = +\hat{N}_r \text{ for } t_0 \leqslant t < t_z & \left.\begin{array}{l}(\xi_{0r},\dot{\xi}_{0r}) \in R_3 \text{ for all } T_f \\ (\xi_{0r},\dot{\xi}_{0r}) \in R_2 \text{ for } T_f \leqslant t_f^0\end{array}\right. \\
N_r(t) = 0 \quad \text{ for } t_z \leqslant t < t_w & \\
N_r(t) = -\hat{N}_r \text{ for } t_w \leqslant t \leqslant T_f & \\
\text{and we will select} & \\
N_r(t) = 0 \quad \text{ for } t_0 \leqslant t < t_1 & (\xi_{0r},\dot{\xi}_{0r}) \in R_2 \text{ for } T_f > t_f^0 \\
N_r(t) = -\hat{N}_r \text{ for } t_1 \leqslant t < t_f^0 & \\
N_r(t) = 0 \quad \text{ for } t_f^0 \leqslant t \leqslant T_f & \\
\text{where} & \\
t_1 = t_0 - \dfrac{1}{2\hat{N}_r}\dot{\xi}_{0r} - \dfrac{\xi_{0r}}{\dot{\xi}_{0r}} & \\
t_f^0 = t_0 + \dfrac{1}{2\hat{N}_r}\dot{\xi}_{0r} - \dfrac{\xi_{0r}}{\dot{\xi}_{0r}} & \\
t_z = \dfrac{1}{2}\left\{T_f + t_0 - \dfrac{\dot{\xi}_{0r}}{\hat{N}_r} - \left[\left(T_f - t_0 + \dfrac{\dot{\xi}_{0r}}{\hat{N}_r}\right)^2 + \dfrac{4\xi_{0r}}{\hat{N}_r} - \dfrac{2\dot{\xi}_{0r}^2}{\hat{N}_r^2}\right]^{\frac{1}{2}}\right\} & \\
t_w = \dfrac{1}{2}\left\{T_f + t_0 - \dfrac{\dot{\xi}_{0r}}{\hat{N}_r} + \left[\left(T_f - t_0 + \dfrac{\dot{\xi}_{0r}}{\hat{N}_r}\right)^2 + \dfrac{4\xi_{0r}}{\hat{N}_r} - \dfrac{2\dot{\xi}_{0r}^2}{\hat{N}_r^2}\right]^{\frac{1}{2}}\right\} &
\end{array}\right\} \tag{5.58b}$$

It is shown in Appen. C that the locus of the first optimal switch time t_z is a section of a second-order parabola in the forth quadrant, having the expression

$$Z_1 = -\left[\frac{3}{2\hat{N}_r} Z_2^2 + \left(T_f - t_0 - \frac{\dot{\xi}_{0r}}{\hat{N}_r}\right) Z_2\right] \tag{5.59}$$

For various values of the modal initial velocity, a family of parabolas will be necessary to describe the state at the first optimal switch time. Clearly, the second optimal switch time t_w occurs when the state trajectory intercepts the γ curve.

Definition

An initial modal state is said to be in reachable zone in the state plane, if the origin can be reached using the appropriate optimal control sequence in the prescribed final time bound.

It is shown in Appen. C that the reachable zone is bounded by two sectors of a second-order parabola

$$Z_1 = -\frac{1}{4\hat{N}_r}\left[Z_2^2 + 2(T_f - t_0)\hat{N}_r Z_2 - (T_f - t_0)^2 \hat{N}_r^2\right] \tag{5.60}$$

and its reflected image about the origin. To guarantee that all rigid body modes are inside the reachable zone, the final time T_f can be determined by the modified Eq.(5.60), or

$$T_f \geqslant t_0 + \max_{r=1,2,\ldots,n_r}\left\{\frac{\dot{\xi}_{0r}}{\hat{N}_r} + \left[2\left(\frac{\dot{\xi}_{0r}}{\hat{N}_r}\right)^2 + 4\,\frac{\xi_{0r}}{\hat{N}_r}\right]^{\frac{1}{2}}\right\} \tag{5.61}$$

for a modal initial state $(\xi_{0r}, \dot{\xi}_{0r}) \in R_1 \cup R_4$. Similarly, for $(\xi_{0r}, \dot{\xi}_{0r}) \in R_2 \cup R_3$, we obtain

$$T_f \geqslant t_0 + \max_{r=1,2,\ldots,n_r}\left\{-\frac{\dot{\xi}_{0r}}{\hat{N}_r} + \left[2\left(\frac{\dot{\xi}_{0r}}{\hat{N}_r}\right)^2 - 4\,\frac{\xi_{0r}}{\hat{N}_r}\right]^{\frac{1}{2}}\right\} \tag{5.62}$$

Clearly, Eqs.(5.61) and (5.62) resemble the minimum-time solution, Eqs.(C1.5) and (C1.6), respectively.

A dimensionless plot of Eqs.(5.51), (5.57), (5.59) and (5.60) is shown in Appen. C, Fig. C.2. The plot provides also a description of reachable zones for the various control regions, and switching curves for the optimal control law, Eqs.(5.58).

5.2.1 Fuel Consumed - RBM

The fuel consumption depends on the initial condition point Ξ in the modal state plane. Refering to Fig. C.2, for a point in region R^- (R^+), the modal fuel depends also on the first and second switch times t_z and t_w as shown in Fig. 5.6 and is given by

$$J_r(N_r) = \int_{t_0}^{t_z} \hat{N}_r \, dt + \int_{t_w}^{t_f} \hat{N}_r \, dt = \hat{N}_r(t_z - t_0 + t_f - t_w) \tag{5.63}$$

For a point in region R^0, the modal fuel is given by

$$J_r(N_r) = \int_{t_1}^{t_f^0} \hat{N}_r \, dt = \hat{N}_r(t_f^0 - t_1) \tag{5.64}$$

Expressions for the times t_0, t_z, t_w, t_f, t_1 and t_f^0 are provided in Eqs.(5.58). The total modal fuel for the RBM's is

obtained by summing all modal fuels in Eqs.(5.63) and (5.64), depending on the different modal initial conditions, or

$$J(\underset{\sim}{N}_{n_r}) = \sum_{r=1}^{n_r} J_r(\hat{N}_r) \tag{5.65}$$

5.3 FUEL-OPTIMAL CONTROL FOR AN ELASTIC MODE

Formulation of the control problem for an Elastic Mode (EM) has a similar pattern, to the one of a rigid body mode. The control of an elastic mode in the modal space is tantamount to controlling a set of linear oscillators system. The derivation of the control law in terms of the costate variables can be accomplished very easily. However, the task of determining the initial conditions of the costate variable is not a straightforward procedure. In practice, a common technique is to assume a final value of the costate variables and run the system backward in time from the origin, using the optimal control law, until the state trajectory intercepts the initial state in the state plane. The idea of running time backwards is most useful for second-order systems, because all the switching is determined by a switching curve. It is of decreasing usefulness as the ord-

er of the system increases, as this would require switching surfaces in the phase space. Clearly, the ability of using second-order system techniques in the analysis of a high-order system is another advantage of the IMSC method.

The differential equations for the elastic modes have the decoupled form

$$\ddot{\xi}_r(t) + \omega_r^2\, \xi_r(t) = N_r(t) \qquad r = 1,2,\ldots,n_e \tag{5.66}$$

where n_e is the number of elastic modes in the control scheme. Using the same state variable definition as in Eq.(5.6d), the modal state vector $\underset{\sim}{x}_r(t)$ satisfies the matrix differential equation

$$\begin{Bmatrix} \dot{x}_{1r}(t) \\ \dot{x}_{2r}(t) \end{Bmatrix} = \begin{bmatrix} 0 & 1 \\ -\omega_r^2 & 0 \end{bmatrix} \begin{Bmatrix} x_{1r}(t) \\ x_{2r}(t) \end{Bmatrix} + \begin{Bmatrix} 0 \\ 1 \end{Bmatrix} N_r(t) \qquad r = 1,2,\ldots,n_e \tag{5.67}$$

Here again, it is the control task to drive the modal plant form an arbitrary initial state given by

$$\underset{\sim}{x}_r(0) = [x_{1r}(0) \quad x_{2r}(0)]^T = [\xi_{0r} \quad \dot{\xi}_{0r}]^T \tag{5.68}$$

to the state origin in the final time t_f, or

$$\underset{\sim}{x}_r(t_f) = \underset{\sim}{0} \tag{5.69}$$

while minimizing the modal fuel expenditure

$$J_r(N_r) = \int_0^{t_f} |N_r(t)|\, dt \qquad r = 1,2,\ldots,n_e \qquad (5.70)$$

The control signal $N_r(t)$ is bounded in magnitude by

$$|N_r(t)| \leqslant \hat{N}_r \qquad r = 1,2,\ldots,n_e \qquad (5.71)$$

while the control bounds are defined by Eq.(5.23).

The modal Hamiltonian associated with Eqs.(5.67) and (5.70) has the form

$$\begin{aligned} H_r(\underset{\sim}{x}_r,\underset{\sim}{p}_r,N_r,t) = |N_r(t)| &+ p_{1r}(t)\, x_{2r}(t) - p_{2r}(t)\, \omega_r^2\, x_{1r}(t) \\ &+ p_{2r}(t)\, N_r(t) \qquad r = 1,2,\ldots,n_e \end{aligned} \qquad (5.72)$$

where the costate variables p_{ir} (i=1,2) are the solution of the adjoint system differential equations

$$\begin{Bmatrix} \dot{p}_{1r}(t) \\ \dot{p}_{2r}(t) \end{Bmatrix} = \begin{bmatrix} 0 & \omega_r^2 \\ -1 & 0 \end{bmatrix} \begin{Bmatrix} p_{1r}(t) \\ p_{2r}(t) \end{Bmatrix} \qquad r = 1,2,\ldots,n_e \qquad (5.73)$$

The minimization of the Hamiltonian H_r with respect to $N_r(t)$, leads to a control law similar to that obtained previously for the rigid body mode solution, namely,

$$N_r(t) = -\hat{N}_r \text{ dez } \{p_{2r}(t)\} \qquad r = 1,2,\ldots,n_e \qquad (5.74)$$

However, here, $p_{2r}(t)$ is the solution to the costate Eqs.(5.73). Rewriting these equations in scalar form, we obtain

$$\ddot{p}_{2r}(t) + \omega_r^2\, p_{2r}(t) = 0 \tag{5.75a}$$

$$p_{1r}(t) = -\,\dot{p}_{2r}(t) \qquad r = 1,2,\ldots,n_e \tag{5.75b}$$

The solution to Eqs.(5.75a) becomes

$$p_{2r}(t) = P_r \sin\,(\omega_r t + \theta_r) \qquad r = 1,2,\ldots,n_e \tag{5.76}$$

where P_r and θ_r are unspecified modal constants, since no boundary conditions were imposed on the costate vector $\underset{\sim}{p}_r(t)$. To determine a control law in Eqs.(5.74) that will drive the state to the origin, these constants must be specified.

To obtain the optimal solution to the state equations, we can rewrite Eqs.(5.67) in scalar form by substituting the optimal control law of Eqs.(5.74), so that

$$\ddot{x}_{1r}(t) + \omega_r^2\, x_{1r}(t) = N_r(t) \tag{5.77a}$$

$$x_{2r}(t) = \dot{x}_{1r}(t) \qquad r = 1,2,\ldots,n_e \tag{5.77b}$$

Equations (5.77) are subject to the boundary conditions (5.68). Considering the elements of control $N_r(t)=0$ and $N_r(t)=\pm\hat{N}_r$, one obtains the solutions

$$x_{1r}(t) = \frac{\dot{\xi}_{0r}}{\omega_r} \sin \omega_r t + \xi_{0r} \cos \omega_r t \tag{5.78a}$$

$$\frac{x_{2r}(t)}{\omega_r} = \frac{\dot{\xi}_{0r}}{\omega_r} \cos \omega_r t - \xi_{0r} \sin \omega_r t \qquad r = 1,2,\ldots,n_e \tag{5.78b}$$

for $N_r(t)=0$ and

$$x_{1r}(t) = \frac{\dot{\xi}_{0r}}{\omega_r} \sin \omega_r t + \left(\xi_{0r} - \frac{\Delta_r}{\omega_r^2}\right) \cos \omega_r t + \frac{\Delta_r}{\omega_r^2} \tag{5.79a}$$

$$\frac{x_{2r}(t)}{\omega_r} = \frac{\dot{\xi}_{0r}}{\omega_r} \cos \omega_r t - \left(\xi_{0r} - \frac{\Delta_r}{\omega_r^2}\right) \sin \omega_r t \quad r = 1,2,\ldots,n_e \tag{5.79b}$$

for $N_r(t)=\pm\hat{N}_r \overset{\Delta}{=} \Delta_r$

State plane trajectories are obtained by eliminating the time t from Eqs.(5.78) and (5.79), with the result

$$x_{1r}^2 + \left(\frac{x_{2r}}{\omega_r}\right)^2 = \xi_{0r}^2 + \left(\frac{\dot{\xi}_{0r}}{\omega_r}\right)^2 \qquad r = 1,2,\ldots,n_e \tag{5.80}$$

$$\left(x_{1r} - \frac{\Delta_r}{\omega_r^2}\right)^2 + \left(\frac{x_{2r}}{\omega_r}\right)^2 = \left(\xi_{0r} - \frac{\Delta_r}{\omega_r^2}\right)^2 + \left(\frac{\dot{\xi}_{0r}}{\omega_r}\right)^2 \qquad r = 1,2,\ldots,n_e \tag{5.81}$$

for $N_r(t)=0$ and $N_r(t)=\Delta_r$, respectively.

Depending upon the modal initial conditions, Eqs.(5.80) and (5.81) represent families of circles in the modal state plane with coordinates x_{1r} and x_{2r}/ω . The centers of these circles lie at 0, $+\hat{N}/\omega_r^2$, $-\hat{N}_r/\omega_r^2$ on the x_{1r} axis for the control actions 0, $+\hat{N}_r$, $-\hat{N}_r$ respectively, as given by

Eqs.(5.74) and (5.76). We designate these families according to the related controls, such as the 0, the $+\hat{N}_r$ and the $-\hat{N}_r$ family. Figure 5.7 shows these circles in the state plane, as well as an arbitrary state trajectory formed by the control sequence $-\hat{N}_r$ for $t_0<t\le t_1$, 0 for $t_1<t\le t_2$, $+\hat{N}_r$ for $t_2,t\le t_3$, 0 for $t_3<t\le t_4$ and $+\hat{N}_r$ for $t_4<t\le t_f$. Clearly, any arbitrary trajectory in the state plane that terminates at the origin, must use circle γ_r^+ or γ_r^- as the last portion of the trajectory.

Based on this observation and utilizing the harmonic nature of the costate functions in Eqs.(5.73), one can construct qualitatively a trajectory pattern in the modal state plane. Figure 5.8 provides a description of the costate function for a certain control sequence, as well as the associated trajectory.

To recover the time from the state plane, we use the definition of the normalized time scale $\tau=\omega t$, where t is the real time. It is shown in Appen. D that

$$\Delta\tau=\Delta\beta \tag{5.82}$$

where $\Delta\beta$ is an angle segment of a circular arc Δs along the trajectory.

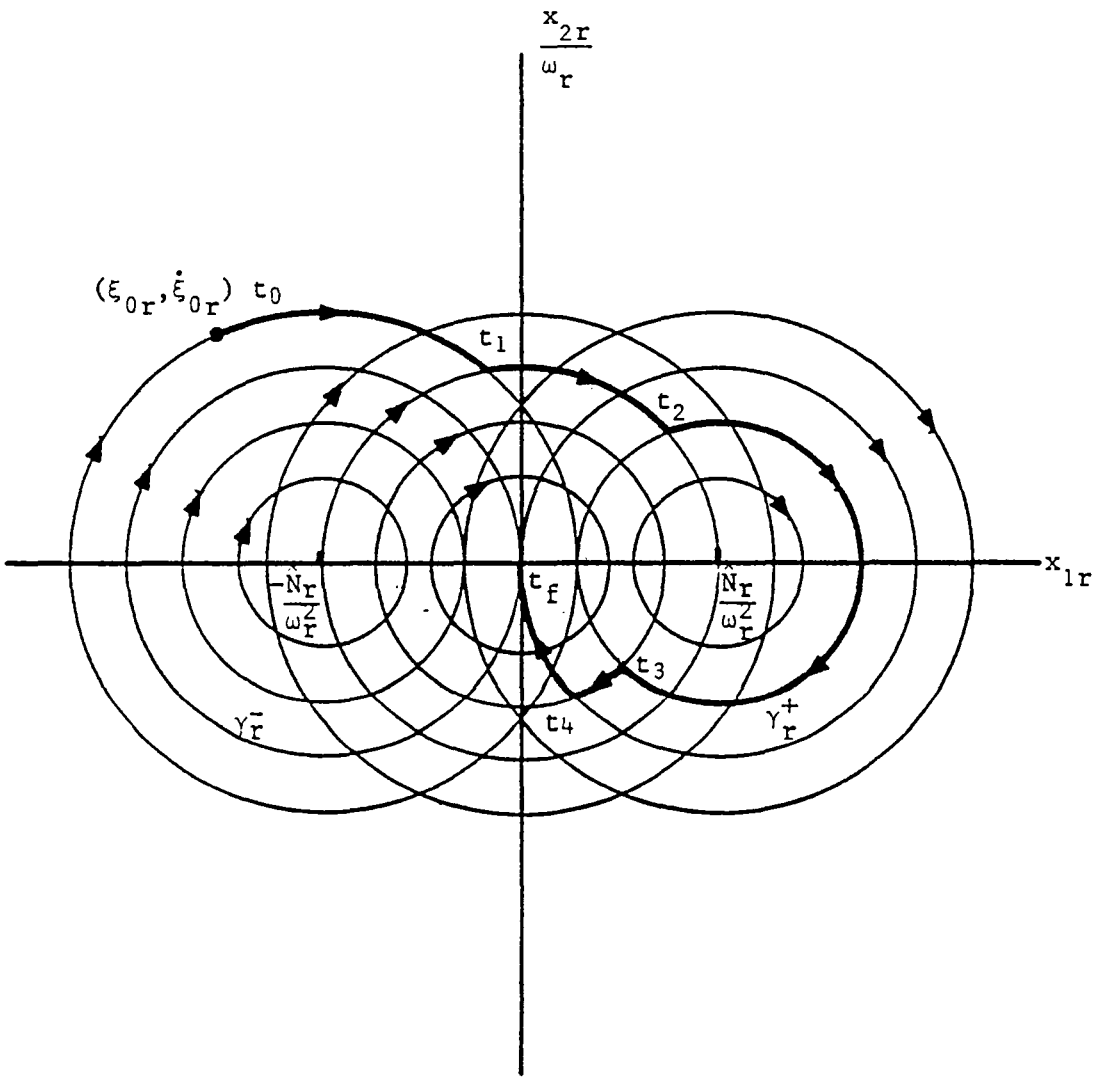

Figure 5.7: Modal State Trajectories Families for EM

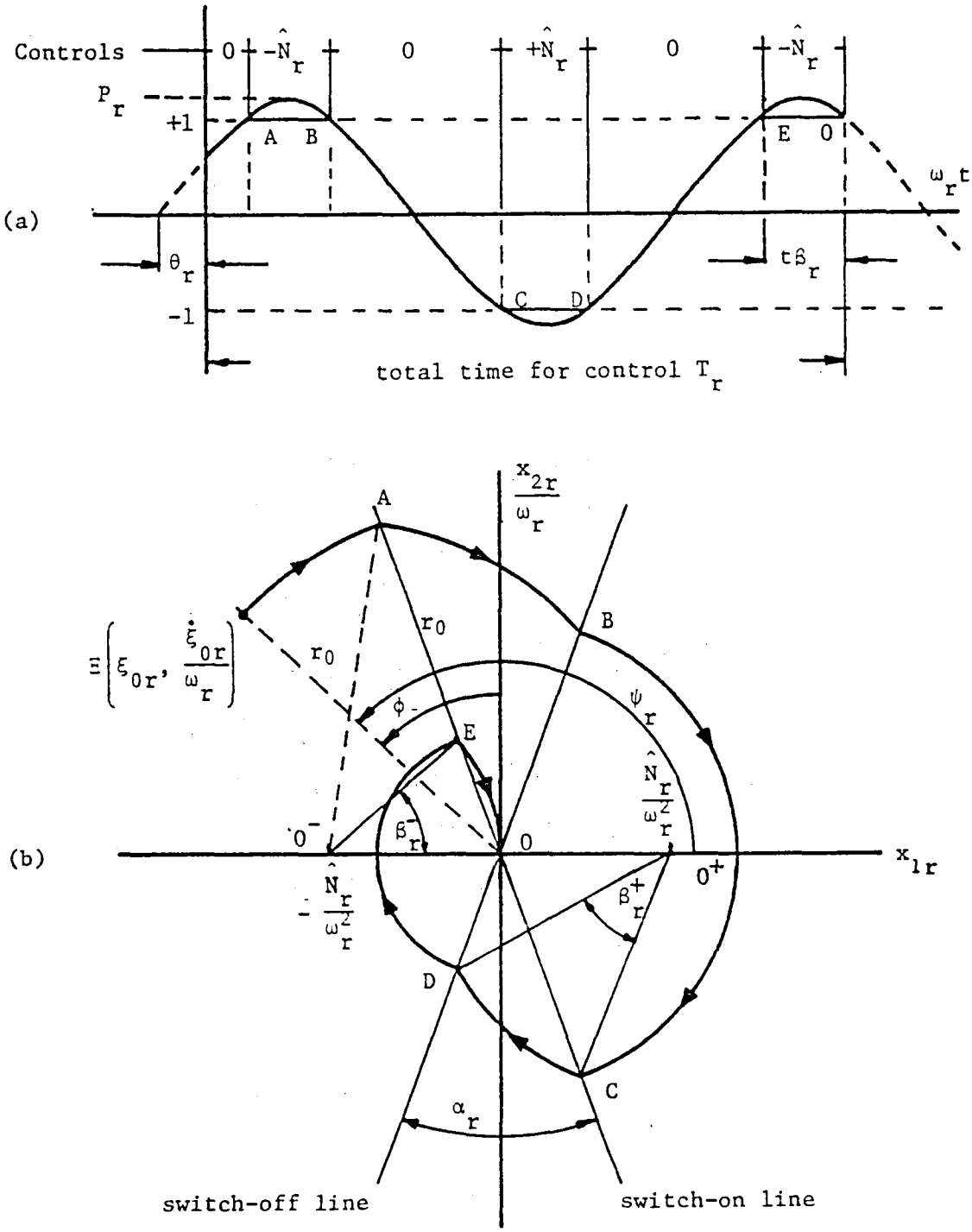

Figure 5.8: Modal State Trajectory vs Modal Costate Function for EM
(a) Modal Costate Function $p_{2r}(t)$
(b) The Associated Modal State Plane Trajectories

Because the optimal controls, Eqs.(5.74) are functions of the costate functions $p_{2r}(t)$, to construct the optimal state trajectory we utilize geometric information available from the description of the costate function. The fact that the trajectory is a path constructed from circular arcs given by Eqs.(5.80) and (5.81) is utilized as well. As can be seen from Fig. 5.8a, all the control portions are of the same duration, i.e., $t_{AB}=t_{CD}=t_{EO}$. This observation, using Eq.(5.82), implies that the angles of the control segments in the state plane must be of the same magnitude, i.e.,

$$\text{angle } (AO^{-}B) = \text{angle } (CO^{+}D) = \text{angle } (EO^{-}O) \triangleq \beta_r \tag{5.83}$$

etc. These observations play an imnportant role in the construction of the state plane trajectory. A simple geometric approach shows that for Eqs.(5.83) to hold true in the state plane, the <u>control</u> <u>sector</u> angle α_r must be symmetric about the x_{2r} axis. In addition, it can be shown that

$$\alpha_r = \beta_r \tag{5.84}$$

These observations enable us to calculate the costate constants P_r and θ_r.

In Appen. D, two cases corresponding to different types of initial condition points in the state plane are investigated. In the first, the point lies <u>outside the control sector ($\phi \geq \alpha/2$),</u>

as shown in Fig. D.2. For this case the costate amplitude constant is obtained as

$$P_r = \left[1 - \left(\frac{r_0\ \omega_r^2}{2n_c\ \hat{N}_r}\right)^2\right]^{-\frac{1}{2}} \tag{5.85}$$

where

$$r_0 = \left(\xi_{0r}^2 + \frac{\dot{\xi}_{0r}^2}{\omega_r^2}\right)^{\frac{1}{2}} \qquad r = 1,2,\ldots,n_e \tag{5.86}$$

is the length of the initial condition position vector in the state plane and n is the number of full non-zero control strokes. The costate phase constant is obtained as

$$\theta_r = \Pi - \psi_r = \pi - \arctan\left(\frac{\dot{\xi}_{0r}}{\omega_r\ \xi_{0r}}\right) \qquad r = 1,2,\ldots,n_e \tag{5.87}$$

where the argument in Eq.(5.87) depends on the quadrant of location of the initial condition point $\Xi(\xi_{0r}, \dot{\xi}_{0r}/\omega_r)$. In the second case, the initial condition point lies <u>inside the control sector ($\phi \leq \alpha'/2$)</u> in the state plane, as shown in Fig. D.3. For this case, the costate amplitude constant is obtained as

$$P_r = \left[1 - \frac{r_0^2 - 2\,\frac{\hat{N}_r}{\omega_r^2}\,r_0\,\sin\phi}{4(n_c^2 - n_c)\left(\frac{\hat{N}_r}{\omega_r^2}\right)^2}\right]^{-\frac{1}{2}} \qquad r = 1,2,\ldots,n_e \tag{5.88}$$

r_0 has the expression of Eq.(5.86).

The costate phase constant for this case has the form

$$\theta_r = \Pi - \psi_r + \delta_r = \Pi - \arctan\left(\frac{\dot{\xi}_{0r}}{\omega_r\ \xi_{0r}}\right) + \delta_r \qquad r = 1,2,\ldots,n_e \qquad (5.89)$$

where, from Appen. D

$$\delta_r = \arcsin\left\{\frac{\dfrac{N_r}{\omega_r^2}\cos\phi}{\left[r_0^2 + \left(\dfrac{\hat{N}_r}{\omega_r^2}\right)^2 - 2r_0\dfrac{\hat{N}_r}{\omega_r^2}\sin\phi\right]^{\frac{1}{2}}}\right\}$$

$$- \arcsin\left\{\frac{\dfrac{N_r}{\omega_r^2}\cos\dfrac{\alpha'}{2}}{\left[r_0^2 + \left(\dfrac{\hat{N}_r}{\omega_r^2}\right)^2 - 2r_0\dfrac{\hat{N}_r}{\omega_r^2}\sin\phi\right]^{\frac{1}{2}}}\right\} \qquad r = 1,2,\ldots,n_e \qquad (5.90)$$

is the phase constant correction factor. In these expressions, $\phi_r = \psi_r - \pi/2$, as can be seen in Fig. 5.8, D.2 and D.3.

5.3.1 Fuel Consumed and Final Time Selection - EM

1. Initial condition point lies outside the control sector

$\phi \geq \alpha/2$

In view of Fig. 5.8, the modal fuel consumed can be calculated as follows:

$$F_r = \hat{N}_r \, n_c \, t_{\alpha r} \tag{5.91}$$

In this expression, $n_c t_{\alpha r}$ is the total time for non-zero control applications. $t_{\alpha r}$ is obtained by using the concept of normalized time, or

$$t_{\alpha r} = \frac{\alpha_r}{\omega_r} \tag{5.92}$$

Using Eq.(D2.6),

$$F_r = \frac{2n_c \, \hat{N}_r}{\omega_r} \arcsin \frac{r_0 \, \omega_r^2}{2n_c \, \hat{N}_r} \tag{5.93}$$

so that letting

$$\frac{r_0 \, \omega_r^2}{2n_c \, \hat{N}_r} = p_1 \qquad 0 \leqslant p_1 \leqslant 1 \tag{5.94}$$

the normalized fuel is obtained from Eq.(5.93) in the form

$$\frac{F_r}{r_0 \, \omega_r} = \frac{1}{p_1} \arcsin p_1 \tag{5.95}$$

Using again Fig. 5.8, the normalized time for solution can be calculated as

$$\tau = \phi + (n_c - 1)\pi + \arcsin p_1 \tag{5.96}$$

Clearly, from Eq.(5.96) $\tau \to \infty$ as $n \to \infty$ or in view of Eq.(5.94), as $p_1 \to 0$. However, the fuel in Eq.(5.95) reaches its abso-

lute minimum at the same time and it is a simple task to show that

$$F_{r\,min} = \lim_{p_1 \to 0} F_r = r_0\,\omega_r \tag{5.97}$$

A similar result was obtained in the case of RBM, where in order to obtain minimum fuel solution, the time had to approach infinity. Here again, a realization of such a solution is made by a selection of finite time for solution, in a similar manner as to the RBM case.

Figure 5.9 provides a description of the normalized fuel given by Eq.(5.95) and the normalized time of Eq.(5.96) for the case $\phi=\pi/2$, $n_c=k_1/p_1$ for various values of k_1, where

$$k_1 = \frac{r_0\,\omega_r^2}{2\hat{N}_r} \tag{5.98}$$

is a modal parameter. For this case, Eq.(5.96) has the special form

$$\tau = \left(\frac{k_1}{p_1} - \frac{1}{2}\right)\pi + \arcsin p_1 \tag{5.99}$$

and, in addition,

$$\lim_{p_1 \to 1} \tau = k_1\,\pi \tag{5.100}$$

2. Initial condition point lies inside the control sector

$\phi \leq \alpha'/2$

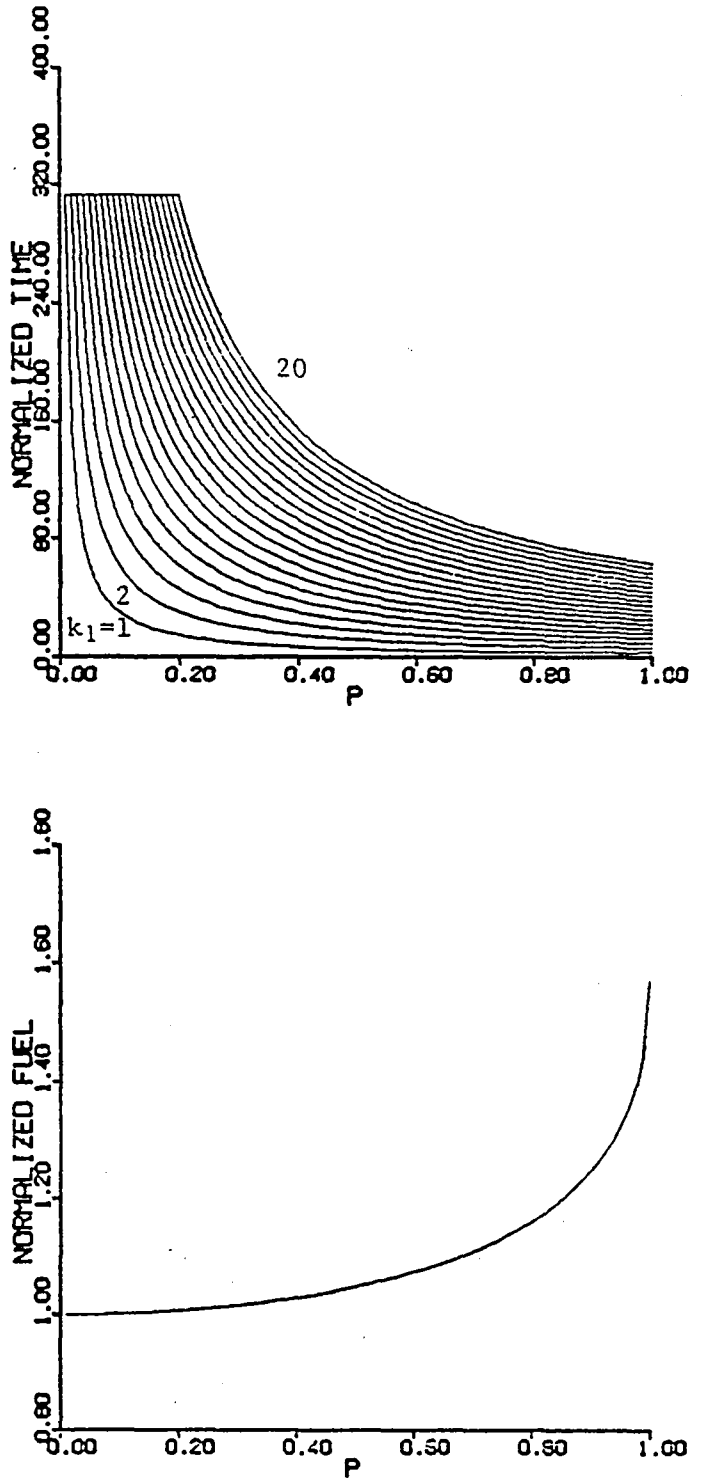

Figure 5.9: Realization of Minimum-Fuel Solution (case 1)

Following a similar pattern, the fuel consumed is obtained as follows

$$F_r = \frac{\hat{N}_r}{\omega_r}\left\{(2n_c-1)\ \arcsin\left[\frac{r_0^2 - 2\frac{\hat{N}_r}{\omega_r^2}\, r_0\ \sin\phi}{4(n_c^2-n_c)}\right]^{\frac{1}{2}} + \phi - \delta\right\} \tag{5.101}$$

Letting

$$\frac{r_0^2 - 2\frac{\hat{N}_r}{\omega_r^2}\, r_0\ \sin\phi}{4(n_c^2 - n_c)\left(\frac{\hat{N}_r}{\omega_r^2}\right)^2} = p_2^2 \qquad 0 \leqslant p_2 \leqslant 1 \tag{5.102}$$

defining the modal parameter

$$\frac{r_0^2 - 2\frac{\hat{N}_r}{\omega_r^2}\, r_0\ \sin\phi}{4\left(\frac{\hat{N}_r}{\omega_r^2}\right)^2} = k_2 \tag{5.103}$$

and inserting Eq.(5.103) into Eq.(5.102), we obtain

$$n_c = \frac{1 + (p_2^2 + 4k_2)^{\frac{1}{2}}}{2p_2} \tag{5.104}$$

Assuming that the correction factor δ is small compared to other terms, Eq.(5.101) can be written as

$$\frac{F_r}{\hat{N}_r/\omega_r} \approx \left[\frac{1 + (p_2^2 + 4k_2)^{\frac{1}{2}}}{p_2} - 1\right] \arcsin p_2 + \phi \tag{5.105}$$

Equation (5.105) represents an expression for the normalized modal fuel.

In view of Fig. D.3a and using the same assumption for δ, the normalized time for solution is obtained in the form

$$\tau = (\eta_1-\eta_2) + (n_c-1)\alpha' + (n_c-1)(\pi-\alpha')$$

$$\simeq \phi + (n_c-1)\pi + \arcsin\left[\frac{r_0^2 - 2\,\frac{\hat{N}_r}{\omega_r^2}\,r_0\,\sin\phi}{4(n_c^2 - n_c)\left(\frac{N_r}{\omega_r^2}\right)^2}\right] \tag{5.106}$$

Using the notation of Eq.(5.102), Eq.(5.106) can be reduced to

$$\tau = \phi + (n_c-1)\pi + \arcsin p_2 \tag{5.107}$$

Clearly, from Eq.(5.107) $\tau\to\infty$ as $n_c\to\infty$, or in view of Eq.(5.102), as $p_2\to 0$. However, the fuel in Eq.(5.105) reaches then its absolute minimum

$$F_{r\,min} \simeq \lim_{p_2\to 0} F_r = \frac{\hat{N}_r}{\omega_r}\,(1 + 2k_2^{\frac{1}{2}}) + \phi \tag{5.108}$$

Using the notation of Eqs.(5.102) and (5.103), the normalized time in Eq.(5.107) can be written as

$$\tau \simeq \phi + \left(\frac{1 + (p_2^2 + 4k_2)^{\frac{1}{2}}}{2p_2} - 1\right)\pi + \arcsin p_2 \tag{5.109}$$

Figure 5.10 provides a description of the normalized fuel of Eq.(5.105) and the normalized time of Eq.(5.109) for the case $\phi=0$. For this case, Eq.(5.109) has the special form

$$\tau \approx \left(\frac{1 + (p_2^2 + 4k_2)^{\frac{1}{2}}}{2p_2} - 1\right)\pi + \arcsin p_2 \tag{5.110}$$

In addition,

$$\lim_{p_2 \to 1} \tau \approx \frac{\pi}{2}(1 + 4k_2)^{\frac{1}{2}} \tag{5.111}$$

After the time for solution has been selected then the modal fuel is calculated according to the process described in Figs. (5.9) and (5.10).

The total modal fuel for the EM's is obtained by summing all the modal fuels in Eqs.(5.95) and (5.105), depending on the different modal initial conditions. A numerical example for the fuel minimization problem is presented in Ch. VI.

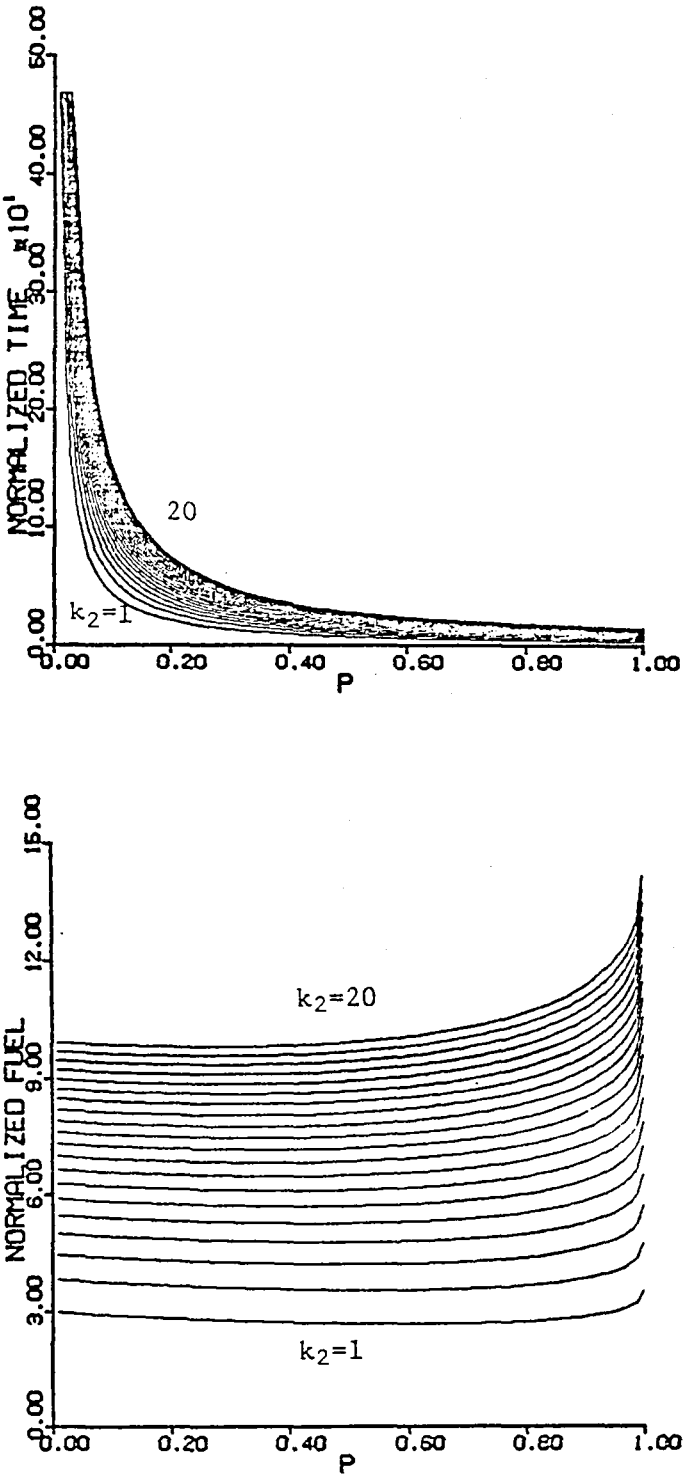

Figure 5.10: Realization of Minimum-Fuel Solution (case 2)

Chapter VI

NUMERICAL EXAMPLES

The control concepts presented in the last three chapters are illustrated by two numerical examples. The equations of motion for the structure were derived by the finite element method, as described in Chapter II. Considering one element per beam member and four members per cable branch, the order of the system displayed in Fig. 1.1 is n=270. For the present examples, a reduced order model of the structure, such as the one displayed in Fig. 2.1, is used. The model has 45 degrees of freedom.

The following structure parameters were considered:

<u>Beam member (aluminum)</u>

length of member	$l=12$ inches
cross-sectional width	$a=2$ inches
cross-sectional thickness	$b=0.25$ inches
mass density	$\rho=9.93\times10^{-2}$ lb/in^3
modulus of elasticity	$E=10\times10^6$ psi
Poisson ratio	$\nu=0.3$
rectangular cross-section torsion factor	$k=0.3$

<u>Cable member (steel)</u>

length of member	$l=20$ inches
equivalent diameter	$d=0.0442$ inches
mass density	$\rho=19.75\times10^{-2}$ lb/in^3
modulus of elasticity	$E=24\times10^6$ psi
Poisson ratio	$\nu=0.3$

Other structure configuration parameters, are as in Fig. 2.1

An eigenvalue problem was solved for the reduced-order system. The first twelve natural frequencies are given in Tab. 6.1 and the associated modes are displayed in Fig. 6.1. The system is excited by initial velocities, generated by an impulsive force, as shown in Fig. 6.2. Mode participation factors for the first twelve modes are displayed in Fig. 6.3, in view of which we retain the first six modes for control, because no further benefits are gained by controlling higher modes.

We propose to control the structure by the IMSC method, which requires as many actuators as the number of controlled modes. Placement of these actuators is based on results obtained in Chapter IV, as well as on the location of the nodal lines in the higher uncontrolled modes. Examining the

first six modes in Fig. 6.1, we observe that four of them have symmetric mode shapes, while the remaining two, have antisymmetric mode shapes. Actuators placed as shown in Fig. 6.4, meet the requirement of Eq.(4.12) for system controllability. Moreover, actuators in this configuration barely excite the seventh, eight and ninth modes, because their locations are on, or close to nodal lines of these higher modes. Clearly, the given impulse at node 8 excites only the symmetric modes. The given actuators configuration represents a symmetric set. To this end, the actuators at nodes 1 and 11 must have identical characteristics to those at nodes 5 and 15 respectively.

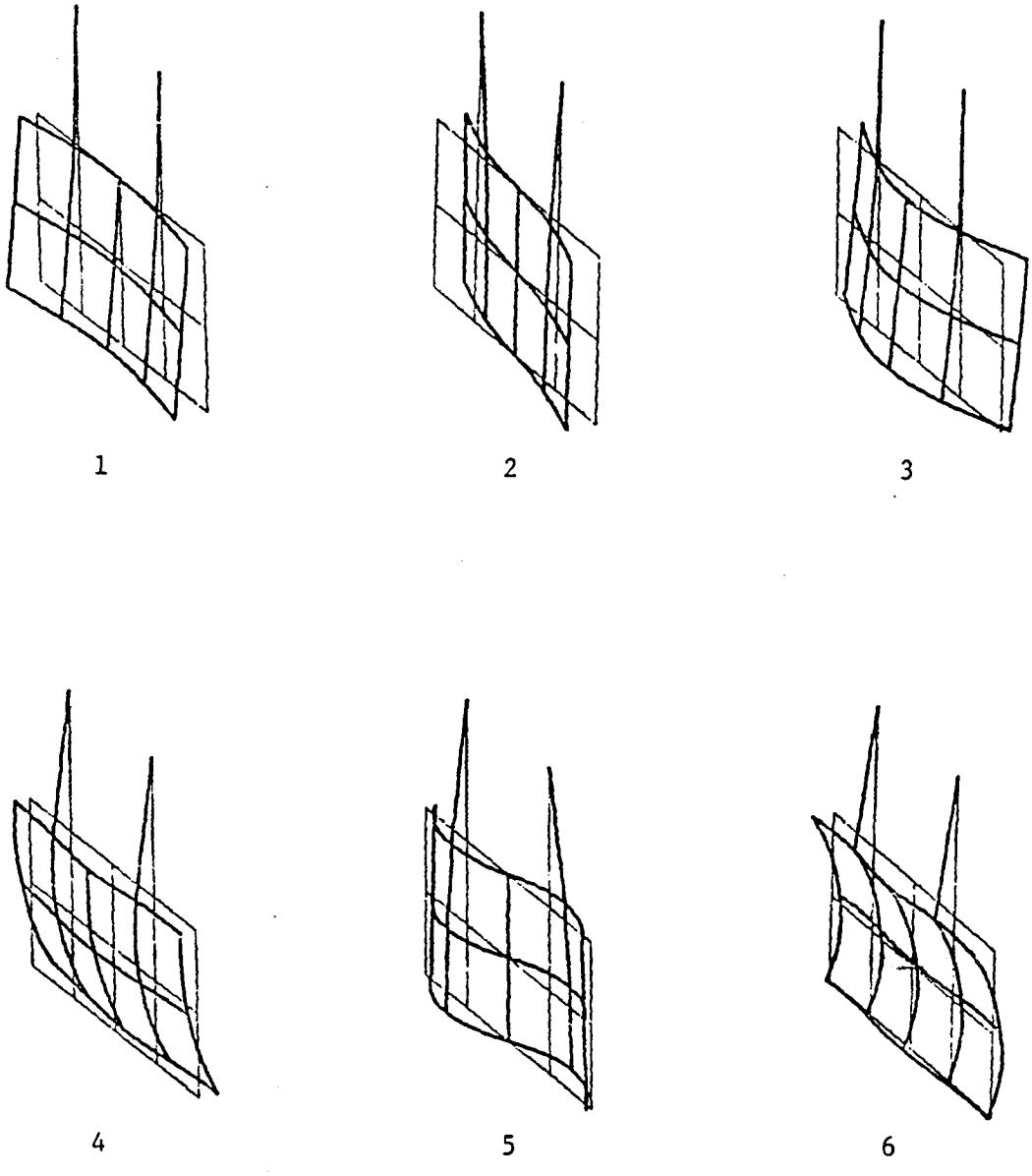

Figure 6.1: The Twelve Lowest Modes of Vibration

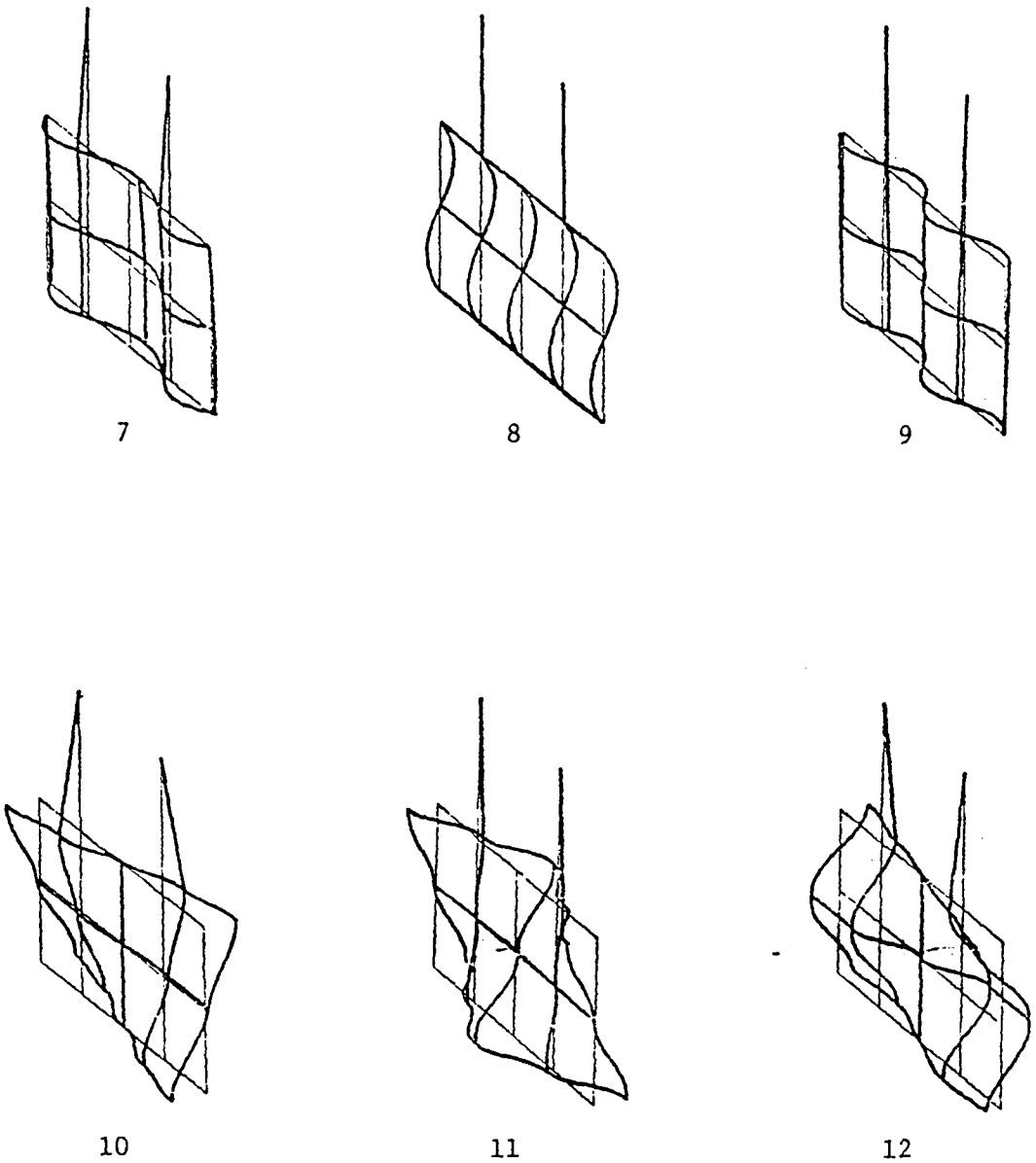

Figure 6.1: (cont.)

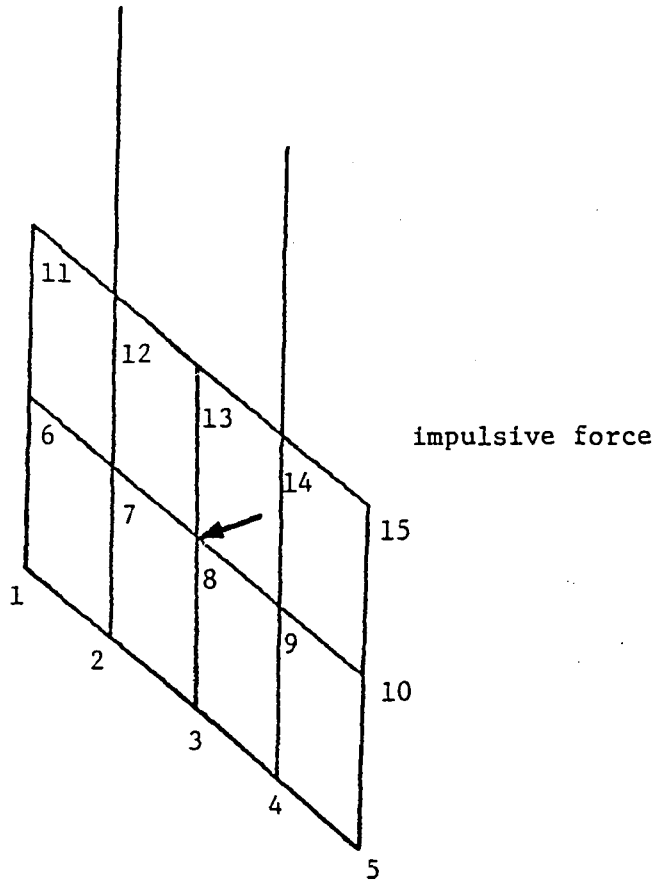

Figure 6.2: System Initial Conditions

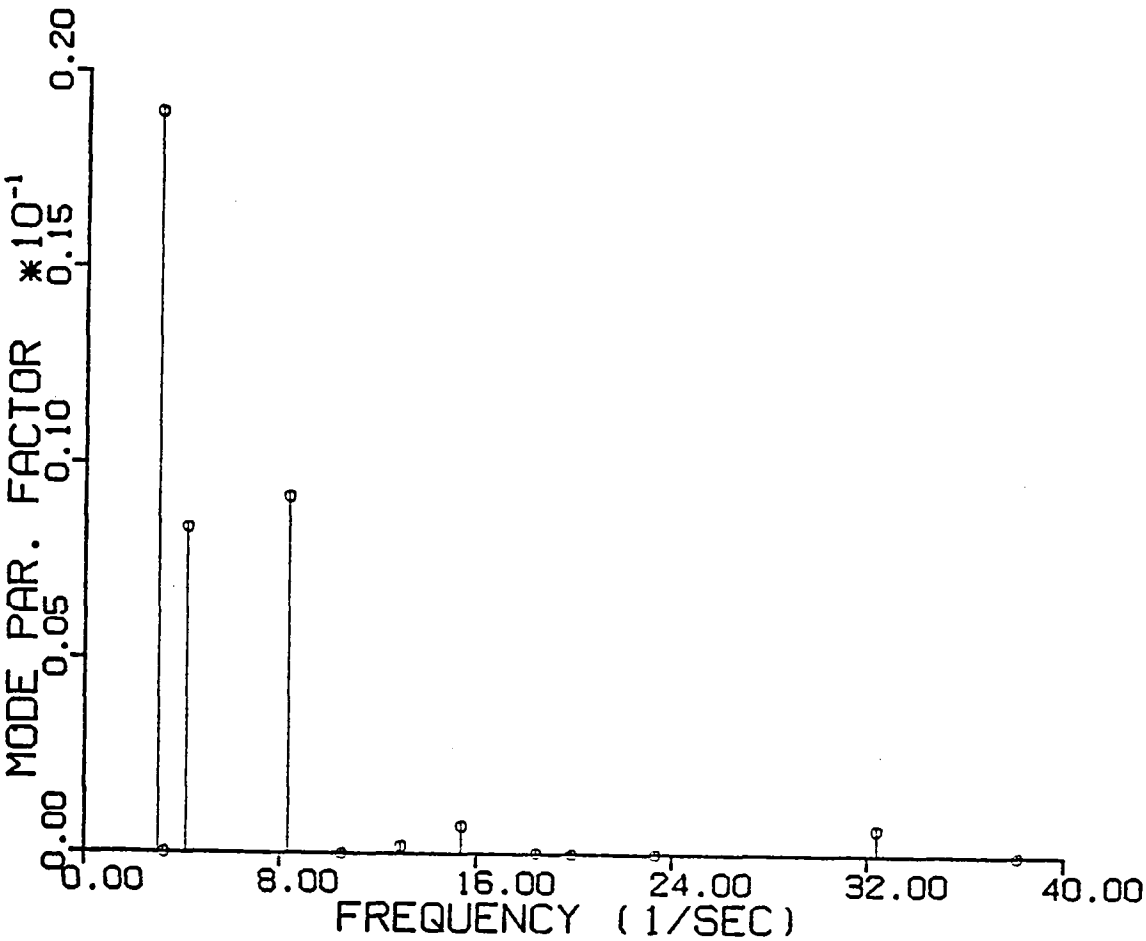

Figure 6.3: Mode Participation Factors

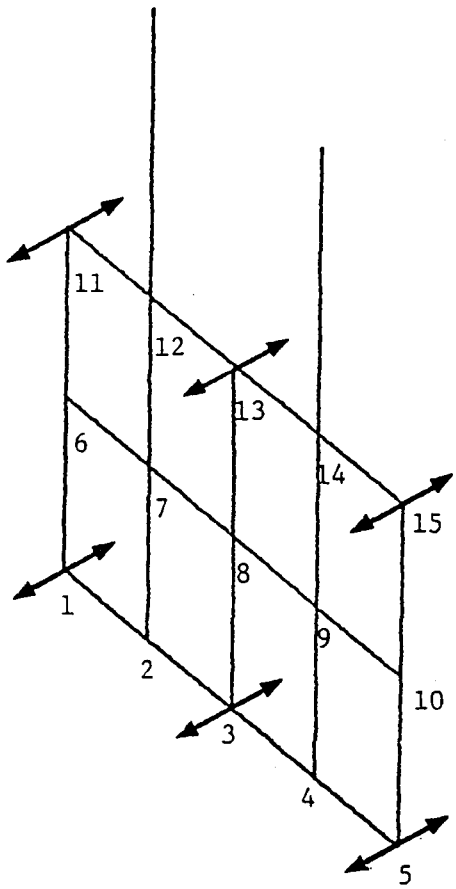

Figure 6.4: Actuators Placement Configuration

6.1 LINEAR OPTIMAL CONTROL WITH QUADRATIC PERFORMANCE INDEX

Implementation of Linear Optimal Control policy, using the IMSC method is based on the derivations of Chapter III. The control effort weighting factors R_r, are chosen so that the lowest controlled mode reach an approximate settling time of 3 seconds for 5% of the initial amplitude. To obtain the appropriate modal damping ratio of ζ=0.33, we use Eq.(3.18) or Fig. 3.1, and select p=4.00. In addition, a structural damping ratio of ζ=0.05 was considered. The response parameters of Eqs.(3.15) are displayed in Tab. 6.1.

The response is presented in the form of the transverse motion in four selected nodes. Figure 6.5 displays the actual response at nodes 1,3,8, and 14 for the uncontrolled as well as for the controlled cases. Figure 6.6 presents the modal forces while Fig. 6.7 presents actuators forces versus time. Finally, assuming that the control forces are proportional to the rate of flow of fuel, Fig. 6.8 provides the total consumed fuel versus time.

TABLE 6.1

System Parameters in the Linear Optimal Control Framework

Mode r	Natural Frequency ω_r	Damping Ratio ζ_r	Modified Frequency ω_{nr}	Damped Frequency ω_{dr}	Phase Angle ψ_r
1	2.995780	0.379679	3.167651	2.930451	0.389449
2	3.259080	0.379679	3.446057	3.188010	0.389449
3	4.161381	0.379679	4.400122	4.070633	0.389449
4	8.371135	0.379679	8.851396	8.188587	0.389449
5	10.537362	0.379679	11.141903	10.307579	0.389449
6	12.932981	0.379679	13.674960	12.650956	0.389449
7	15.402695				
8	18.471893				
9	19.938034				
10	23.332260				
11	32.394440				
12	38.127151				

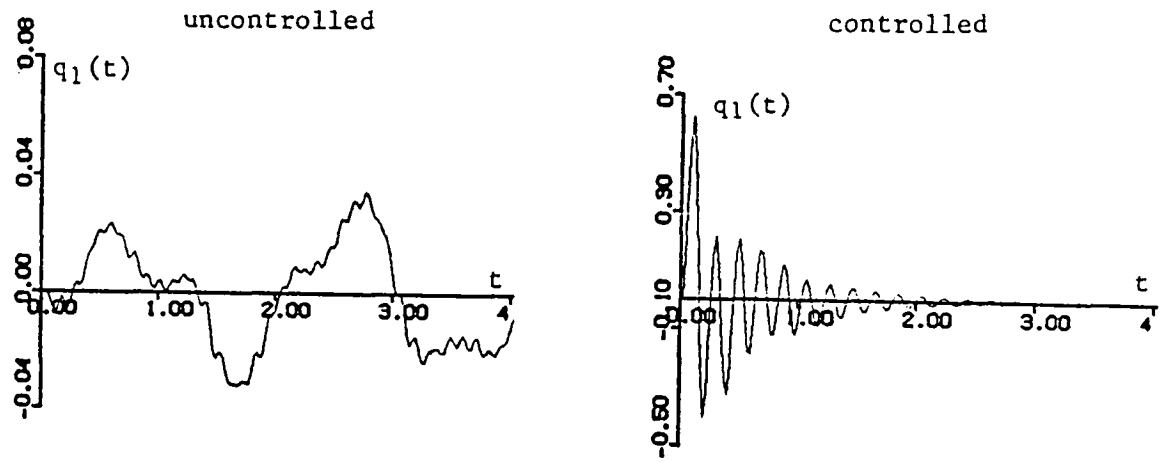

node 1

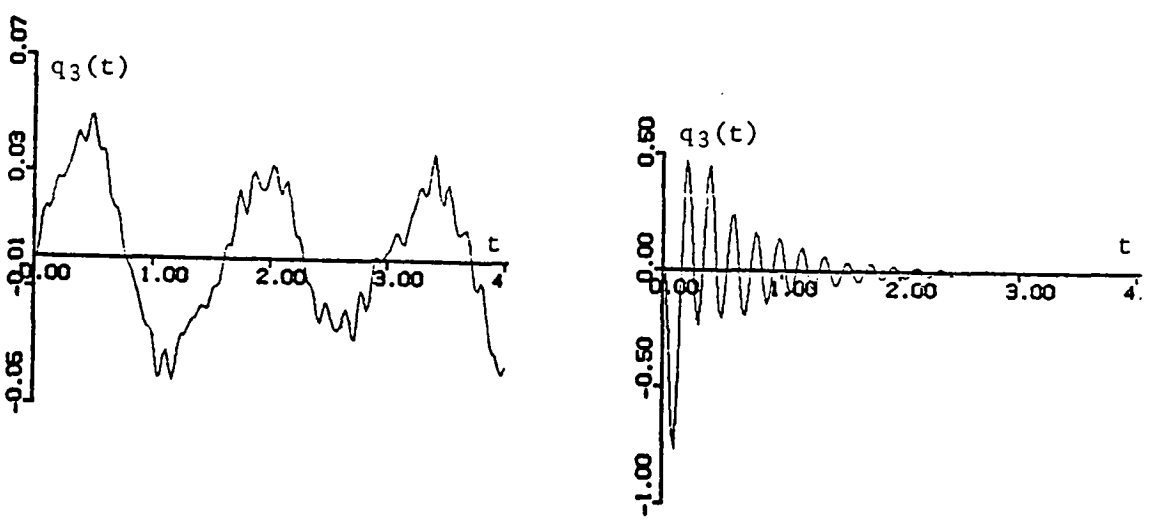

node 3

Figure 6.5: Actual Response at Nodes 1,3,8 and 14

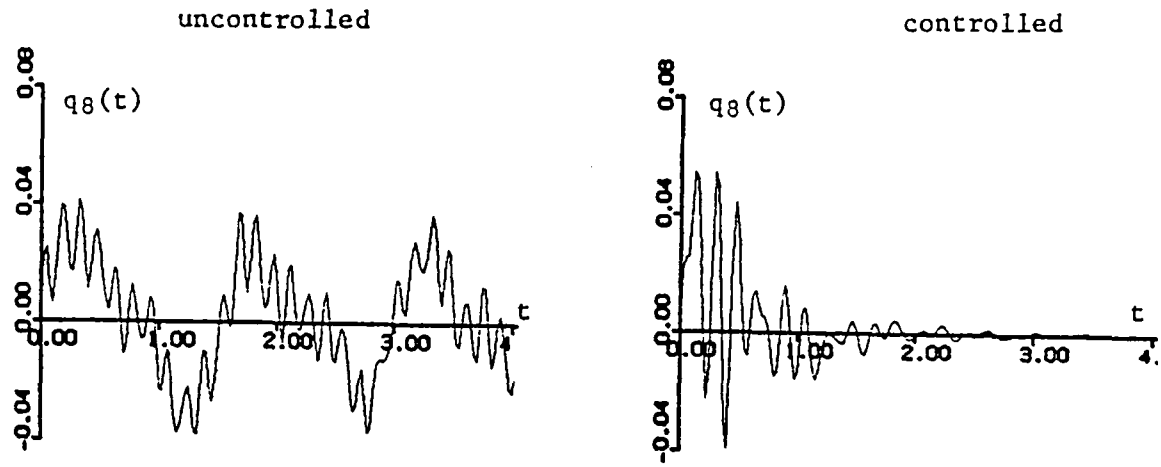

node 8

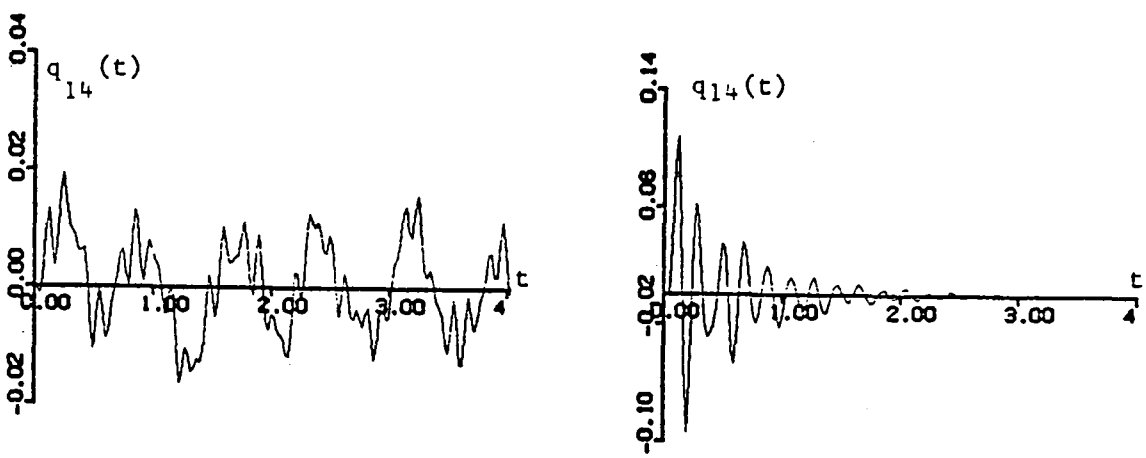

node 14

Figure 6.5: (cont.)

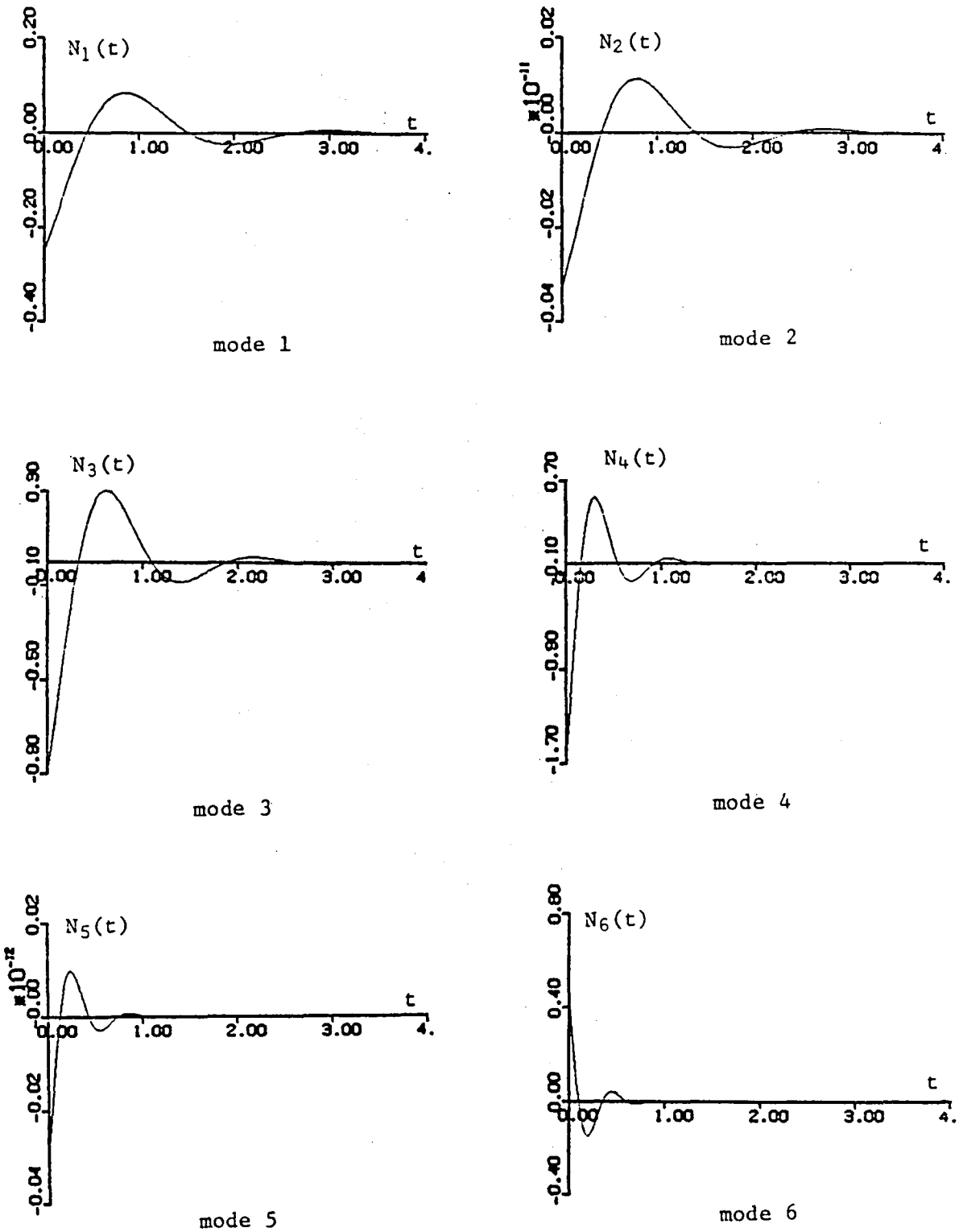

Figure 6.6: Modal Control Forces vs Time

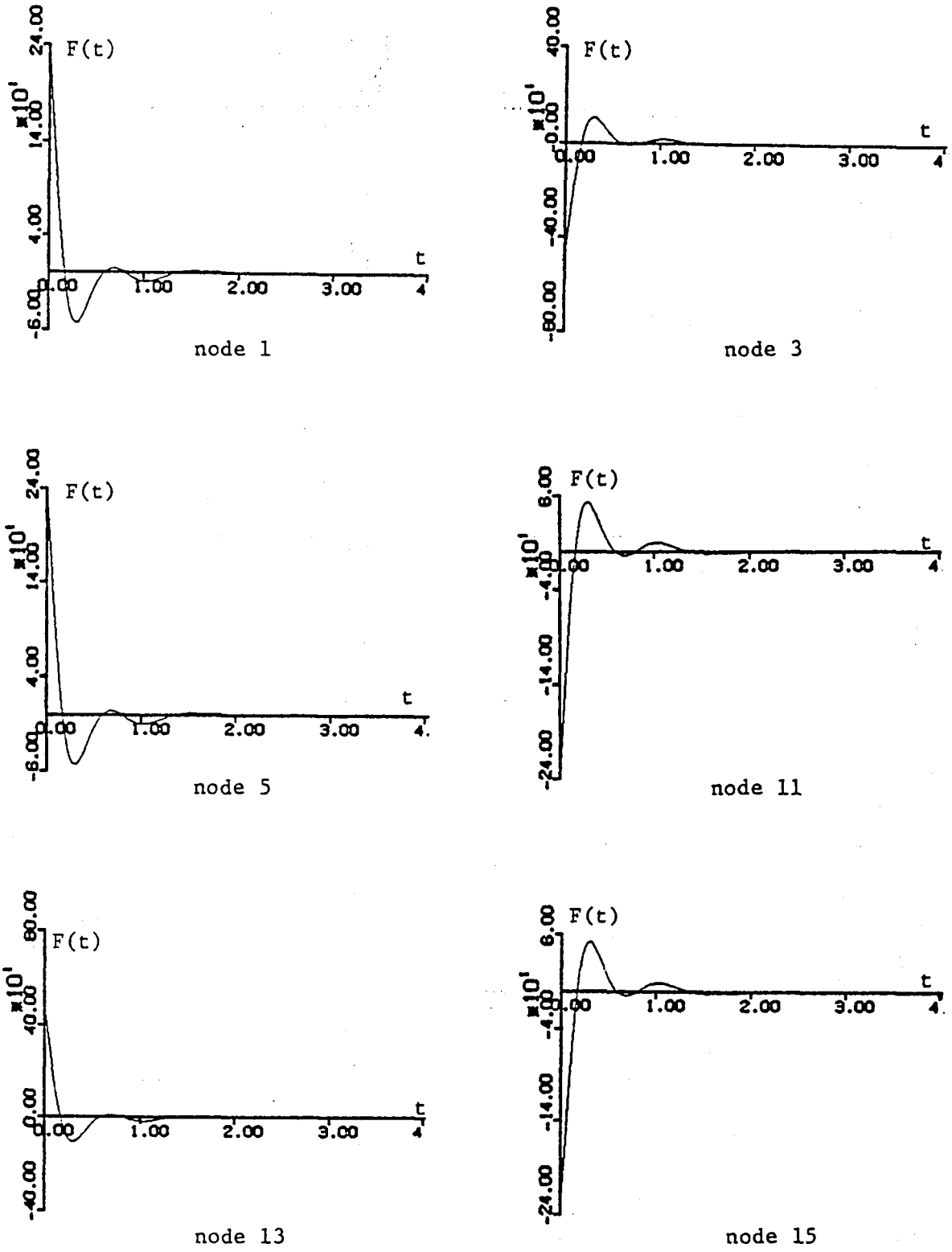

Figure 6.7: Actuators Forces vs Time

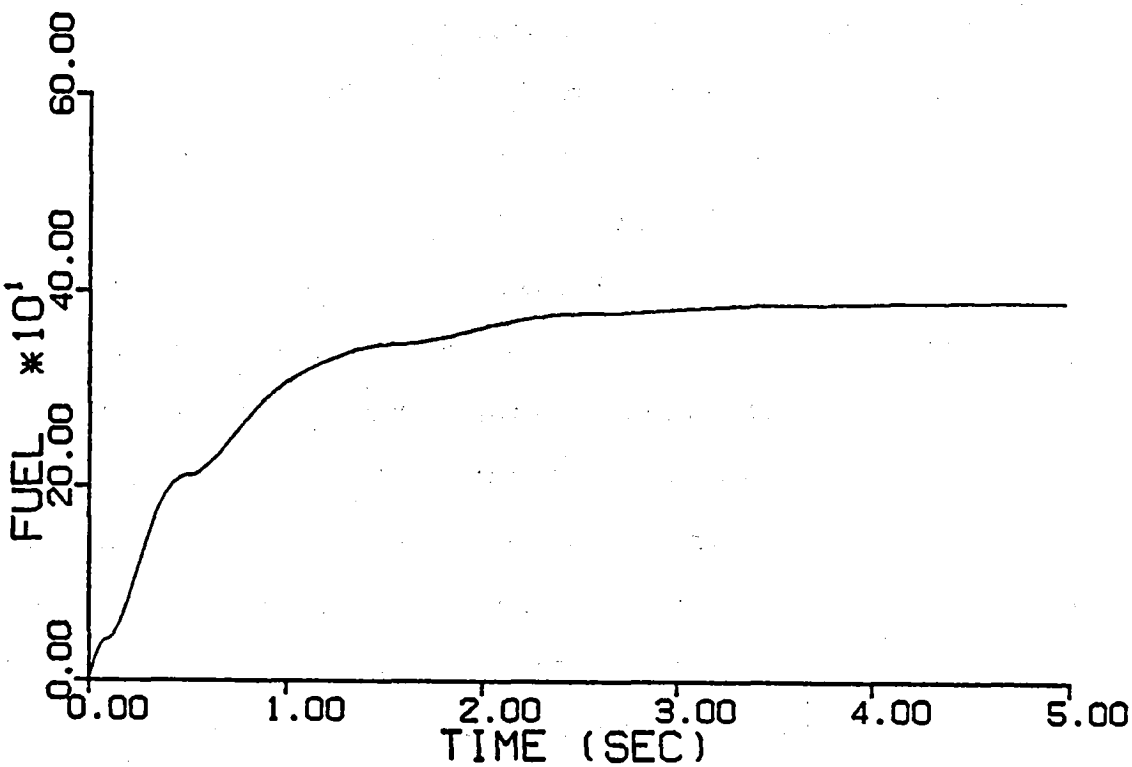

Figure 6.8: Total Consumed Fuel

6.2 MINIMUM-FUEL PROBLEM

Implementation of Minimum-Fuel Control policy, using the IMSC method is based on the derivations of Chapter V. It has been shown that the modal minimum fuel control is nonlinear of the "bang-off-bang" type. Most of the control techniques for this type of problem were developed as state(phase)- plane concepts. Therefore it proves convenient to show how the control task is achieved for each mode in the control scheme, using state-plane trajectories. Table 6.2 provides the system parameters for three cases of control bounds. The modal state-plane trajectories for these cases are shown in Fig. 6.9. Figure 6.10 presents the modal on-off control forces, while Fig. 6.11 presents actuators quantized forces versus time. Finally, assuming that the control forces are proportional to the rate of flow of fuel, Fig. 6.12 gives the total consumed fuel versus time.

A comparison between fuel consumption in the linear optimal control design, Fig. 6.8, and the minimum fuel design, Fig. 6.12, reveals a saving of about 20% for the latter.

TABLE 6.2

System Parameters in the Minimum-Fuel Control Framework

Case	Control Bound M	Mode r	Modal State-Plane Initial Conditions r_0	ψ (rad)	Number of Control Strokes n_c	Modal Final Time t_f (sec)
1	100	1	0.039649	0.0	3	2.27
		2	0.0	0.0	-	-
		3	0.074399	0.0	7	4.71
		4	0.033788	0.0	15	5.34
		5	0.0	0.0	-	-
		6	0.003797	-3.14	6	1.03
2	180	1	0.039649	0.0	2	1.20
		2	0.0	0.0	-	-
		3	0.074399	0.0	5	3.16
		4	0.033788	0.0	9	3.08
		5	0.0	0.0	-	-
		6	0.003797	-3.14	4	0.53
3	200	1	0.039649	0.0	2	1.20
		2	0.0	0.0	-	-
		3	0.074399	0.0	4	2.44
		4	0.033788	0.0	8	2.71
		5	0.0	0.0	-	-
		6	0.003797	-3.14	4	0.53

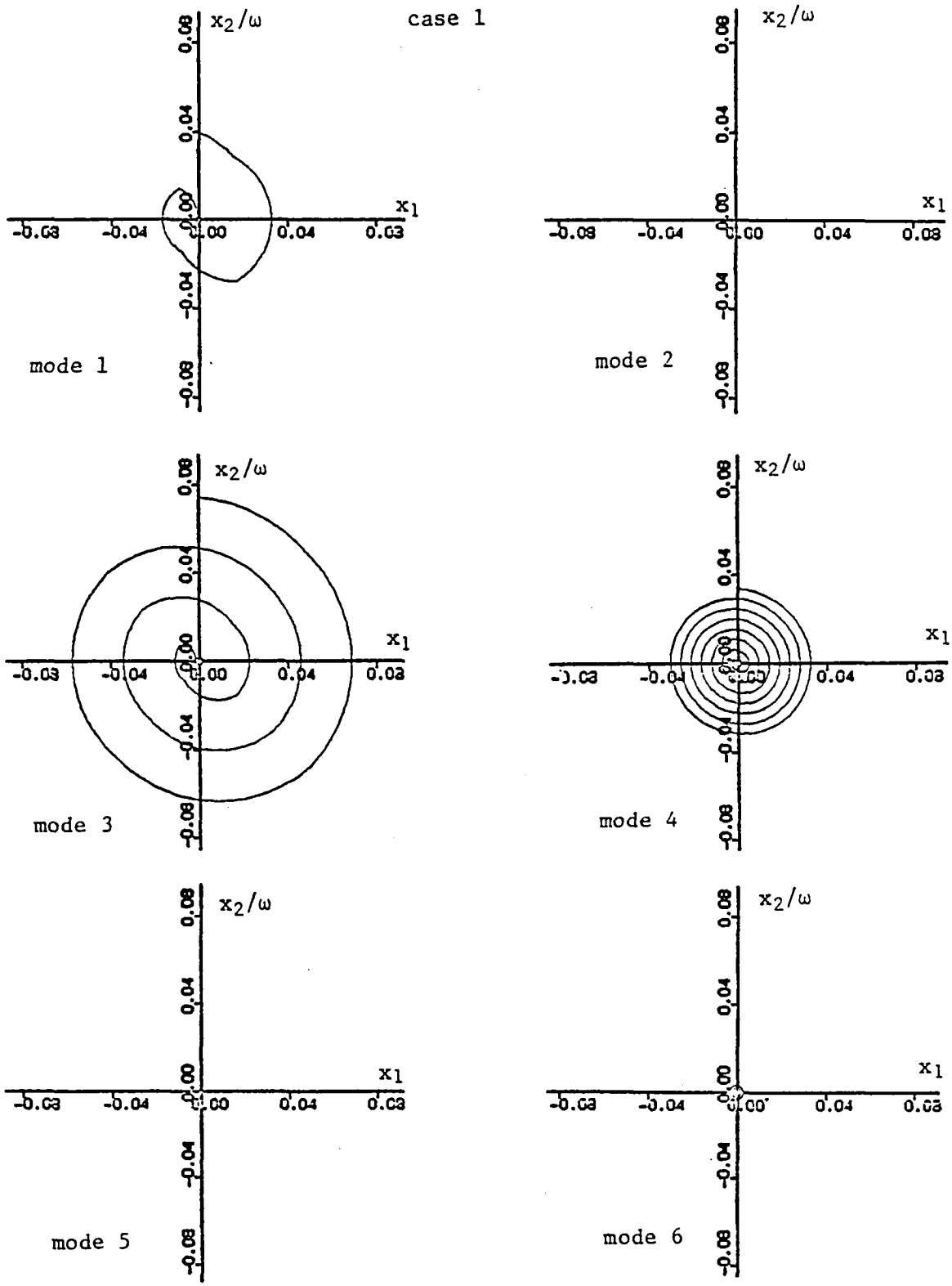

Figure 6.9: Modal State-Plane Trajectories (Cases 1,2,3)

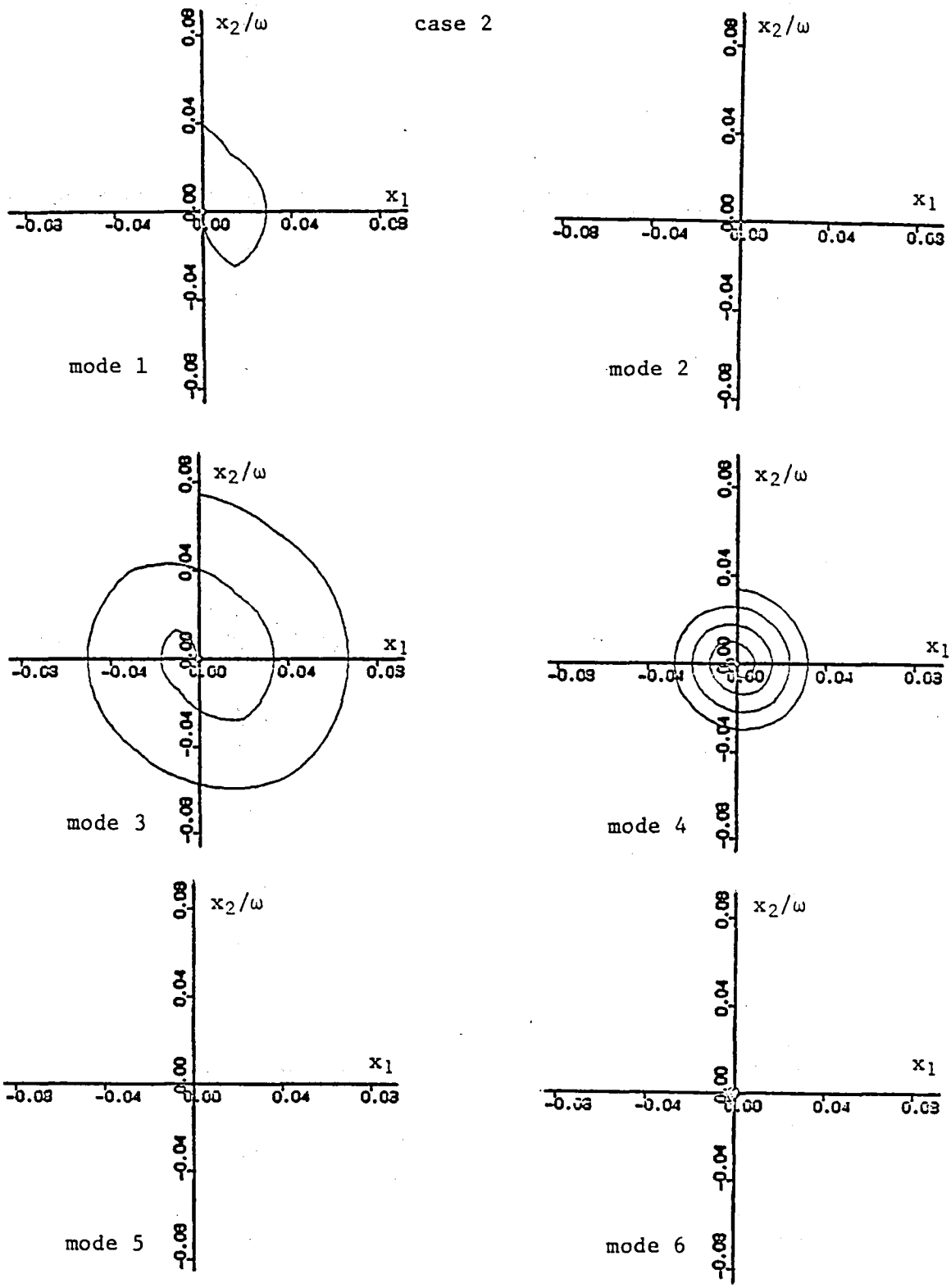

Figure 6.9: (cont.)

case 3

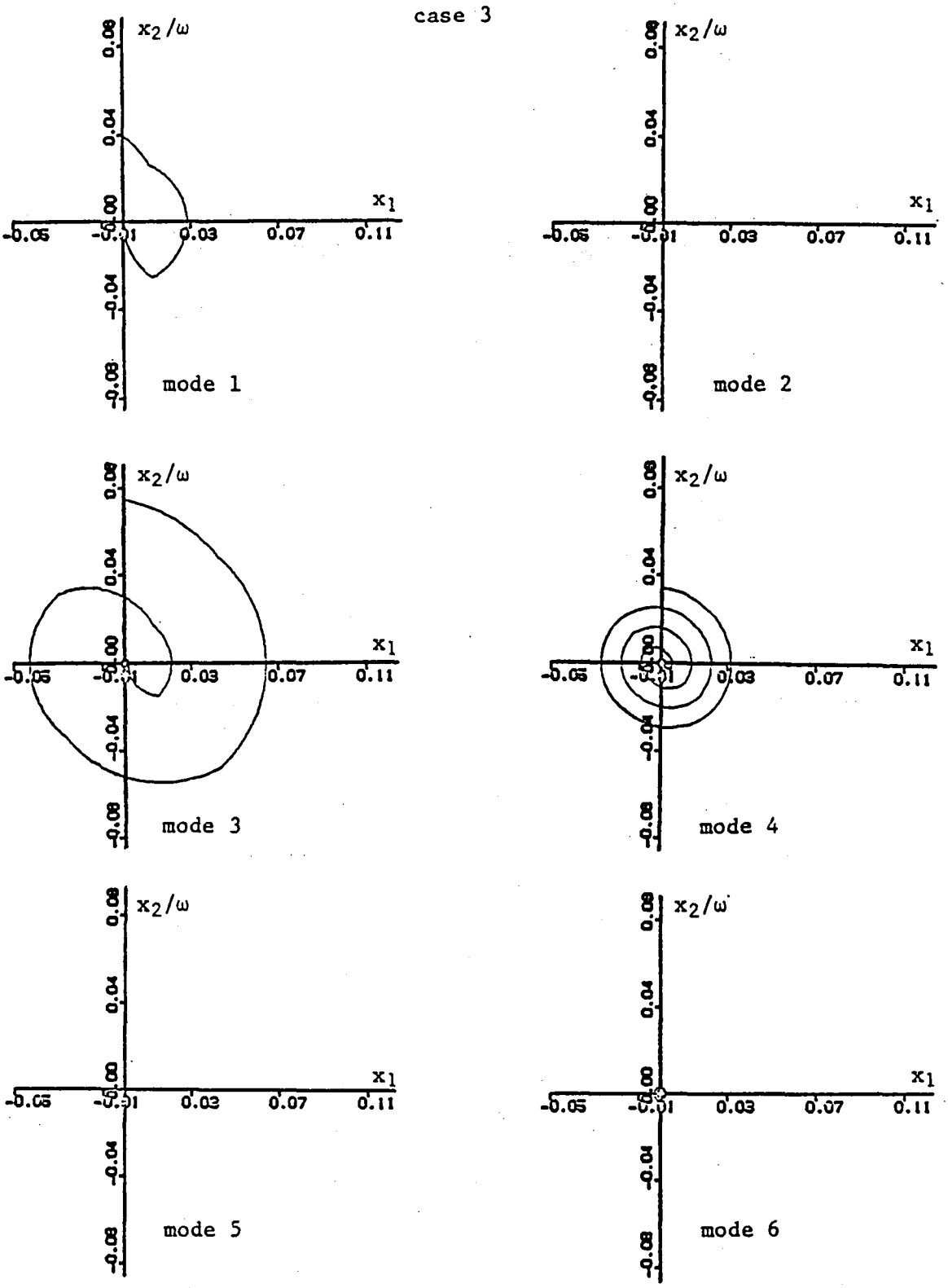

Figure 6.9: (cont.)

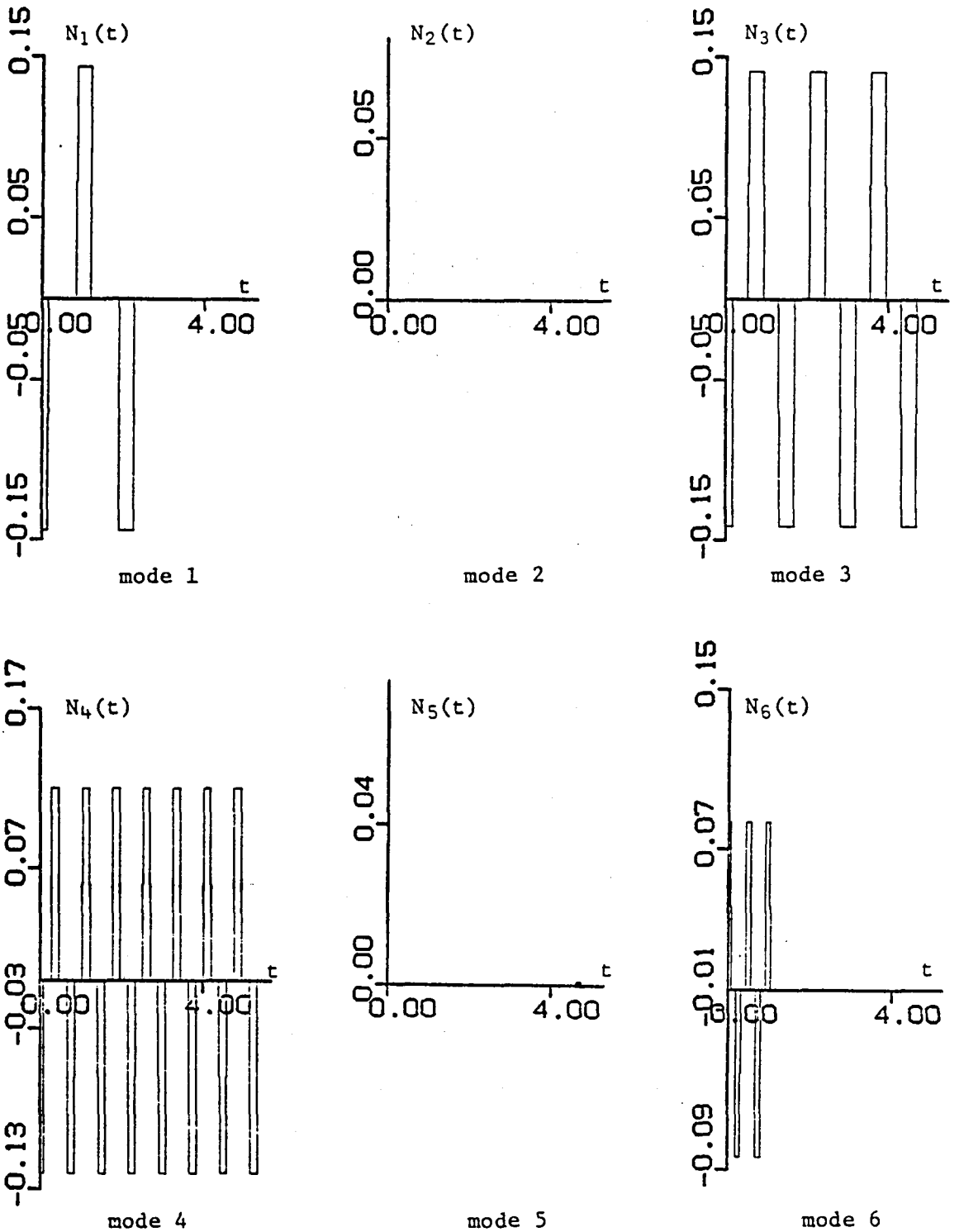

Figure 6.10: Modal Control Forces vs Time (Case 1)

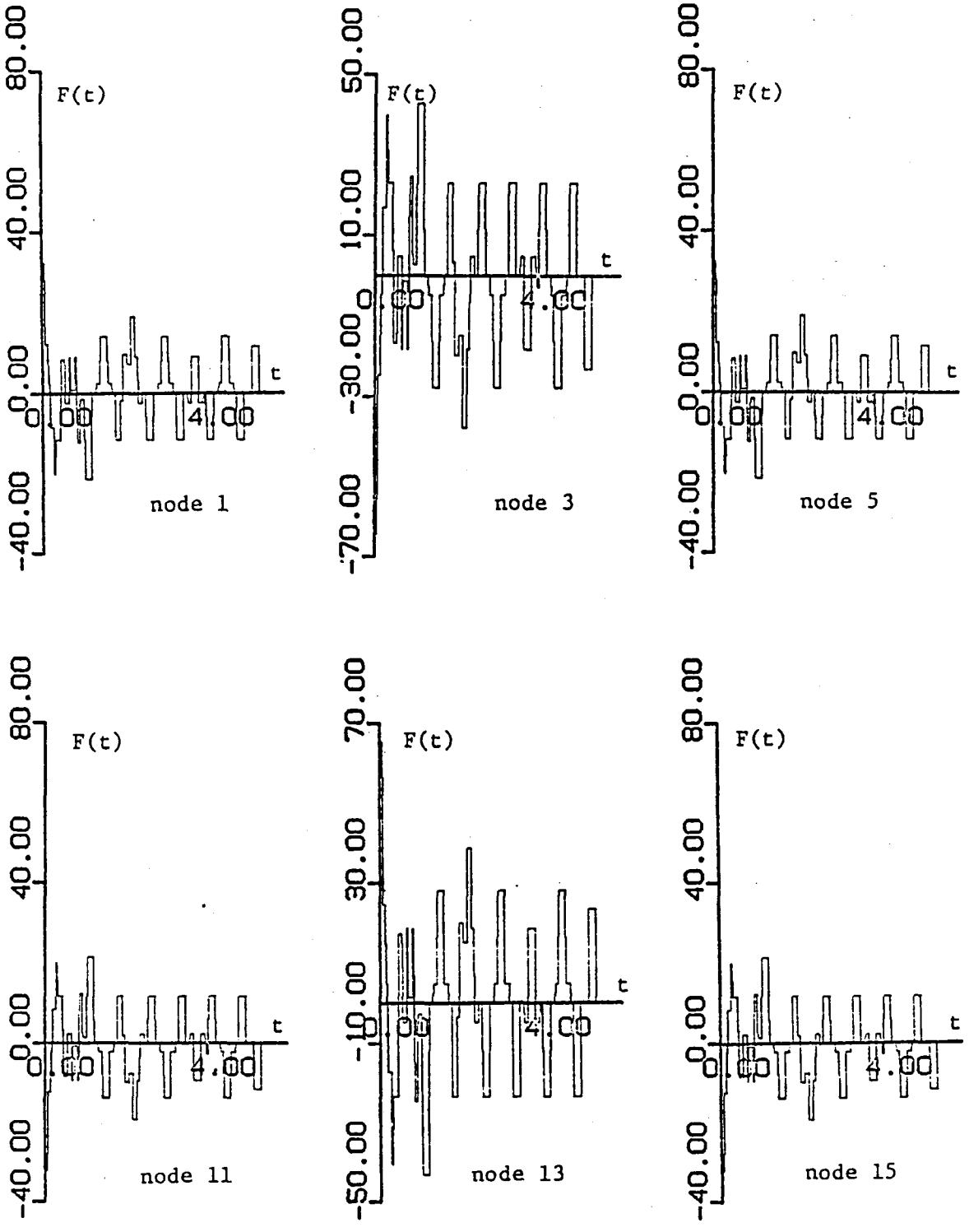

Figure 6.11: Actuators Forces vs Time (Case 1)

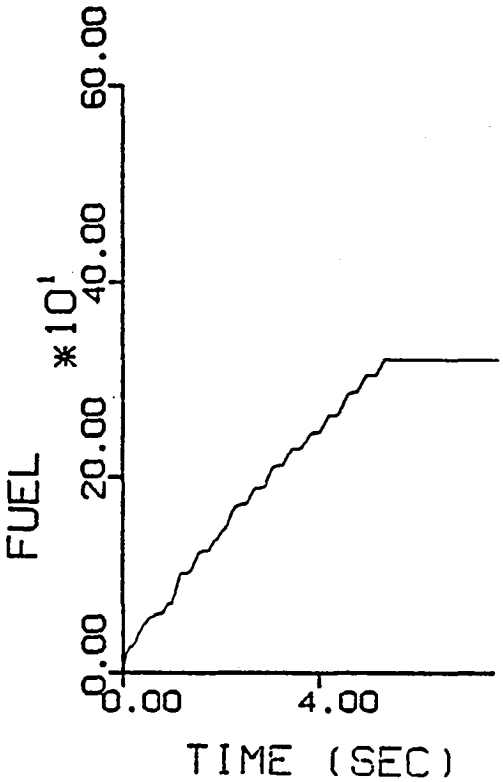

Figure 6.12: Total Consumed Fuel (Case 1)

Chapter VII

CONCLUSIONS AND RECOMMENDATIONS

Recent designs of large structures require distributed-parameter models described by partial differential equations. Exact solutions to these equations are limited to relatively simple geometries. However, in most practical problems, closed-form solutions are not feasible and system discretization is unavoidable. The discretization process converts the distributed-parameter system equations into a coupled multivariable linear eqations of motion. Control of the high-order model is not feasible due to computation limitations and errors that arise in modeling the higher modes by the discretization process. The fundamental problem of active control of flexible systems is the control of a large-order system, using a much smaller-order controller. The particular number of modes chosen to represent the truncated system model is often difficult to justify. One can measure the significance of the modes by computing their participation factors in generating the actual response.

The increased order of models representing modern structures and the associated control problems have provided

the motivation for developing methods permitting analysis of such systems, and solutions to the control problems with little computation effort. Such a method is the Independent Modal Space Control (IMSC). Using this method, the 2n-order coupled system equations of motiom is reduced to n independent second-order modal space systems. This approach allows complete flexibility as to which mode to control, because the control law is designed in the modal space for each mode independently. The ability of using second-order system techniques in the analysis of a high-order system is a distinct advantage typical of the IMSC method and not possible for any other method.

In this study, IMSC method was employed in the design of a linear optimal control law, as well as in the design of a minimum-fuel control law for a two dimensional domain problem. Due to the use of the IMSC method, some response performance indices, like settling time, can simply be met. At the same time, no control forces were applied to the modes that were not excited. These tasks are very hard to achieve, if not impossible, by any other method.

An important factor in any control scheme is the placement of the actuators. Actuators placement becomes even

more critical when two dimensional domains are considered in conjunction with the IMSC method, especially if the system possesses some symmetry properties. In such cases, actuators placement must be carefully made to prevent the occurence of a singular mode participation matrix. Because actuators location affect this matrix directly, knowledge of the modes shape permits a correct actuators placement. Relating to the modes shape of such systems, a method was developed in this study as to how to recognize such singular cases just by examining the location, as well as the type of actuators used in the control framework. This method is very helpful in the design and placement of actuators, as well as of sensors when the IMSC method is applied to two-dimensional domain problems.

The minimum-fuel problem is a very important one in space vehicles, especially in those designed for lengthy missions. The amount of fuel available for control is at times limited to such an extent that fuel economy is the predominant factor in control system design. The explicit dependence of the control on the instantaneous values of the state variables in a coupled high-order system, is a very complex task, and for most practical cases it remains an unsolved problem. In these cases, a trial and error process

is unavoidable for the state determination. Such a process may be reasonable for a low-order system (fourth order at most), but certainly not for a high-order system, where the computational difficulties are insurmontable. The control task is made considerably simpler by using the IMSC method, which obviates the complexity inherent in a high-order system. In this study, IMSC method was employed, and the difficult minimum-fuel problem for a 2n-order coupled system was reduced to n fuel minimization problems for a decoupled set of n second-order modal space systems. In using the IMSC method, one must minimize modal cost functions instead of a global cost function. This decomposition allows the use of second-order system techniques in the control scheme rather than the multivariable system control techniques, which are hard to implement.

In the derivation of the minimum-fuel control problem via the IMSC method, the condition number of the mode participation matrix plays an important role in determining actuators efficiency. Observing the characteristics of the actuators quantized forces, one can easily determine this effectiveness to be less than 70%. It is suggested that further research be carried out on the dependence of the condition number on actuators placement and how to decrease

this condition number in order to increase actuators effectiveness.

The fuel minimization technique depends on correct switching times in the process of driving the modes to the system origin. Variations in these times create an offset in reaching the final state. Further study of the sensitivity of these switching times to parameters variation and their influence on the final state is strongly recommended.

REFERENCES

1. Meirovitch, L. (editor), Proceedings of the First VPI&SU/AIAA Symposium on Dynamics and Control of Large Flexible Spacecraft, June 1977, Blacksburg, Virginia

2. Meirovitch, L. (editor), Proceedings of the Second VPI&SU/AIAA Symposium on Dynamics and Control of Large Flexible Spacecraft, June 1979, Blacksburg, Virginia

3. Meirovitch, L. (editor), Proceedings of the Third VPI&SU/AIAA Symposium on Dynamics and Control of Large Flexible Spacecraft, June 1981, Blacksburg, Virginia

4. Balas, M. J., "Active Control of Flexible Systems", Journal of Optimization Theory and Applications, Vol. 25, No. 3, 1978, pp. 415-436

5. Balas, M. J. and Canavin, J. R., "An Active Control System Philosophy for a Class of Large Space Structures", Proceedings of the First VPI&SU/AIAA Symposium on Dynamics and Control of Large Flexible Spacecraft, Meirovitch, L. (editor), June 1977, Blacksburg, Virginia, pp. 271-285

6. Meirovitch, L., Van Landingham, H. F. and Öz, H., "Control of Spinning Flexible Spacecraft by Modal Synthesis", Acta Astronautica, Vol. 4, no. 9/10, Sept./Oct. 1977, pp. 985-1010

7. Meirovitch, L. and Öz, H., "Modal-Space Control of Distributed Gyroscopic Systems", Journal of Guidance and Control, Vol. 3, No. 2, March-April 1980, pp. 140-150

8. Meirovitch, L. and Öz, H., "Active Control of Structures by Modal Synthesis", Structural Control, Leipholz, H. H. E. (editor), North-Holland Publishing Co., 1980, pp. 505-521

9. Öz, H. and Meirovitch, L., "Optimal Modal-Space Control of Flexible Gyroscopic Systems", Journal of Guidance and Control, Vol. 3, No. 3, May-June 1980, pp. 218-226

10. Meirovitch, L. and Baruh, H., "Optimal Control of Damped Flexible Gyroscopic Systems", Journal of Guidance and Control, Vol. 4, No. 2, March-April 1981, pp. 157-163

11. Meirovitch, L., Baruh, H. and Öz, H., "A Comparison of Control Techniques for Large Flexible Systems", Journal of Guidance, Control, and Dynamics, Vol. 6, No. 4, July-Aug. 1983, pp. 302-310.

12. Meirovitch, L. and Baruh, H., "Control of Self-Adjoint distributed Parameter Systems", Journal of Guidance, Control, and Dynamics, Vol. 5, No. 1, Jan.-Feb. 1982, pp. 60-66

13. Meirovitch, L., Computational Methods in Structural Dynamics, Sijthoff-Noordhoff, The Netherlands, 1980.

14. Baruh, H. and Meirovitch, L., "On the Placement of Actuators in the Control of Distributed-Parameter Systems", Proceedings of the AIAA Dynamics Specialist Conference, April 1981, pp. 611-620

15. Lindberg, R. E. and Longman, R. W., "On the Number and Placement of Actuators for Independent Modal Space Control", presented as Paper No. 82-1436 at the AIAA/AAS Astrodynamics Conference, San Diego, California, August 9-11, 1982

16. Kirk, D. E., Optimal Control Theory, Prentice-Hall Englewood Cliffs, N.J., 1970

17. Athans, M. and Falb, P., L., Optimal Control: An Introduction to the Theory and Its Applications, McGraw-Hill Book Co., N.Y., 1966

18. Athanassiades, M., "Optimal Control for Linear Time Invariant Plants with Time-, Fuel-, and Energy Constraints", IEEE Trans. Appl. Ind., Vol. 81, 1963, pp. 321-325

19. Athans, M., "Minimum Fuel Feedback Control Systems: Second Order Case", IEEE Trans. Appl. Ind., Vol. 82, 1963, pp. 8-17

20. Athans, M., "Fuel-Optimal Control of a Double Integral Plant with Response Time Constraint", IEEE Trans. Appl. Ind., Vol. 83, 1964, pp. 240-246

21. Athans, M., "Minimum Fuel Control of Second Order Systems with Real Poles", IEEE Trans. Appl. Ind., Vol. 83, 1964, pp. 148-153

22. Foy, W. H., "Fuel Minimization In Flight Vehicle Attitude Control", IEEE Trans. Autom. Control, Vol. AC-8, 1963, pp. 84-88

23. Flugge-Lotz, I., Discontinuous and Optimal Control, McGraw-Hill Book Co., N.Y., 1968

24. Meirovitch, L., Analytical Methods in Vibrations, The Macmillan Co., London, 1967

25. Dym, C. L., Shames, I. H., Solid Mechanics - A Variational Approach, McGraw-Hill Book Co., 1973

26. Meirovitch, L. and Öz, H., "Modal-Space Control of Large Flexible Spacecraft Possessing Ignorable Coordinates", Journal of Guidance and Control, Vol. 3, No. 6, Nov.-Dec. 1980, pp. 569-577

27. Meirovitch, L., Elements of Vibration Analysis, McGraw-Hill Book Co., 1975

28. Karlin, S., Total Positivity, Stanford University Press, Stanford, California, 1968

29. Franklin, J. N., Matrix Theory, Prentice-Hall, Englewood Cliffs, N.J., 1969

Appendix A

LAPLACE EXPANSION FOR DETERMINANTS

See also Karlin [28], Chapter 0.

The classical Laplace expansion for determinants has the form

$$\det A\begin{pmatrix}1 & 2 & \dots & n\\ 1 & 2 & \dots & n\end{pmatrix} = \sum (-1)^{\sum_{k=1}^{p}(i_k+j_k)} \det A\begin{pmatrix}i_1 & i_2 & \dots & i_p\\ j_1 & j_2 & \dots & j_p\end{pmatrix} \cdot \det A\begin{pmatrix}i_1' & i_2' & \dots & i_{n-p}\\ j_1' & j_2' & \dots & j_{n-p}'\end{pmatrix} \tag{A.1}$$

where

$$A\begin{pmatrix}i_1 & i_2 & \dots & i_p\\ j_1 & j_2 & \dots & j_p\end{pmatrix}$$

denotes the minor of the matrix A obtained by the selected rows $i_1, i_2, \dots, i_p$ and selected columns $j_1, j_2, \dots, j_p$.

In the sum, there are $\binom{n}{p}$ terms as the number of selections of ordered p indices. The sum is extended over all p-tuples $1 \le j_1 < j_2 < \dots < j_p \le n$, where $j_1', j_2', \dots, j_{n-p}'$ denote the

complementary set of indices to $j_1, j_2, \ldots, j_p$ in $1, 2, \ldots, n$, arranged in natural order, and similarly $i'_1, i'_2, \ldots, i'_{n-p}$ denote the complementary set of indices to $i_1, i_2, \ldots, i_p$ in $1, 2, \ldots, n$.

<u>Example 1</u>

Expand the determinant

$$\det A = \begin{vmatrix} a_{11} & a_{12} & a_{13} & a_{14} \\ a_{21} & a_{22} & a_{23} & a_{24} \\ a_{31} & a_{32} & a_{33} & a_{34} \\ a_{41} & a_{42} & a_{43} & a_{44} \end{vmatrix} \tag{A.2}$$

using Laplace expansion.

For the expansion, we will select two fixed rows, for example, the second and the third rows. The number of terms in the expansion will be

$\binom{n}{p} = \binom{4}{2} = 6$

Using Eq.(A.1)

$$
\begin{aligned}
\det A = {} & + \begin{vmatrix} a_{21} & a_{22} \\ a_{31} & a_{32} \end{vmatrix} \begin{vmatrix} a_{13} & a_{14} \\ a_{43} & a_{44} \end{vmatrix} - \begin{vmatrix} a_{21} & a_{23} \\ a_{31} & a_{33} \end{vmatrix} \begin{vmatrix} a_{12} & a_{14} \\ a_{42} & a_{44} \end{vmatrix} \\
& + \begin{vmatrix} a_{21} & a_{24} \\ a_{31} & a_{34} \end{vmatrix} \begin{vmatrix} a_{12} & a_{13} \\ a_{42} & a_{43} \end{vmatrix} + \begin{vmatrix} a_{22} & a_{23} \\ a_{32} & a_{33} \end{vmatrix} \begin{vmatrix} a_{11} & a_{14} \\ a_{41} & a_{44} \end{vmatrix} \\
& - \begin{vmatrix} a_{22} & a_{24} \\ a_{32} & a_{34} \end{vmatrix} \begin{vmatrix} a_{11} & a_{13} \\ a_{41} & a_{43} \end{vmatrix} + \begin{vmatrix} a_{23} & a_{24} \\ a_{33} & a_{34} \end{vmatrix} \begin{vmatrix} a_{11} & a_{12} \\ a_{41} & a_{42} \end{vmatrix}
\end{aligned}
\tag{A.3}
$$

<u>Example 2</u>

We attempt to control the first six modes in a n=45 order system, where the actuators are placed as shown in Fig. A.1.

The mode participation matrix $U_C^T B$ for this case is

$$
\begin{array}{c}
\text{mode shape} \\ \downarrow \\ S \\ A \\ S \\ S \\ A \\ S
\end{array}
\begin{array}{c}
\begin{array}{cccccc} 17 & 18 & 23 & 24 & 29 & 30 \end{array} \leftarrow \text{actuator \#} \\
\begin{pmatrix}
a_1 & a_2 & a_3 & 0 & a_1 & -a_2 \\
b_1 & b_2 & 0 & b_4 & -b_1 & b_2 \\
c_1 & c_2 & c_3 & 0 & c_1 & -c_2 \\
d_1 & d_2 & d_3 & 0 & d_1 & -d_2 \\
e_1 & e_2 & 0 & e_4 & -e_1 & e_2 \\
f_1 & f_2 & f_3 & 0 & f_1 & -f_2
\end{pmatrix}
\end{array}
= U_C^T B
\tag{A.4}
$$

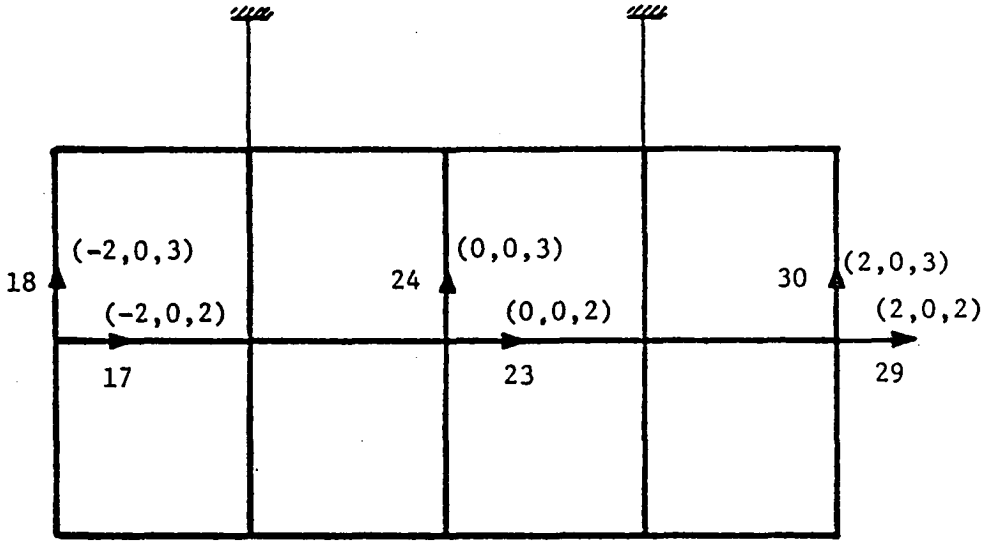

Figure A.1: Beam Lattice with Symmetric Actuators Configuration

where "S" and "A" denote symmetric and antisymmetric modes, respectively. Here, p+h=2+1=3 and s=4. Hence, p+h<s and the proposition states clearly that for this case, the mode participation matrix is singular. It is an easy task to show this, using rows and columns elementary transformation. We change the rows order having first the symmetric modes and then the antisymmetric modes (not necessary), so that

$$\begin{array}{c} S \\ S \\ S \\ S \\ A \\ A \end{array} \begin{pmatrix} a_1 & a_2 & a_3 & 0 & a_1 & -a_2 \\ c_1 & c_2 & c_3 & 0 & c_1 & -c_2 \\ d_1 & d_2 & d_3 & 0 & d_1 & -d_2 \\ f_1 & f_2 & f_3 & 0 & f_1 & -f_2 \\ b_1 & b_2 & 0 & b_4 & -b_1 & b_2 \\ e_1 & e_2 & 0 & e_4 & -e_1 & e_2 \end{pmatrix} \tag{A.5}$$

Substracting 1st column from the 5th and adding the 2nd to the 6th, we obtain

$$\begin{pmatrix} a_1 & a_2 & a_3 & 0 & 0 & 0 \\ c_1 & c_2 & c_3 & 0 & 0 & 0 \\ d_1 & d_2 & d_3 & 0 & 0 & 0 \\ f_1 & f_2 & f_3 & 0 & 0 & 0 \\ b_1 & b_2 & 0 & b_4 & -2b_1 & 2b_2 \\ e_1 & e_2 & 0 & e_4 & -2e_1 & 2e_2 \end{pmatrix} \tag{A.6}$$

Then, expanding the determinant of (A.6), we obtain

$$\det(\ ) = -\ b_4 \begin{vmatrix} a_1 & a_2 & a_3 & 0 & 0 \\ c_1 & c_2 & c_3 & 0 & 0 \\ d_1 & d_2 & d_3 & 0 & 0 \\ f_1 & f_2 & f_3 & 0 & 0 \\ e_1 & e_2 & 0 & -2e_1 & -2e_2 \end{vmatrix} + e_4 \begin{vmatrix} a_1 & a_2 & a_3 & 0 & 0 \\ c_1 & c_2 & c_3 & 0 & 0 \\ d_1 & d_2 & d_3 & 0 & 0 \\ f_1 & f_2 & f_3 & 0 & 0 \\ b_1 & b_2 & 0 & -2b_1 & -2b_2 \end{vmatrix}$$

$$= 0 + 0 = 0 \tag{A.7}$$

which means that $U_C^T B$ is singular.

Appendix B

MINIMUM FUEL CONTROL WITH UNSPECIFIED FINAL TIME: RIGID BODY MODE

See also Athans [17].

To obtain the minimum-fuel solution and to indicate the set of initial states for which no minimum-fuel solution exists, we divide the x_1-x_2 state plane into four sets, using the γ^+ and γ^- curves defined by Eqs.(5.51) and (5.52) respectively, and the x_{1r} axis.

We recall the following equations to describe the state plane trajectories for $N_r(t)=0$, and $N_r(t)=\pm\hat{N}_r \stackrel{\Delta}{=} \Delta_r$.
Solution to the state equations

$$x_{1r}(t) = \xi_{0r} + \dot{\xi}_{0r}\, t \tag{B.1}$$

$$x_{2r}(t) = \dot{\xi}_{0r} \tag{B.2}$$

for $N_r(t)=0$

$$x_{1r}(t) = \xi_{0r} + \dot{\xi}_{0r}\, t + \frac{1}{2}\Delta_r\, t^2 \tag{B.3}$$

$$x_{2r}(t) = \dot{\xi}_{0r} + \Delta_r\, t \tag{B.4}$$

for $N_r(t)=\pm\hat{N}_r \stackrel{\Delta}{=} \Delta_r$

The state plane trajectories are

$$x_{2r}(t) = \dot{\xi}_{0r} = \text{const} \qquad , \text{ for } N_r(t) = 0 \tag{B.5}$$

$$x_{1r}(t) = \xi_{0r} - \frac{1}{2\Delta_r}\dot{\xi}_{0r}^2 + \frac{1}{2\Delta_r}x_{2r}^2 \quad , \quad \text{for } N_r(t) = \pm\hat{N}_r = \Delta_r \tag{B.6}$$

The regions in the state plane are described in Fig. B.1. Now we show the regions of existance and non-existance for a minimum-fuel solution.

B.1 REGION R1

If the initial state is in region R_1, given by Eq.(5.54a), or region R_3, given by Eq.(5.54c) (note that the switching curve γ is not included), then a minimum-fuel solution for the control driving the plant to the origin does not exist.

For any $N_r(t)$, we have from the second state equation $\dot{x}_{2r}(t)=N_r(t)$, which implies that

$$x_{2r}(t) = \dot{\xi}_{0r} + \int_{t_0}^{t} N_r(\tau)d\tau \tag{B1.1}$$

from which

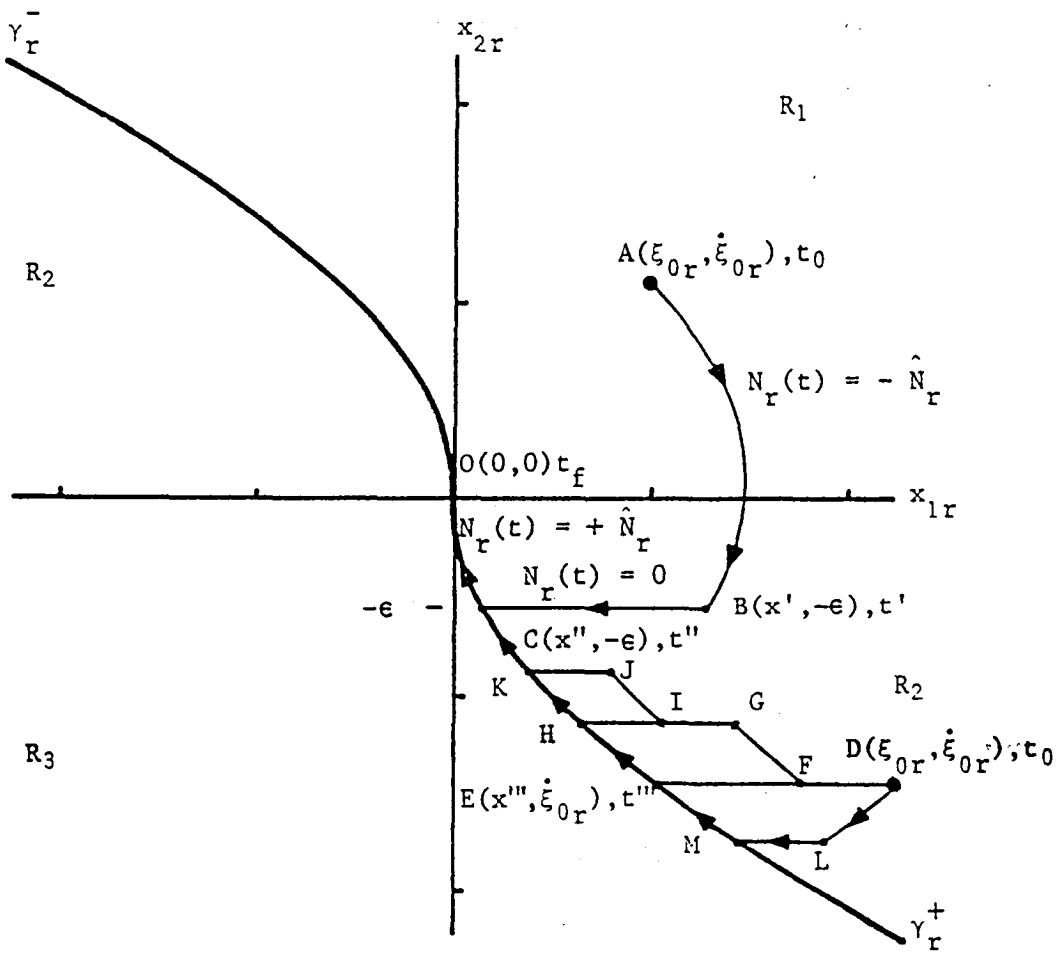

Figure B.1: Control Dependence on Initial Condition Point for RBM Regions R_1, R_2, R_3, R_4 Are Defined by Eq. (5.54).

$$\left| \int_{t_0}^{t} N_r(\tau)d\tau \right| = \left| x_{2r}(t) - \dot{\xi}_{0r} \right| \tag{B1.2}$$

Dividing the path to the origin ABCO into segments on which the control is a constant function of time, we can calculate the consumed fuel

$$\begin{aligned} J_r(N_r) &= \int_{t_0}^{t'} |N_r(t)|dt + \int_{t'}^{t''} |N_r(t)|dt + \int_{t''}^{t_f} |N_r(t)|dt \\ &= |-\epsilon - \dot{\xi}_{0r}| + |-\epsilon -(-\epsilon)| + |0 - (-\epsilon)| = |\dot{\xi}_{0r}| + 2\epsilon \end{aligned} \tag{B1.3}$$

The elapsed time for this operation can be calculated as follows:

on AB

$$t' - t_0 = \frac{\dot{\xi}_{0r} + \epsilon}{\hat{N}_r} \tag{B1.4}$$

on BC

$$t'' - t' = \frac{x''-x'}{-\epsilon} = \frac{\xi_{0r} + \frac{1}{2\hat{N}_r}\dot{\xi}_{0r}^2 - \frac{\epsilon^2}{\hat{N}_r}}{\epsilon} \tag{B1.5}$$

on CO

$$t_f - t'' = \frac{\epsilon}{\hat{N}_r} \tag{B1.6}$$

The final time t_f is

$$t_f = t_0 + \frac{\dot{\xi}_{0r} + \epsilon}{\hat{N}_r} + \frac{\xi_{0r} + \frac{1}{2\hat{N}_r}\dot{\xi}_{0r}^2}{\epsilon} \tag{B1.7}$$

Clearly, the fuel in Eq.(B1.3) will reach its minimum in the limit as $\epsilon \to 0$. The required fuel, then, approaches the lower bound on fuel expenditure. However, as $\epsilon \to 0$, the elapsed time in Eq.(B1.7) increases without bounds, $t_f \to \infty$. Hence, the fuel required can be arbitrarily close to, but never attain the lower bound. This means that a <u>minimum-fuel control does not exist.</u>

B.2 REGION R2

If the initial state is in region R_4 given by Eq.(5.54d), or region R_2 given by Eq.(5.54b), then <u>the minimum-fuel solution</u> for the control driving the plant to the origin <u>is not unique.</u>

In this statement we excluded the case in which the initial state is on the switching curve γ_r. For such a case it is clear that a minimum-fuel solution exists and it is unique. $\{+\hat{N}_r\}$ is applied to an initial state on γ_r^+ as well as $\{-\hat{N}_r\}$ to an initial state on γ_r^-. Any other initial state can be represented by point D in Fig. B.1

Clearly, the fuel consumption would be the same for all paths DEO, DFGHO, DFGIJKO

$$J_r(N_r) = |\dot{\xi}_{0r}| \tag{B2.1}$$

Hence, there are infinitely many ways of reaching the origin from D with the same amount of fuel. The associated control sequences with paths DEO, DFGHO and DFGIJKO are $\{0,+\hat{N}_r\}$, $\{0,+\hat{N}_r,0,+\hat{N}_r\}$ and $\{0,+\hat{N}_r,0,+\hat{N}_r,0,+\hat{N}_r\}$, respectively. The last two sequences, are certainly not from the set of candidates for the fuel-optimal control in Eq.(5.46), that minimize the Hamiltonian absolutely. In contrast to the same fuel consumption for those paths, the response time t_f is different. The shortest response time among all minimum-fuel controls mentioned above is the one associated with path DEO and is given as

$$t_f = t_0 + \frac{x''' - \xi_{0r}}{\dot{\xi}_{0r}} + \frac{0 - \dot{\xi}_{0r}}{\hat{N}_r} = t_0 - \left(\frac{1}{2\hat{N}_r}\dot{\xi}_{0r} + \frac{\xi_{0r}}{\dot{\xi}_{0r}}\right) \tag{B2.2}$$

Finally, the control sequence $\{-N_r,0,+N_r\}$ along path DLMO cannot be fuel-optimal although it belongs to the set of candidates for the fuel-optimal control in Eq.(5.46).

To show this, we assume that $\{-\hat{N}_r,0,+\hat{N}_r\}$ is fuel-optimal in driving the plant from its initial state at D to the origin. This control sequence is ploted in Fig. 5.3i, from which we can draw conclusions concerning the costate function $p_{2r}(t)$. Using Eqs.(5.45), in view of Fig. 5.3i at t=0, we obtain

$$p_{2r}(0) = \eta_{2r} > 1 \qquad p_{1r}(0) = \eta_{1r} \tag{B2.3}$$

Because $N_r(0)=-\hat{N}_r$, substitution of Eq.(B2.3) into the Hamiltonian Eq.(5.41) at t=0 yields

$$H_r\Big|_{t=0} = |-\hat{N}_r| + \eta_{1r}\,\dot{\xi}_{0r} + \eta_{2r}\,(-\hat{N}_r) \tag{B2.4}$$

Because the final time t_f is free and the Hamiltonian does not depend explicitly on time, the Hamiltonian must vanish on the extremal trajectory. The relation $\hat{N}_r(1-\eta_{2r})<0$ implies that $\eta_{1r}\dot{\xi}_{0r}>0$. But, $(\xi_{0r},\dot{\xi}_{0r})\in R_4$, so that $\dot{\xi}_{0r}<0$, from which we obtain $\eta_{1r}<0$. In view of this result, we have $\eta_{1r}<0$ and $\eta_{2r}>1$ such that from the costate equation, Eq.(5.45b), we obtain

$$p_{2r}(t) = \eta_{2r} - \eta_{1r}\,t > \eta_{2r} > 1 \qquad \text{for all } t > 0 \tag{B2.5}$$

This corresponds to Fig. 5.3c with the associate control sequence $\{-\hat{N}_r\}$, which contradicts the assumed sequence $\{-\hat{N}_r,0,+\hat{N}_r\}$. Hence, the latter control sequence cannot be fuel-optimal.

Appendix C

MINIMUM-FUEL CONTROL WITH BOUNDED FINAL TIME: RIGID BODY MODE

See also Athans [17].

C.1 MINIMUM-TIME SOLUTION

It will prove convenient to begin with the expression for the minimum-time solution. This expression appears frequently in the derivation for the minimum-fuel problem as it provides the lower bound for the final time. Figure C.1 describes a minimum-time optimal trajectory, where the optimal control law is a sequence as $\{-\hat{N}_r, +\hat{N}_r\}$ or $\{+\hat{N}_r, -\hat{N}_r\}$ for an initial state in region R^- or R^+ respectively. Regions R^- and R^+ are the parts of the state plane created by the γ curve such that R^- is to the right of this curve and R^+ is to the left.

For an initial state in region R^-

$$z_1 = \xi_{0r} + \dot{\xi}_{0r}\, t_1 - \frac{1}{2}\hat{N}_r\, t_1^2 \tag{C1.1}$$

$$z_2 = \dot{\xi}_{0r} - \hat{N}_r\, t_1 \tag{C1.2}$$

$$0 = z_1 + z_2\, t_2 + \frac{1}{2}\hat{N}_r\, t_2^2 \tag{C1.3}$$

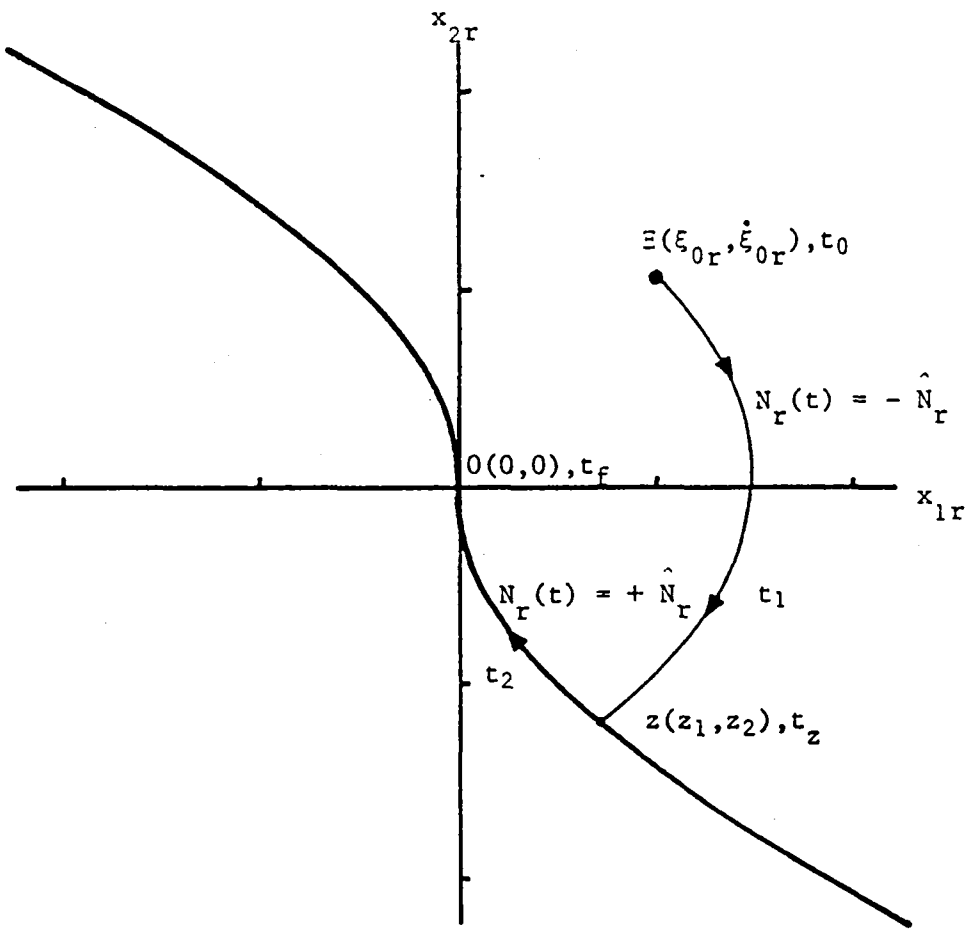

Figure C.1: State Plane Minimum-Time Trajectory for RBM

$$0 = z_2 + \hat{N}_r\, t_2 \tag{C1.4}$$

where $t_1 = t_z - t_0$ and $t_2 = t_f - t_z$. From Eqs.(C.1) (C.2) and (C.3) (C.4), we obtain

$$t_f = t_1 + t_2 = t_0 + \frac{\dot{\xi}_{0r}}{\hat{N}_r} + \left(\frac{2\dot{\xi}_{0r}^2}{\hat{N}_r^2} + \frac{4\xi_{0r}}{\hat{N}_r}\right)^{\frac{1}{2}} \tag{C1.5}$$

For an initial state in region R^+, we obtain in a similar way

$$t_f = t_0 - \frac{\dot{\xi}_{0r}}{\hat{N}_r} + \left(\frac{2\dot{\xi}_{0r}^2}{\hat{N}_r^2} - \frac{4\xi_{0r}}{\hat{N}_r}\right)^{\frac{1}{2}} \tag{C1.6}$$

C.2 SWITCHING TIMES TZ, TW

Refering to Fig. 5.6, t_z is the first switch time and t_w is the second. The determination of these times is done upon solving the following trajectories equation $((\xi_{0r}, \dot{\xi}_{0r}) \in R_1 \cup R_4)$

path Ξ-Z

$$z_1 = \xi_{0r} + \dot{\xi}_{0r}\,(t_z - t_0) - \frac{1}{2}\hat{N}_r(t_z - t_0)^2 \tag{C2.1}$$

$$z_2 = \dot{\xi}_{0r} - \hat{N}_r(t_z - t_0) \tag{C2.2}$$

path Z-W

$$w_1 = z_1 + z_2(t_w - t_z) \tag{C2.3}$$

$$w_2 = z_2 \tag{C2.4}$$

path W-O

$$0 = w_1 + w_2\,(t_f - t_w) + \frac{1}{2}\,\hat{N}_r\,(T_f - t_w)^2 \tag{C2.5}$$

$$0 = w_2 + \hat{N}_r\,(T_f - t_w) \tag{C2.6}$$

We express t_z and t_w in terms of the initial state $(\xi_{0r}, \dot{\xi}_{0r})$ and the prescribed final time T_f. Using Eqs.(C2.4) (C2.5) and (C2.6), we obtain

$$w_1 = \frac{1}{2}\,\frac{z_2^2}{\hat{N}_r} \tag{C2.7}$$

From Eqs.(C2.4) and (C2.6)

$$t_w = T_f + \frac{z_2}{\hat{N}_r} \tag{C2.8}$$

and from Eq.(C2.2)

$$t_z - t_0 = \frac{1}{\hat{N}_r}\,(\dot{\xi}_{0r} - z_2) \tag{C2.9}$$

Substituting Eq.(C2.9) into Eq.(C2.1), we obtain

$$z_1 = \xi_{0r} + \frac{\dot{\xi}_{0r}}{2\hat{N}_r} - \frac{z_2^2}{2\hat{N}_r} \tag{C2.10}$$

From Eqs.(C2.8) and (C2.9)

$$t_w - t_z = \frac{2z_2}{\hat{N}_r} - \frac{\dot{\xi}_{0r}}{\hat{N}_r} + T_f - t_0 \tag{C2.11}$$

Substitution of Eqs.(C2.7) (C2.10) and (C2.11) into Eq.(C2.3), yields a quadratic equation in Z_2 in terms of the initial state and the final time

$$z_2^2 + [\hat{N}_r(T_f - t_0) - \dot{\xi}_{0r}]z_2 + \left(\hat{N}_r\ \xi_{0r} + \frac{\dot{\xi}_{0r}}{2}\right) = 0 \qquad \text{(C2.12)}$$

which has the solution

$$z_2 = -\frac{1}{2}\,[\hat{N}_r(T_f - t_0) - \dot{\xi}_{0r}] \pm \frac{1}{2}\left\{[\hat{N}_r(T_f - t_0\ ) - \dot{\xi}_{0r}]^2 - 4\left[\hat{N}_r\ \xi_{0r} + \frac{\dot{\xi}_{0r}^2}{2}\right]^{\frac{1}{2}}\right\} \qquad \text{(C2.13)}$$

In view of Eq.(C1.5), the terms in the curly brackets in Eq.(C2.13) add up to a positive value. Moreover, Eq.(C2.11) and knowledge that $t_w - t_z > 0$ imply $Z_2 > -1/2 \cdot [\hat{N}_r(T_f - t_0) - \dot{\xi}_{0r}]$, so that only the plus sign in Eq.(C2.13) is applicable. Substitution of Eq.(C2.13) into Eq.(C2.9) and into Eq.(C2.8), yields

$$t_z = \frac{1}{2}\left\{T_f + t_0 + \frac{\dot{\xi}_{0r}}{\hat{N}_r} - \left[\left(T_f - t_0 - \frac{\dot{\xi}_{0r}}{\hat{N}_r}\right)^2 - \frac{4\xi_{0r}}{\hat{N}_r} - \frac{2\dot{\xi}_{0r}^2}{\hat{N}_r^2}\right]^{\frac{1}{2}}\right\} \qquad \text{(C2.14)}$$

$$t_w = \frac{1}{2}\left\{T_f + t_0 + \frac{\dot{\xi}_{0r}}{\hat{N}_r} + \left[\left(T_f - t_0 - \frac{\dot{\xi}_{0r}}{\hat{N}_r}\right)^2 - \frac{4\xi_{0r}}{\hat{N}_r} - \frac{2\dot{\xi}_{0r}^2}{\hat{N}_r^2}\right]^{\frac{1}{2}}\right\} \qquad \text{(C2.15)}$$

respectively.

C.3 FIRST SWITCH TIMES LOCI

Substitution of Eqs.(C2.7) and (C2.11) into Eq.(C2.3), yields the equation for the loci of the first optimal switch time t_z

$$Z_1 = -\left[\frac{3}{2\hat{N}_r} Z_2^2 + \left(T_f - t_0 - \frac{\dot{\xi}_{0r}}{\hat{N}_r}\right) Z_2\right] \tag{C3.1}$$

$(Z_1, Z_2) \in R_4$

C.4 BOUNDARIES FOR THE REACHABLE STATES

Since t_z and t_w are real, the terms in the square brackets in Eq.(C2.14) or Eq.(C2.15) must add to be a positive value. This condition yields the expression for the boundary to all modal initial conditions that can reach the origin in the prescribed final time bound, or

$$Z_1 \leqslant -\frac{1}{4\hat{N}_r} [Z_2^2 + 2(T_f - t_0)\, \hat{N}_r\, Z_2 - (T_f - t_0)^2\, \hat{N}_r^2] \tag{C4.1}$$

$(Z_1, Z_2) \in R_1 \cup R_4$ Eq.(C4.1)can be modified to allow the determination of the minimum final time bound for a given system, such that all the initial states in the control scheme will be located in the reachable zone.

$$T_f \geqslant t_0 + \max_{r=1,2,\ldots,n_r} \left\{\frac{\dot{\xi}_{0r}}{\hat{N}_r} + \left[2\left(\frac{\dot{\xi}_{0r}}{\hat{N}_r}\right)^2 + 4\,\frac{\xi_{0r}}{\hat{N}_r}\right]^{\frac{1}{2}}\right\}_{(\xi_{0r}, \dot{\xi}_{0r}) \in R_1 \cup R_4} \tag{C4.2}$$

similarly,

$$T_f \geqslant t_0 + \max_{r=1,2,\ldots,n_r} \left\{ \frac{-\dot{\xi}_{0r}}{\hat{N}_r} + \left[2\left(\frac{\dot{\xi}_{0r}}{\hat{N}_r}\right)^2 - 4\,\frac{\xi_{0r}}{\hat{N}_r} \right]^{\frac{1}{2}} \right\}_{(\xi_{0r},\dot{\xi}_{0r})\in R_2 U R_3} \tag{C4.3}$$

Obviously, Eqs.(C4.2) and (C4.3) resemble the form of the minimum-time solution, in Eqs.(C1.5) and (C1.6), respectively.

C.5 PLOT OF THE MODAL STATE PLANE

Figure C.2 presents a nondimensional plot of the modal state plane. The following scale factors have been used

$$x_{1r} = \tilde{x}_{1r}\,\hat{N}_r\,(T_f - t_0)^2 \tag{C5.1}$$

$$x_{2r} = \tilde{x}_{2r}\,\hat{N}_r\,(T_f - t_0) \tag{C5.2}$$

Inserting Eqs.(C5.1) and (C5.2) into Eqs.(5.57) (C3.1) and (C4.1), we obtain the following nondimensional forms:

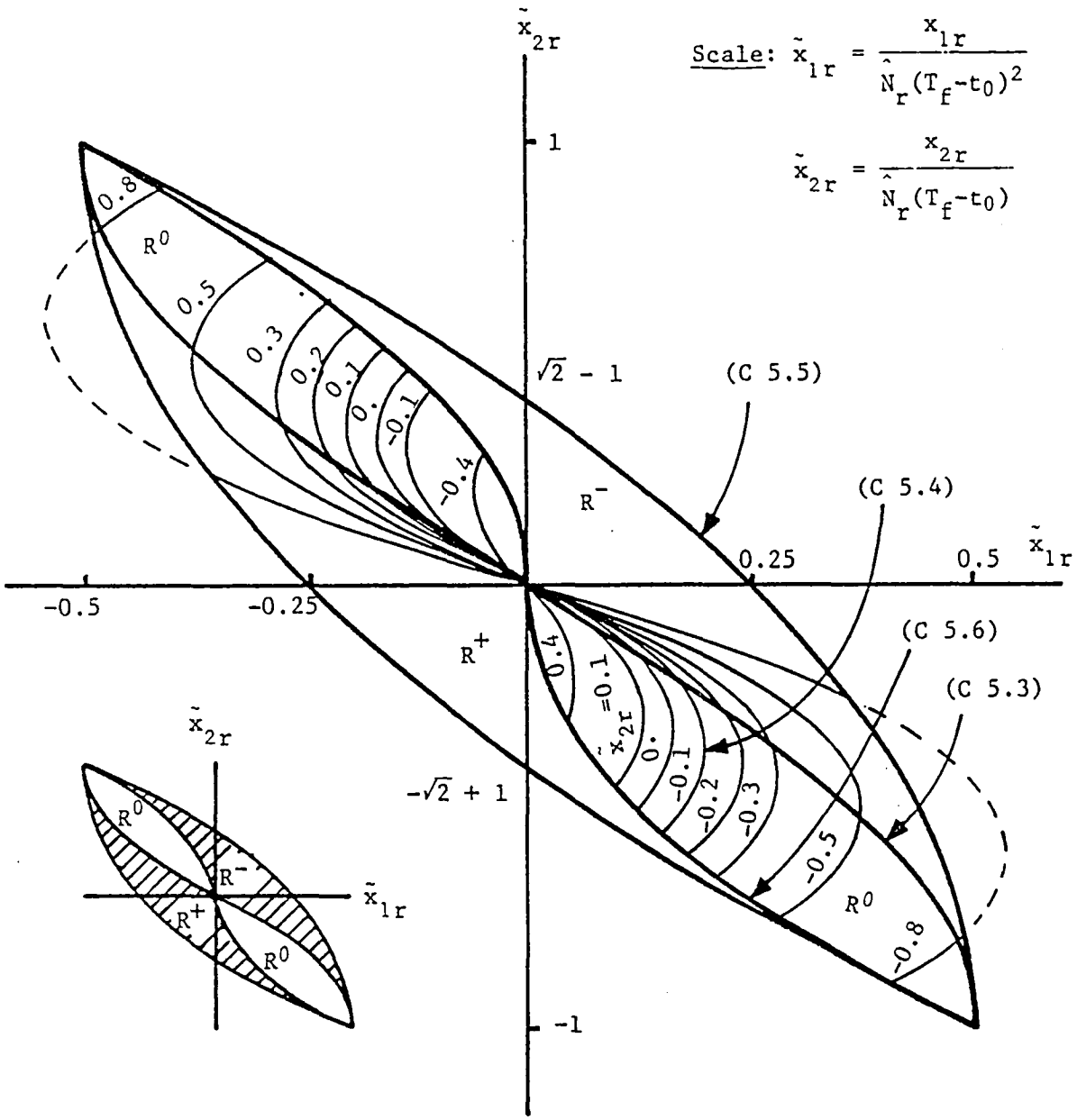

Figure C.2: Optimal Control Regions and Switching Curves in the Modal State Plane for RBM

1. For Eq.(5.57) - the curve that isolates modal initial states reaching the origin in less then the final time T_f

$$\tilde{\xi}_{0r} = -\left(\frac{1}{2}\,\dot{\tilde{\xi}}_{0r}^2 + \dot{\tilde{\xi}}_{0r}\right) \tag{C5.3}$$

2. For Eq.(C3.1) - the family of the first switching curves depending on the modal initial velocity

$$\tilde{Z}_1 = -\left[\frac{3}{2}\,\tilde{Z}_2^2 + (1 - \dot{\tilde{\xi}}_{0r})\,\tilde{Z}_2\right] \tag{C5.4}$$

for $\dot{\tilde{\xi}}_{0r}$=const.

3. For Eq.(C4.1) - the boundary curve for the reachable states

$$\tilde{\xi}_{0r} = -\frac{1}{4}\,(\dot{\tilde{\xi}}_{0r}^2 + 2\dot{\tilde{\xi}}_{0r} - 1) \tag{C5.5}$$

4. For Eq.(5.51) - the γ_r^+ curve, which is the final switching curve

$$\tilde{Z}_1 = \frac{1}{2}\,\tilde{Z}_2^2 \tag{C5.6}$$

Note that Eqs.(C5.3)-(C5.6) describe only one half of the plot in Fig. C.2, while the other part was obtained using the symmetry about the origin.

Regions R^-, R^0, R^+ in the plot designate the following control sequences to reach the origin. From region

1. R^- : $\{-\hat{N}_r, 0, +\hat{N}_r\}$
2. R^0 : $\{0, +\hat{N}_r\}$ fourth quadrant

   $\{0, -\hat{N}_r\}$ second quadrant
3. R^+ : $\{+\hat{N}_r, 0, -\hat{N}_r\}$

Appendix D

MINIMUM-FUEL CONTROL: ELASTIC MODE

See also Flugge-Lotz [23].

D.1 TIME SCALING OF THE STATE PLANE TRAJECTORIES

Figure D.1 displays the construction for one short interval. Because time increases in clockwise direction in the state plane, the radius line R rotates in a clockwise direction. A positve increment Δs along the solution curve and a positive increment $\Delta\beta$ as well, are likewise taken in the clockwise direction of increasing time. From the geometry of the figure, we obtain

$$\frac{\Delta x_1}{\Delta s} = \frac{x_2}{\omega R} \tag{D1.1}$$

Using the relations $\Delta\beta=\Delta s/R$, $\Delta x_1=x_2\Delta t$ and the definition for normalized time $\tau=\omega t$, where t is real time, we obtain

$$\Delta\tau = \Delta\beta \tag{D1.2}$$

Equation (D1.2) implies that the normalized time is equal to the sector angle of the circle or circle approximation increment Δs of the state plane trajectory.

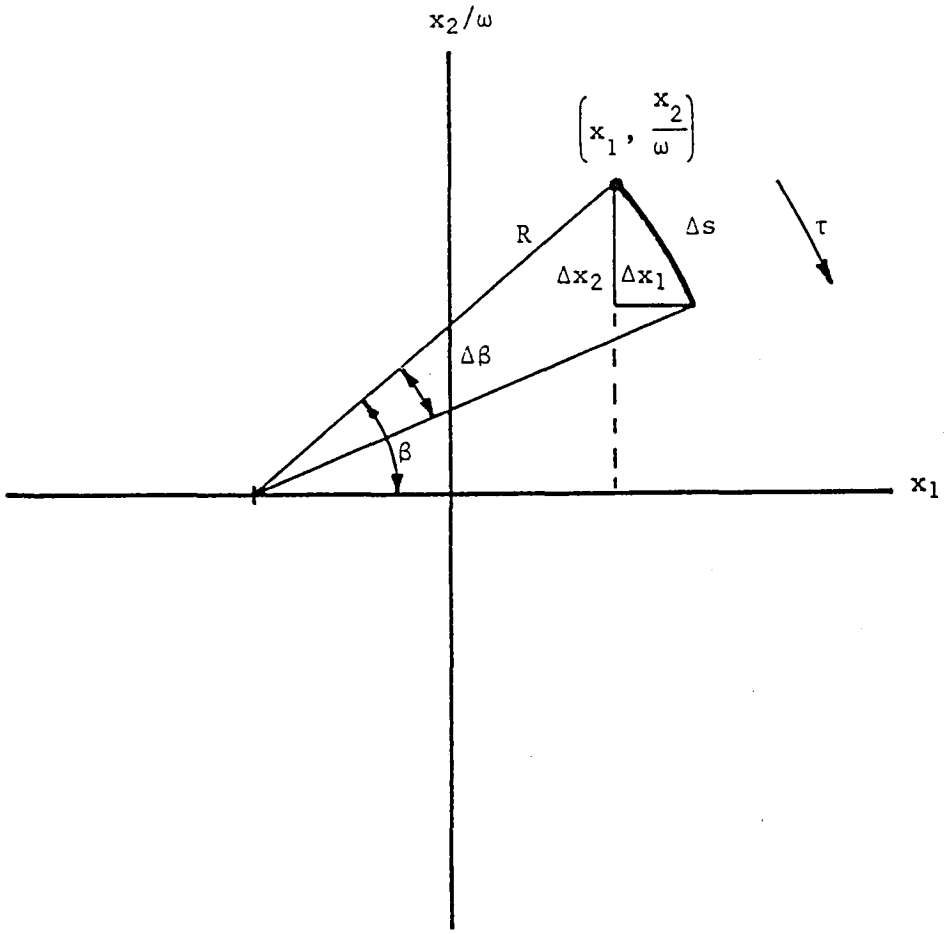

Figure D.1: Time Recovery from State Plane Description

D.2 DETERMINATION OF THE COSTATE CONSTANTS FOR INITIAL CONDITION POINT OUTSIDE THE CONTROL SECTOR

The determination of the amplitude P and phase angle θ in the costate equation $p_2(t)=P\bullet\sin(\omega t+\theta)$ for a point outside the control sector, is based on the following relations from Fig. D.2a

$$\overline{O^- A}^2 = r_0^2 + \left(\frac{\hat{N}_r}{\omega^2}\right)^2 - 2r_0 \frac{\hat{N}_r}{\omega^2} \cos\left(\frac{\pi}{2} - \frac{\alpha}{2}\right) \tag{D2.1}$$

$$\overline{O^- B}^2 = \overline{OB}^2 + \left(\frac{\hat{N}_r}{\omega^2}\right)^2 - 2\,\overline{OB}\,\frac{\hat{N}_r}{\omega^2} \cos\left(\frac{\pi}{2} + \frac{\alpha}{2}\right) \tag{D2.2}$$

Because $O^-A=O^-B$, we obtain

$$\Delta r_0 = 2\,\frac{\hat{N}_r}{\omega^2} \sin\frac{\alpha}{2} \tag{D2.3}$$

Note that $\Delta r_0=r_0-OB$ is the decrease in the distance of the state from the origin of the state plane during one nonzero control stroke. Clearly, each such control action decreases this distance in equal steps. Defining the integer n_c as the total number of control actions, we must have

$$n_c\,\Delta r_0 = r_0 \tag{D2.4}$$

to reach the origin, where

$$r_0 = \left(\xi_0^2 + \frac{\dot{\xi}_0^2}{\omega^2}\right)^{\frac{1}{2}} \tag{D2.5}$$

Substitution of Eq.(D2.3) into (D2.4), yields

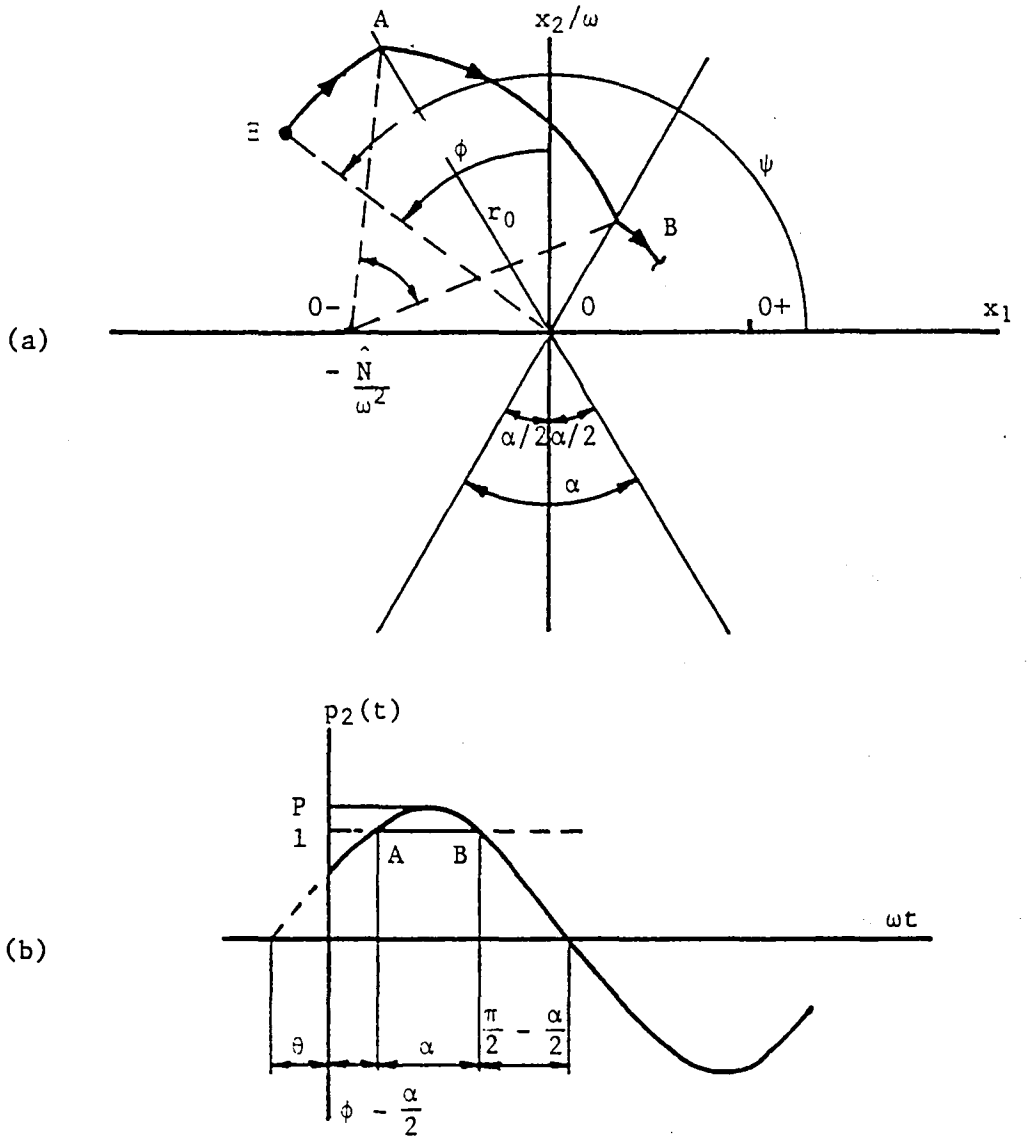

Figure D.2: Initial Condition Point Outside the Control Sector for EM
(a) State Plane Trajectory
(b) Costate Function

$$\sin\frac{\alpha}{2} = \frac{r_0\ \omega^2}{2n_c\ \hat{N}} \leqslant 1 \tag{D2.6}$$

so that the only restriction on n_c becomes

$$n_c > \text{Integer}\left\{\frac{r_0\ \omega^2}{2\hat{N}}\right\} \tag{D2.7}$$

The solution to the costate equation is given in Eq.(5.73) as

$$p_2 = P\sin(\omega t + \theta) \tag{D2.8}$$

Writing Eq.(D2.8) for point B in Fig. D.2b, we obtain

$$1 = P\sin\left(\frac{\pi}{2} + \frac{\alpha}{2}\right) \tag{D2.9}$$

from which, the amplitude constant P is obtained as

$$P = \frac{1}{\cos\frac{\alpha}{2}} = \left[1 - \left(\frac{r_0\ \omega^2}{2n_c\ \hat{N}}\right)^2\right]^{-\frac{1}{2}} \tag{D2.10}$$

The phase angle θ is obtained directly from Fig. D.2b. Clearly,

$$\theta + \left(\phi - \frac{\alpha}{2}\right) + \alpha + \left(\frac{\pi}{2} - \frac{\alpha}{2}\right) = \pi \tag{D2.11}$$

from which

$$\theta + \phi + \frac{\pi}{2} = \pi \tag{D2.12}$$

and because

$$\phi + \frac{\pi}{2} = \psi \tag{D2.13}$$

we obtain

$$\theta = \pi - \psi = \pi - \arctan\left(\frac{\dot{\xi}_{0r}}{\omega\ \xi_{0r}}\right) \tag{D2.14}$$

where the argument in Eq.(D2.14) depends on the quadrant of the initial condition point $(\xi_0, \dot{\xi}_0/\omega)$.

D.3 DETERMINATION OF THE COSTATE CONSTANTS FOR INITIAL CONDITION POINT INSIDE THE CONTROL SECTOR

The determination of the amplitude P and phase angle θ in the costate equation $p_2(t)=P\bullet\sin(\omega t+\theta)$ for a point inside the control sector, is based on the following relations from Fig. D.3a

$$\overline{O^{-}\Xi}^2 = r_0^2 + \left(\frac{\hat{N}}{\omega^2}\right)^2 - 2r_0\frac{\hat{N}}{\omega^2}\cos\left(\frac{\pi}{2} - \phi\right) \tag{D3.1}$$

$$\overline{O^{-}B}^2 = \overline{OB}^2 + \left(\frac{\hat{N}}{\omega^2}\right)^2 - 2\overline{OB}\frac{\hat{N}}{\omega^2}\cos\left(\frac{\pi}{2} + \frac{\alpha'}{2}\right) \tag{D3.2}$$

Because $O^{-}\Xi=O^{-}B$,

$$r_0^2 - \overline{OB}^2 = 2\frac{\hat{N}}{\omega^2}\left(r_0\sin\phi + \overline{OB}\sin\frac{\alpha'}{2}\right) \tag{D3.3}$$

As in Eq.(D2.4),

$$(n_c-1)\Delta r_0 = \overline{OB} \tag{D3.4}$$

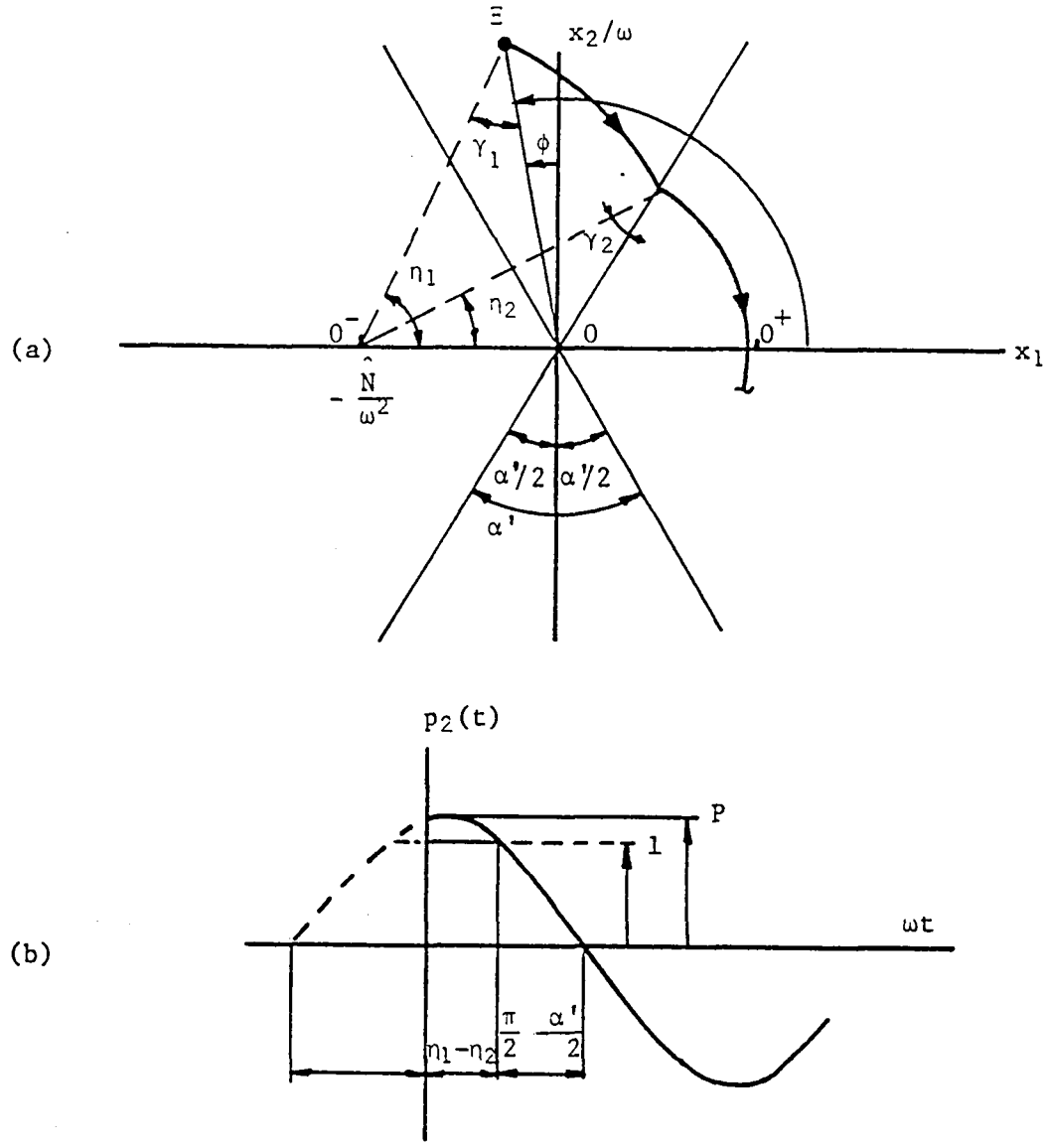

Figure D.3: Initial Condition Point Inside the Control Sector for EM
(a) State Plane Trajectory
(b) Costate Function

where $n_c - 1$ is the number of full nonzero control strokes and Δr_0 has the expression of Eq.(D2.3). Substitution of Eqs.(D2.3) and (D3.4) into Eq.(D3.3), yields

$$\sin^2 \frac{\alpha'}{2} = \frac{r_0^2 - 2 \frac{\hat{N}}{\omega^2} r_0 \sin\varphi}{4(n_c^2 - n_c)\left(\frac{\hat{N}}{\omega^2}\right)^2} \tag{D3.5}$$

Using the same argument as for Eqs.(D2.8) and (D2.9), we obtain the amplitude constant P for this case as

$$P = \left[1 - \frac{r_0^2 - 2 \frac{\hat{N}}{\omega^2} r_0 \sin\phi}{4(n_c^2 - n_c)\left(\frac{\hat{N}}{\omega^2}\right)^2}\right]^{-\frac{1}{2}} \tag{D3.6}$$

The phase angle θ is obtained directly from Fig. D.3b. Clearly,

$$\theta + (\eta_1 - \eta_2) + \frac{\pi}{2} - \frac{\alpha'}{2} = \pi \tag{D3.7}$$

From Fig. D.3a we obtain the relations

$$\eta_1 + \gamma_1 + \left(\frac{\pi}{2} - \phi\right) = \eta_2 + \gamma_2 + \left(\frac{\pi}{2} + \frac{\alpha'}{2}\right) = \pi \tag{D3.8}$$

from which

$$\eta_1 - \eta_2 = \gamma_2 - \gamma_1 + \phi + \frac{\alpha'}{2} \tag{D3.9}$$

Substitution of Eq.(D3.9) into Eq.(D3.7), yields

$$\theta + \gamma_2 - \gamma_1 + \frac{\pi}{2} + \phi = \pi \tag{D3.10}$$

or

$$\theta = \pi - \psi + \delta \tag{D3.11}$$

where $\delta=\gamma_1-\gamma_2$, is a correction factor to the phase angle θ. γ_1 and γ_2 are obtained from the triangular relations in Fig. D.3a, or

$$\sin \gamma_1 = \frac{\sin\left(\frac{\pi}{2} - \phi\right)}{\overline{O\Xi}} \frac{\hat{N}}{\omega^2} = \frac{\frac{\hat{N}}{\omega^2} \cos\phi}{\left[r_0^2 + \left(\frac{\hat{N}}{\omega^2}\right)^2 - 2r_0 \frac{\hat{N}}{\omega^2} \sin\phi\right]^{\frac{1}{2}}} \tag{D3.12}$$

$$\sin \gamma_2 = \frac{\sin\left(\frac{\pi}{2} + \frac{\alpha'}{2}\right)}{\overline{OB}} \frac{\hat{N}}{\omega^2} = \frac{\frac{N}{\omega^2} \cos \frac{\alpha'}{2}}{\left[r_0^2 + \left(\frac{\hat{N}}{\omega^2}\right)^2 - 2r_0 \frac{\hat{N}}{\omega^2} \sin\phi\right]^{\frac{1}{2}}} \tag{D3.13}$$

It is easy to show that $\delta=0$ for the case where the initial condition point is outside the control sector ($\phi>\alpha/2$).

1. Report No.	2. Government Accession No.	3. Recipient's Catalog No.
NASA CR-3760		

4. Title and Subtitle	5. Report Date
CONTROL OF LARGE FLEXIBLE SPACECRAFT BY THE INDEPENDENT MODAL-SPACE CONTROL METHOD	January 1984
	6. Performing Organization Code
7. Author(s)	8. Performing Organization Report No.
Leonard Meirovitch and Joram Shenhar	
9. Performing Organization Name and Address	10. Work Unit No.
Virginia Polytechnic Institute and State University Department of Engineering Science and Mechanics Blacksburg, VA 24061	11. Contract or Grant No. NAG1-225
12. Sponsoring Agency Name and Address	13. Type of Report and Period Covered Contractor Report
National Aeronautics and Space Administration Washington, DC 20546	14. Sponsoring Agency Code

15. Supplementary Notes

Langley Technical Monitor: Raymond C. Montgomery
Interim Report

16. Abstract

The problem of control of a large-order flexible structure in the form of a plate-like lattice by the Independent Modal-Space Control (IMSC) method is presented. The equations of motion are first transformed to the modal space, thus obtaining internal (plant) decoupling of the system. Then, the control laws are designed in the modal space for each mode separately, so that the modal equations of motion are rendered externally (controller) decoupled. This complete decoupling applies both to rigid-body modes and elastic modes. The application of linear optimal control, in conjunction with a quadratic performance index, is first reviewed.

For one-dimensional structures, the actuators placement represents no problem if the IMSC method is used. In the case of two-dimensional or three-dimensional structures, care must be exercised in the selection of the actuators locations so as to avoid singularity of the modal participation matrix, thus ensuring controllability. Some criteria for the actuators locations are developed.

The minimum-fuel problem has important implications for various space missions. Yet, solutions of the problem have been limited to very low-order systems. A solution for high-order systems is proposed here by the IMSC method, whereby the problem is reduced to a number of modal minimum-fuel problems for the controlled modes.

17. Key Words (Suggested by Author(s))	18. Distribution Statement
Modal control Large space structures Active damping	Unclassified - Unlimited Subject Category 13

19. Security Classif. (of this report)	20. Security Classif. (of this page)	21. No. of Pages	22. Price
Unclassified	Unclassified	214	A10

N-305

For sale by the National Technical Information Service, Springfield, Virginia 22161

☆U.S. GOVERNMENT PRINTING OFFICE: 1984-739-010/48 REGION NO. 4

National Aeronautics and
Space Administration

Washington, D.C.
20546

Official Business
Penalty for Private Use, $300

SPECIAL FOURTH CLASS MAIL
BOOK

Postage and Fees Paid
National Aeronautics and
Space Administration
NASA-451

U.S. MAIL

NASA

POSTMASTER: If Undeliverable (Section 158
Postal Manual) Do Not Return